Supplementary Information

Discovery of Benzoxazole-Thiazolidinone Hybrids as Promising Antibacterial Agents against *Staphylococcus aureus* and *Enterococcus* Species

Vijay Sai Krishna Cheerala[a], Abdul Akhir[b], Deepanshi Saxena[b], Rahul Maitra[b], Sidharth Chopra[b,c,*] and Sundaresan Chittor Neelakantan[a*]

[a]Department of Chemistry, Sri Sathya Sai Institute of Higher Learning, Brindavan Campus, Bengaluru, 560067, Karnataka, India

[b]Division of Molecular Microbiology and Immunology, CSIR-Central Drug Research Institute, Sector 10, Sitapur Road, Lucknow - 226031, Uttar Pradesh, India

[c] AcSIR: Academy of Scientific and Innovative Research (AcSIR), Ghaziabad, 201002, India

Corresponding Author

Sidharth Chopra:Tel:+91-7652032958, email: skhopra007@gmail.com

Sundaresan Chittor Neelakantan: Tel: +91-7975943998. Email: cnsundaresan@sssihl.edu.in

Table of contents

1. Characterization details of B-T hybrids (BT3 – BT26)

BT3: M.P. 275-277 °C; λ_{max}(THF): 360 nm; ν_{max} (cm^{-1}): 3159 (N-H thiazolidinone), 3062 (C-H aromatic), 1717 (C=O thiazolidinone), 1598 (C=N); ^{1}HNMR (400 MHz, DMSO-d6): δ 13.31 (s, 1H), 7.93 (s, 1H), 7.79 – 7.44 (m, 6H), 7.33 (m, 2H); ^{13}C NMR (100 MHz, DMSO-d6): δ167.24, 163.35, 162.27, 148.74, 141.57, 134.89, 132.51, 131.69, 130.90, 129.80, 128.76, 128.67, 128.02, 125.08, 124.85, 119.16, 110.85; Mass (*m/z*): 355.9404 [M+H^+]

BT4: M.P. 262-264 °C; λ_{max}(THF): 360 nm; ^{1}HNMR (400 MHz, DMSO-d6): δ 13.26 (s, 1H), 7.80 (s, 1H), 7.79 (t, *J* = 1.6 Hz, 1H), 7.71 (m, 1H), 7.64 (m, 3H), 7.58 (m, 1H), 7.33 (m, 2H); ^{13}C NMR (100 MHz, DMSO-d6): δ 167.68, 163.72, 162.41, 158.40, 148.74, 141.72, 134.78, 133.90, 130.98, 125.02, 124.73, 124.03, 122.13, 119.11, 118.45, 116.52, 110.80; Mass (*m/z*): 355.9400 [M+H^+]

BT5: M.P. 287-289 °C; λ_{max}(THF): 365 nm; ν_{max} (cm^{-1}): 3162 (N-H thiazolidinone), 3049 (C-H aromatic), 1719 (C=O thiazolidinone), 1602(C=N); ^{1}HNMR (400 MHz, DMSO-d6): δ13.22 (s, 1H), 7.82 (s, 1H), 7.77 – 7.60 (m, 6H) 7.34 (m, 2H); ^{13}C NMR (100 MHz, DMSO-d6): δ 13C NMR (101 MHz, DMSO) δ 167.06, 162.83, 161.88, 148.30, 141.20, 135.22, 132.09, 131.89 (2C), 129.58 (2C), 124.63, 124.58, 124.36, 118.66, 110.39; Mass (*m/z*): 355.9403 [M+H^+]

BT6: M.P. 301-302 °C; λ_{max}(THF): 360 nm; ^{1}HNMR (400 MHz, DMSO-d6): δ 13.27 (s, 1H), 7.84 – 7.56 (m, 5H), 7.55 – 7.27 (m, 4H); Mass (*m/z*): 339.9716 [M+H^+]

BT7: M.P. 279-281 °C; λ_{max}(THF): 360 nm; ^{1}HNMR (400 MHz, DMSO-d6): δ 13.23 (s, 1H), 7.80 (s, 1H), 7.72 (m, 1H), 7.64 (m, 2H), 7.53 (dt, *J* = 7.6, 2.3 Hz, 2H), 7.34 (m, 3H); ^{13}C NMR (100 MHz, DMSO-d6): δ 13C NMR (101 MHz, DMSO) δ 167.39, 163.97, 163.16, 162.27, 161.54, 148.73, 141.62, 135.99, 132.18, 131.94, 126.24, 125.87, 124.90, 119.18, 117.78, 117.31, 110.80; Mass (*m/z*): 339.9715 [M+H^+]

BT8: M.P. 312-314 °C; λ_{max}(THF): 363 nm; ^{1}HNMR (400 MHz, DMSO-d6): 1H NMR (400 MHz, DMSO) δ 13.20 (s, 1H), 7.85 (s, 1H), 7.79 (d, *J* = 8.6 Hz, 1H), 7.78 (d, *J* = 8.6 Hz, 1H), 7.72 (m, 1H), 7.66 (m, 1H), 7.47 (t, *J* = 8.6 Hz, 2H), 7.35 (m, 2H); ^{13}C NMR (100 MHz, DMSO-d6): δ 167.14, 164.27, 161.92, 161.77, 148.28, 141.22, 132.81, 132.72, 132.16, 129.83, 124.61, 124.33, 123.50, 118.66, 116.81, 116.59, 110.38 ; Mass (*m/z*): 339.9715 [M+H^+]

BT9: M.P. 283-284 °C; λ_{max}(THF): 365 nm; ^{1}HNMR (400 MHz, DMSO-d6): δ 13.21 (s, 1H), 7.80 (m, 3H), 7.64 (m, 4H), 7.33 (m, 2H); ^{13}C NMR (100 MHz, DMSO-d6): δ 13C NMR (101 MHz, DMSO) δ 13C NMR (101 MHz, DMSO) δ 167.04, 162.79, 161.85, 148.29, 141.19, 132.48 (2C), 132.39, 132.01 (2C), 131.96, 124.65, 124.61, 124.34, 124.15, 118.65, 110.38.; Mass (*m/z*): 399.8826 [M+H^{+}], 401.8805 [M+2+H^{+}].

BT10: M.P. 261-263 °C; λ_{max}(THF): 385 nm; v_{max} (cm^{-1}): 3162 (N-H thiazolidinone), 3055 (C-H aromatic), 1683 (C=O thiazolidinone), 1583 (C=N); ^{1}HNMR (400 MHz, DMSO-d6): δ 13.11(s, 1H), 10.82(s, 1H), 8.04 (s, 1H), 7.72(m, 1H), 7.64(m, 1H), 7.51 (dd, J = 7.9, 1.6 Hz, 1H), 7.33(m, 3H), 7.09 (d, *J* = 8.2 Hz, 1H), 7.04 (td, *J* = 7.6, 1.1 Hz, 1H); ^{13}C NMR (100 MHz, DMSO-d6): δ13C NMR (101 MHz, DMSO) δ 167.40, 163.56, 162.07, 157.62, 148.25, 141.31, 132.55, 128.86, 128.69, 124.53, 124.20, 122.04, 120.01, 119.74, 118.61, 116.38, 110.30; Mass (*m/z*): 337.9762 [M+H^{+}]

BT11: M.P. 282-284 °C; λ_{max}(THF): 371 nm; v_{max} (cm^{-1}): 3136 (N-H thiazolidinone), 3063 (C-H aromatic), 1698 (C=O thiazolidinone), 1581 (C=N); ^{1}HNMR (400 MHz, DMSO-d6): δ 13.15 (s, 1H), 9.99 (s, 1H), 7.73 (s, 1H), 7.74 (m, 1H), 7.65 (m, 1H), 7.40 (t, *J* = 8.07, 7.95 Hz, 1H), 7.35 (m, 2H), 7.15 (d, *J* = 7.95 Hz, 1H), 7.10 (s, 1H), 6.94 (dd, *J* = 1.83, 1.71, 8.19, 8.07 Hz, 1H); ^{13}C NMR (100 MHz, DMSO-d6): δ 167.69, 163.72, 162.40, 158.40, 148.75, 141.72, 134.76, 133.89, 130.97, 125.00, 124.75, 124.02, 122.12, 119.10, 118.44, 116.51, 110.80; Mass (*m/z*): 338.0593 [M+H^{+}]

BT12: M.P. 310-312 °C; λ_{max}(THF): 388 nm; v_{max} (cm^{-1}): 3119 (N-H thiazolidinone), 3048 (C-H aromatic), 1690 (C=O thiazolidinone), 1557 (C=N); ^{1}HNMR (400 MHz, DMSO-d6): δ 13.04 (s, 1H), 10.41 (s, 1H), 7.74 (s, 1H), 7.73 (m, 1H), 7.65 (m, 1H), 7.58 (d, *J* = 8.6 Hz, 2H), 7.34 (m, 2H), 6.99 (d, *J* = 8.6 Hz, 2H); ^{13}C NMR (100 MHz, DMSO-d6): δ 167.80, 163.77, 162.53, 160.66, 148.68, 141.80, 134.30, 133.25 (2C), 124.94, 124.61, 124.48, 119.57, 119.08, 116.95 (2C), 110.73; Mass (*m/z*): 338.0521 [M+H^{+}]

BT13: M.P. 267-269 °C; λ_{max}(THF): 359 nm; v_{max} (cm^{-1}): 3080 (N-H thiazolidinone), 3045 (C-H aromatic), 1725(C=O thiazolidinone); 1592 (C=N), 1515/1340 (NO2); ^{1}HNMR (400 MHz, DMSO-d6): δ 13.29 (s, 1H), 8.26 (dd, *J* = 8.3, 1.2 Hz, 1H), 8.06 (s, 1H), 7.98 (td, *J* = 7.6, 1.3 Hz, 1H), 7.84 (dd, *J* = 7.8, 1.4 Hz, 1H), 7.78 (td, *J* = 7.9, 1.4 Hz, 1H), 7.64 (m, 2H), 7.30 (m, 2H); ^{13}C NMR (100

MHz, DMSO-d6): δ166.37, 163.05, 161.85, 148.23, 147.71, 141.06, 134.83, 131.19, 130.45, 129.82, 129.30, 128.26, 125.56, 124.60, 124.37, 118.64, 110.38; Mass (*m/z*): 366.9641 [M+H$^+$]

BT14: M.P. 260-261 °C; λ_{max}(THF): 358 nm; v_{max} (cm^{-1}): 3124 (N-H thiazolidinone), 3061 (C-H aromatic), 1702 (C=O thiazolidinone), 1579 (C=N), 1531/1352 (NO2); ^{1}HNMR (400 MHz, DMSO-d6): δ 13.31 (s, 1H), 8.55 (t, *J* = 2.0 Hz, 1H), 8.32 (dd, *J* = 8.2, 2.0 Hz, 1H), 8.11 (dt, *J* = 8.0, 1.1 Hz, 1H), 7.96 (s, 1H), 7.89 (t, *J* = 8.0 Hz, 1H), 7.69 (m, 1H), 7.65 (m, 1H), 7.34 (m, 2H); ^{13}C NMR (100 MHz, DMSO-d6): δ 167.31, 162.96, 162.24, 148.77, 141.56, 135.98, 135.30, 131.48, 131.21, 127.23, 125.24, 125.12, 125.08, 124.88, 119.14, 110.87; Mass (*m/z*): 366.9629 [M+H$^+$]

BT15: M.P. 287-288 °C; λ_{max}(THF): 376 nm; v_{max} (cm^{-1}): 3100 (N-H thiazolidinone), 3050 (C-H aromatic), 1719 (C=O thiazolidinone), 1596(C=N), 1521/1343 (NO2); ^{1}HNMR (400 MHz, DMSO-d6): δ 13.32 (s, 1H), 8.42 (d, *J* = 8.6 Hz, 2H), 7.96 (d, *J* = 8.6, 2H), 7.93 (s, 1H), 7.71 (m, 1H), 7.66 (m, 1H), 7.35 (m, 2H); Mass (*m/z*): 366.9623 [M+H$^+$]

BT16: M.P. 251-252 °C; λ_{max}(THF): 366 nm; v_{max} (cm^{-1}): 3119 (N-H thiazolidinone), 3056 (C-H aromatic), 1693 (C=O thiazolidinone), 1574 (C=N); ^{1}HNMR (400 MHz, DMSO-d6): δ 13.18 (s, 1H), 7.79 (s, 1H), 7.72 (m, 1H), 7.64 (m, 1H), 7.53 (t, *J* = 8.2 Hz, 1H), 7.33 (m, 2H), 7.27 (m, 2H), 7.11 (ddd, *J* = 8.4, 2.5, 0.9 Hz, 1H), 3.83 (s, 3H); ^{13}C NMR (100 MHz, DMSO-d6): δ 167.06, 163.09, 161.93, 159.68, 148.27, 141.21, 134.49, 133.16, 130.60, 124.57, 124.31, 124.14, 121.93, 118.70, 116.17, 116.12, 110.35, 55.35; Mass (*m/z*): 351.9907 [M+H$^+$]

BT17: M.P. 281-282°C; λ_{max}(THF): 383 nm; v_{max} (cm^{-1}): 3155 (N-H thiazolidinone), 3058 (C-H aromatic), 1712 (C=O thiazolidinone), 1593 (C=N); ^{1}HNMR (400 MHz, DMSO-d6): δ 13.07 (s, 1H), 7.76 (s, 1H), 7.71 (m, 1H), 7.66 (d, J = 8.8 Hz, 1H), 7.63 (m, 1H), 7.32 (m, 2H), 7.15 (d, J = 8.8 Hz, 1H), 3.84 (s, 3H); ^{13}C NMR (100 MHz, DMSO-d6): δ 167.25, 163.18, 162.02, 161.24, 148.25, 141.29, 133.35, 132.44, 125.58, 124.55, 124.21, 120.43, 118.59, 115.10, 110.32, 55.57; Mass (*m/z*): 351.9900 [M+H$^+$]

BT18: M.P. 271-272 °C; λ_{max}(THF): 393 nm; v_{max} (cm^{-1}): 3424(O-H), 3135 (N-H thiazolidinone), 1698(C=O thiazolidinone), 1567 (C=N); ^{1}HNMR (400 MHz, DMSO-d6): δ 13.03 (s, 1H), 10.06 (s, 1H), 7.74 (s, 1H), 7.69 (m, 1H), 7.62 (m, 1H), 7.32 (m, 3H), 7.19 (dd, *J* = 8.3, 2.1 Hz, 1H), 7.01 (d, *J* = 8.3 Hz, 1H), 3.86 (s, 3H); ^{13}C NMR (100 MHz, DMSO-d6): δ 167.30, 163.46, 162.13, 149.76,

148.25, 148.03, 141.31, 134.14, 124.55, 124.50, 124.17, 123.87, 119.52, 118.59, 116.38, 115.37, 110.29, 55.74; Mass (*m/z*): 367.9825 [M+H$^+$]

BT19: M.P. 273-274 °C; λ_{max}(THF): 392 nm; ^{1}HNMR (400 MHz, DMSO-d6): δ 13.06 (s, 1H), 9.65 (s, 1H), 7.72 (m, 1H), 7.68 (s, 1H), 7.64 (m, 1H), 7.33 (m, 2H), 7.2 (m, 1H), 7.14 (m, 2H), 3.86 (s, 3H); ^{13}C NMR (100 MHz, DMSO-d6): δ 167.30, 163.36, 162.06, 150.37, 148.27, 147.02, 141.34, 133.86, 125.77, 124.55, 124.21, 124.09, 120.17, 118.59, 116.03, 112.53, 110.32, 55.76; Mass (*m/z*): 367.9829 [M+H$^+$]

BT20: M.P. 314-316 °C; λ_{max}(THF): 448 nm; ν_{max} (cm^{-1}): 3110 (N-H thiazolidinone), 3045 (C-H aromatic), 1683 (C=O thiazolidinone), 1570 (C=N); ^{13}C NMR (100 MHz, DMSO-d6): δ 166.77, 162.82, 161.61, 151.06, 147.58, 140.81, 133.87, 131.97 (2C), 123.83, 123.39, 119.22, 117.81, 115.06, 111.56 (2C), 109.60, 39.00; Mass (*m/z*): 365.0191 [M+H$^+$]

BT21: M.P. 251-252 °C; λ_{max}(THF): 398 nm; ν_{max} (cm^{-1}): 3118 (N-H thiazolidinone), 3061 (C-H aromatic), 1696 (C=O thiazolidinone), 1576 (C=N); ^{1}HNMR (400 MHz, DMSO-d6): δ 13.15 (s, 1H), 7.79 (s, 1H), 7.71 (m, 1H), 7.65 (d, *J* = 8.5 Hz, 2H), 7.64 (m, 1H), 7.47 (d, *J* = 8.5 Hz, 2H), 7.34 (m, 2H), 2.56 (s, 3H); ^{13}C NMR (100 MHz, DMSO-d6): δ 167.19, 162.98, 161.97, 148.28, 142.74, 141.26, 132.93, 130.74, 129.18, 125.86, 124.58, 124.27, 122.16, 118.61, 110.35, 14.04; Mass (*m/z*): 367.9641 [M+H$^+$]

BT22: M.P. 326-327 °C; λ_{max}(THF): 385 nm; ν_{max} (cm^{-1}): 3113 (N-H thiazolidinone), 3046 (C-H aromatic), 1690 (C=O thiazolidinone), 1566 (C=N); ^{1}HNMR (400 MHz, DMSO-d6): δ 13.13 (s, 1H), 8.09 (s, 1H), 8.08 (m, 1H), 7.75 (d, *J* = 1.6 Hz, 1H) 7.72 (m, 1H), 7.65 (m, 1H), 7.38 – 7.30 (m, 3H); ^{13}C NMR (100 MHz, DMSO-d6): δ 13C NMR (101 MHz, DMSO) δ 166.95, 162.51, 161.98, 148.26, 141.24, 137.18, 135.32, 133.78, 129.10, 126.33, 124.59, 124.28, 121.02, 118.64, 110.35; Mass (*m/z*): 327.9392 [M+H$^+$]

BT23: M.P. 319-321 °C; λ_{max}(THF): 384 nm; ν_{max} (cm^{-1}): 3119 (N-H thiazolidinone), 3042 (C-H aromatic), 1786 (C=O thiazolidinone), 1575 (C=N); ^{1}HNMR (400 MHz, DMSO-d6): δ 13.03 (s, 1H), 8.20 (d, *J* = 1.8 Hz, 1H), 7.71 (m, 1H), 7.65 (s, 1H), 7.64 (m, 1H), 7.33 (m, 2H), 7.20 (d, *J* = 3.5 Hz, 1H), 6.81 (dd, *J* = 3.5, 1.8 Hz, 1H); ^{13}C NMR (100 MHz, DMSO-d6): δ 166.99, 164.13, 162.11,

149.50, 148.26, 148.09, 141.35, 124.56, 124.20, 120.37, 119.63, 119.45, 118.54, 113.78, 110.31; Mass (*m/z*): 311.9642 [M+H$^+$]

BT24: M.P. 292-294 °C; λ_{max}(THF): 371 nm; ν_{max} (cm^{-1}): 3162 (N-H thiazolidinone), 3069 (C-H aromatic), 1724 (C=O thiazolidinone), 1589 (C=N); ^{1}HNMR (400 MHz, DMSO-d6): δ 13.02, 8.88 (s, 1H), 7.98 (td, *J* = 7.5, 1.5 Hz, 1H), 7.92 (m, 1H), 7.87 (s, 1H), 7.74 (m, 1H), 7.64 (m, 1H), 7.48 (ddd, *J* = 7.5, 4.8, 1.5 Hz, 1H), 7.35 (pd, *J* = 7.4, 1.5 Hz, 2H).; ^{13}C NMR (100 MHz, DMSO-d6): δ 167.31, 162.09, 151.49, 149.66, 148.37, 141.47, 137.62, 129.63, 128.09, 127.75, 124.51, 124.20, 124.18, 118.63, 110.30; Mass (*m/z*): 322.9786 [M+H$^+$]

BT25: M.P. 259-261°C; λ_{max}(THF): 388 nm; ^{1}HNMR (400 MHz, DMSO-d6): δ 1H NMR (400 MHz, DMSO) δ1H NMR (400 MHz, DMSO) δ 13.15 (s, 1H), 11.14 (s, 1H), 7.88 (s, 1H), 7.68 (m, 1H), 7.61 (m, 1H), 7.43 (d, *J* = 2.6 Hz, 1H), 7.37 (dd, *J* = 8.8, 2.6 Hz, 1H), 7.31 (m, 2H), 7.08 (d, *J* = 8.8 Hz, 1H); ^{13}C NMR (100 MHz, DMSO-d6): δ 13C NMR (101 MHz, DMSO) δ 167.20, 163.11, 161.98, 156.24, 148.28, 141.23, 131.84, 127.99, 127.36, 124.56, 124.28, 123.96, 123.00, 121.72, 118.66, 118.03, 110.33; Mass (*m/z*): 371.9312 [M+H$^+$]

BT26: M.P. 278-279 °C; λ_{max}(THF): 387 nm; ^{1}HNMR (400 MHz, DMSO-d6): δ 13.13 (s, 1H), 11.00 (s, 1H), 7.87 (s, 1H), 7.67 (m, 1H), 7.62 (m, 1H), 7.56 (d, J = 2.4 Hz, 1H), 7.49 (dd, J = 8.8, 2.4 Hz, 1H), 7.32 (m, 2H), 6.95 (d, J = 8.8 Hz, 1H); ^{13}C NMR (100 MHz, DMSO-d6): δ 167.12, 163.10, 161.97, 156.43, 148.28, 141.22, 134.70, 131.04, 127.34, 124.56, 124.28, 124.04, 122.37, 118.62, 118.36, 110.57, 110.34; Mass (*m/z*): 415.8757 [M+H$^+$], 417.8737 [M+2+H$^+$]

2. $^{1}H/^{13}C$-NMR Spectra of B-T hybrids

$^{1}H/^{13}C$-NMR spectra of BT1

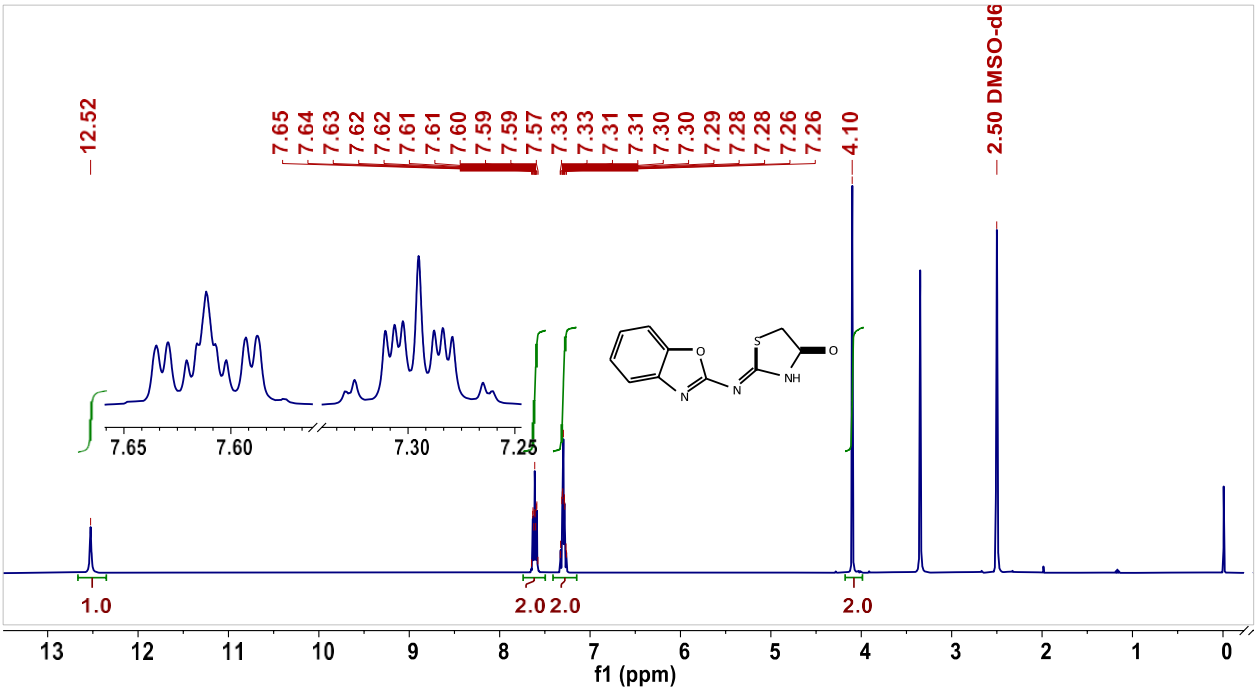

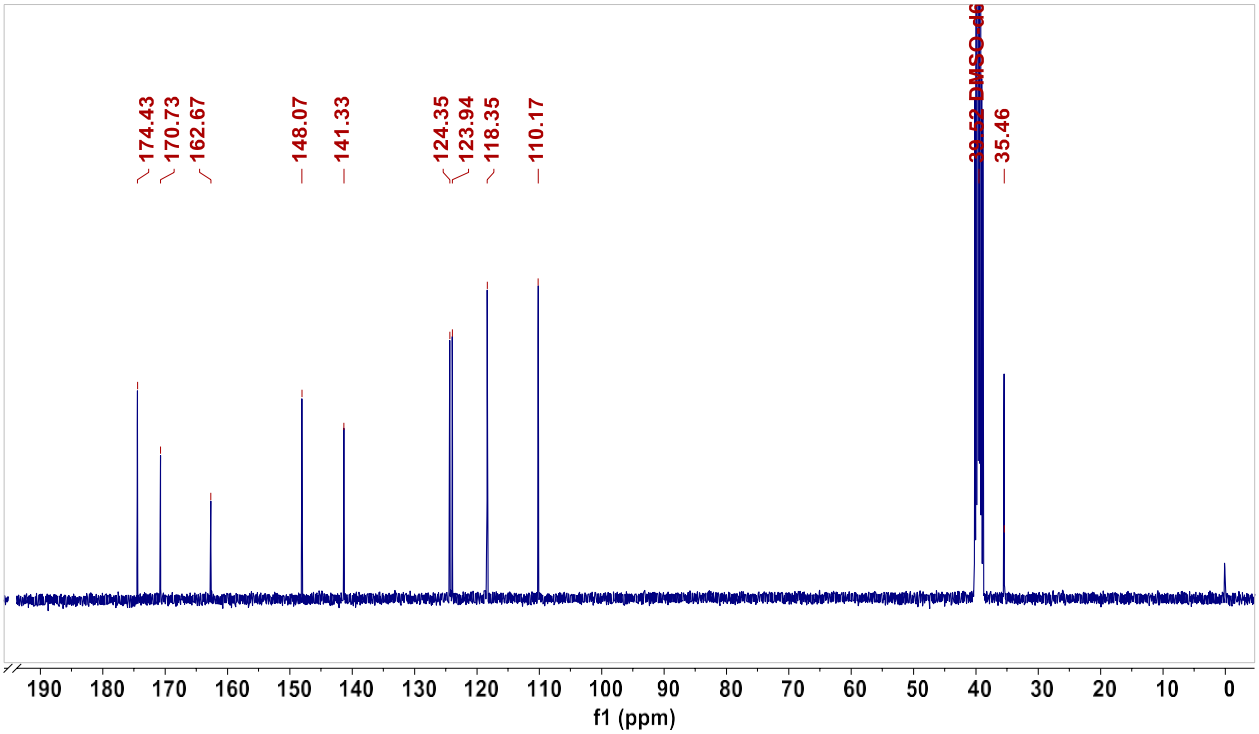

$^{1}H/^{13}C$-NMR spectra of BT8

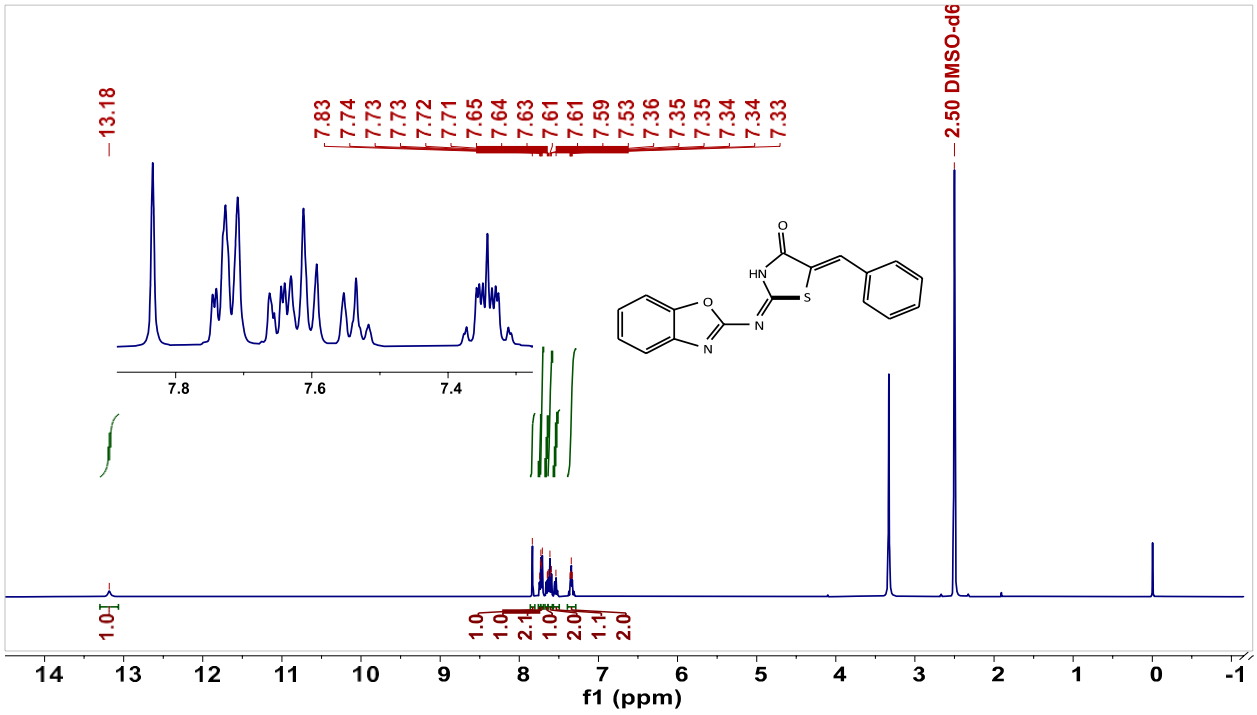

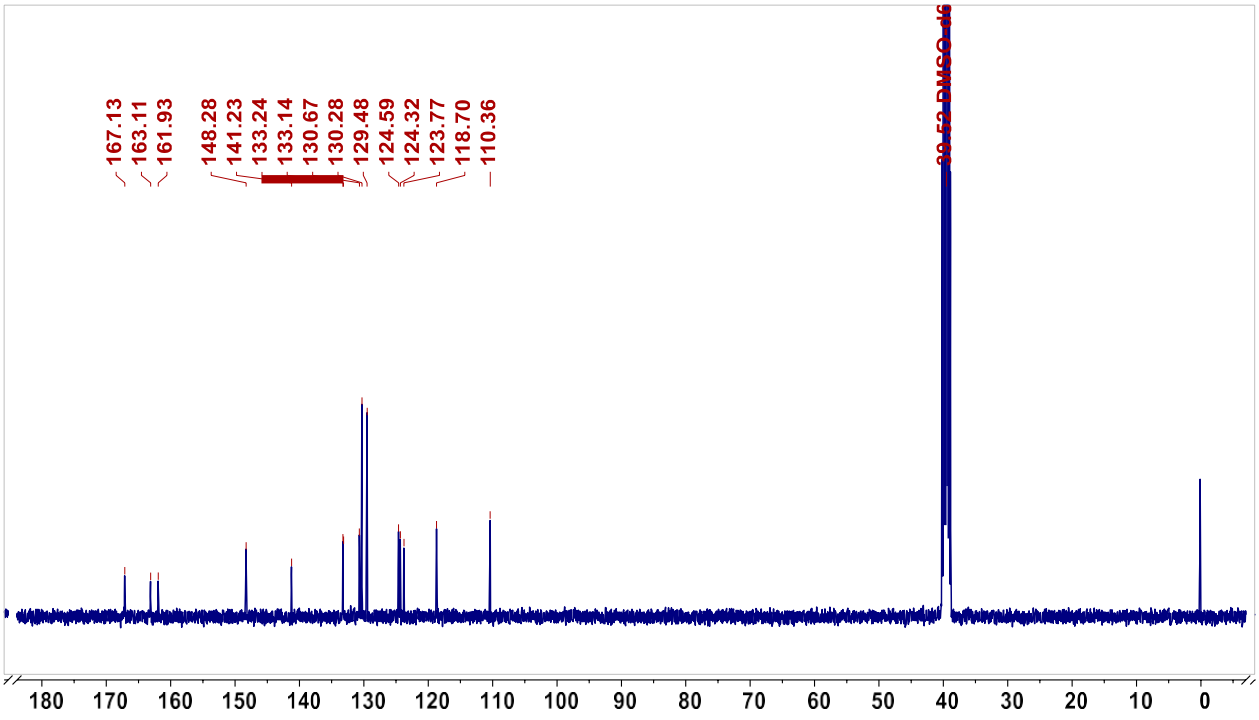

$^{1}H/^{13}C$-NMR spectra of BT9

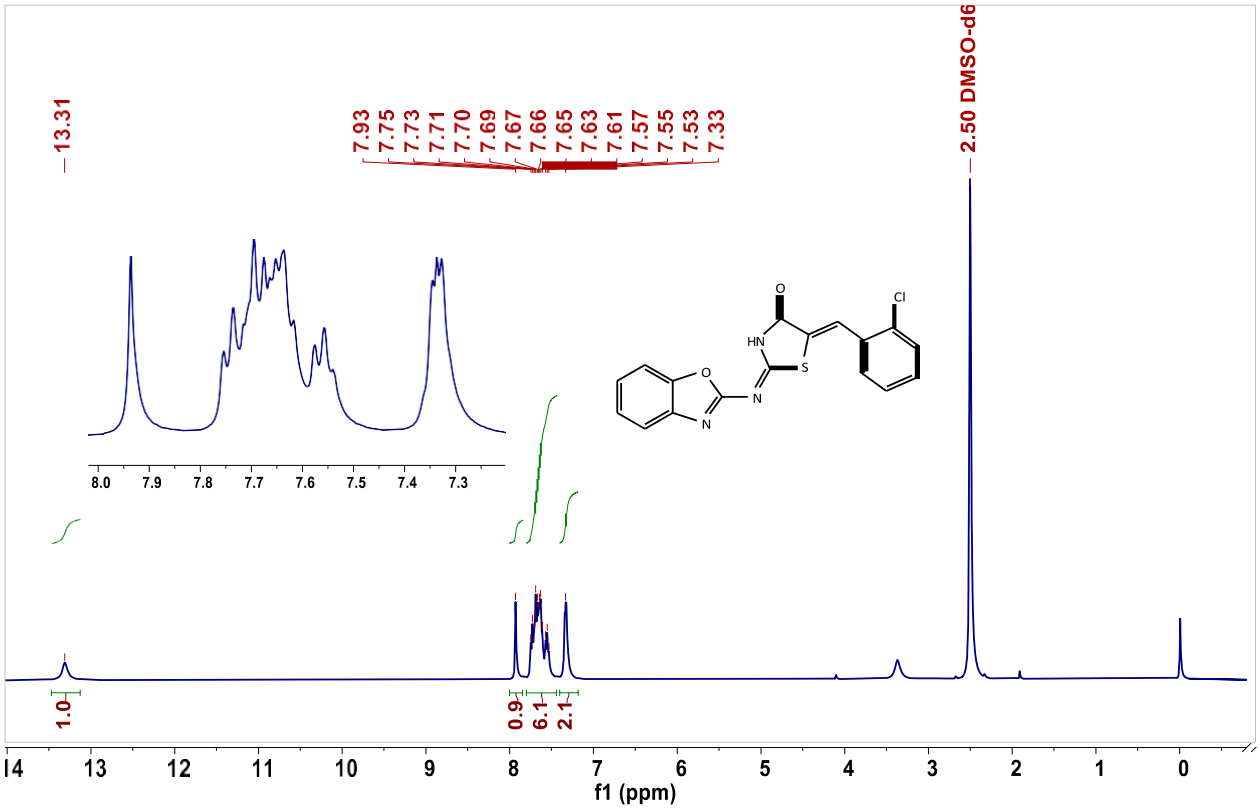

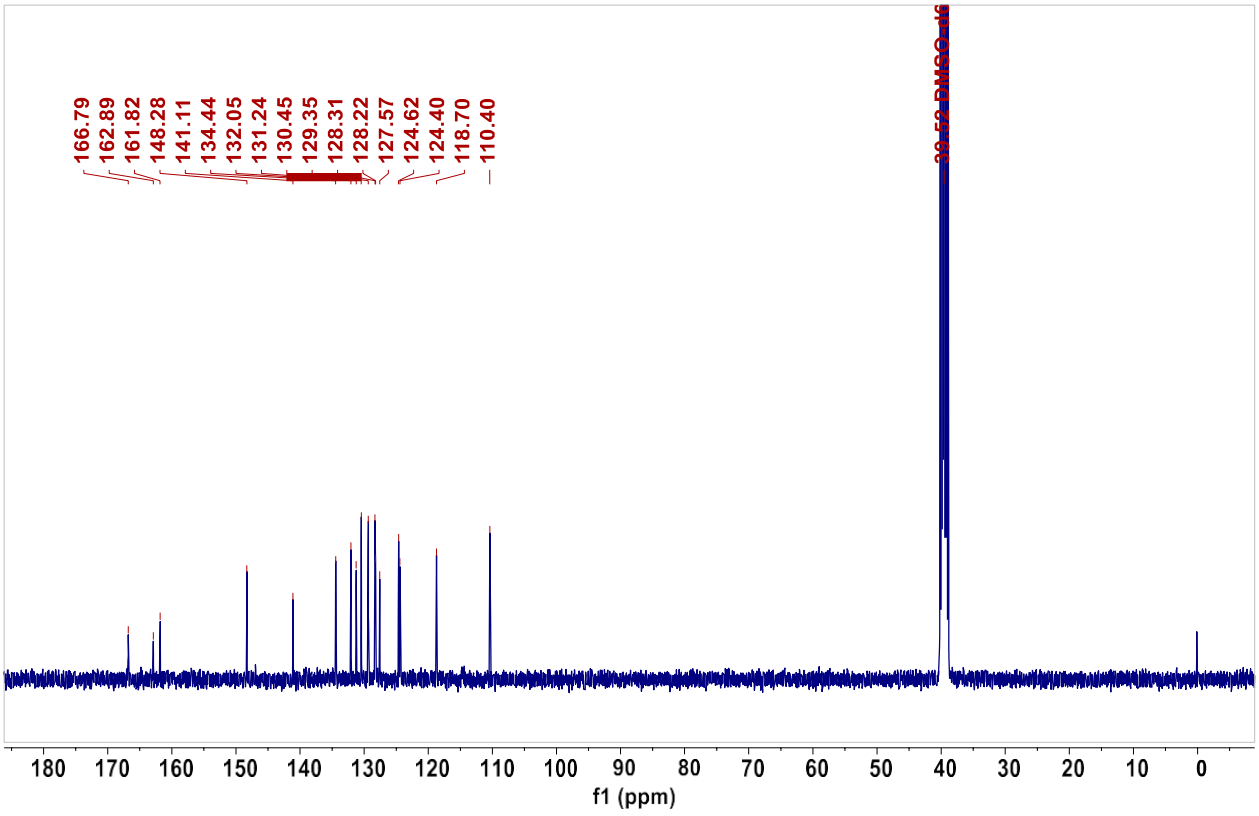

$^{1}H/^{13}C$-NMR spectra of BT

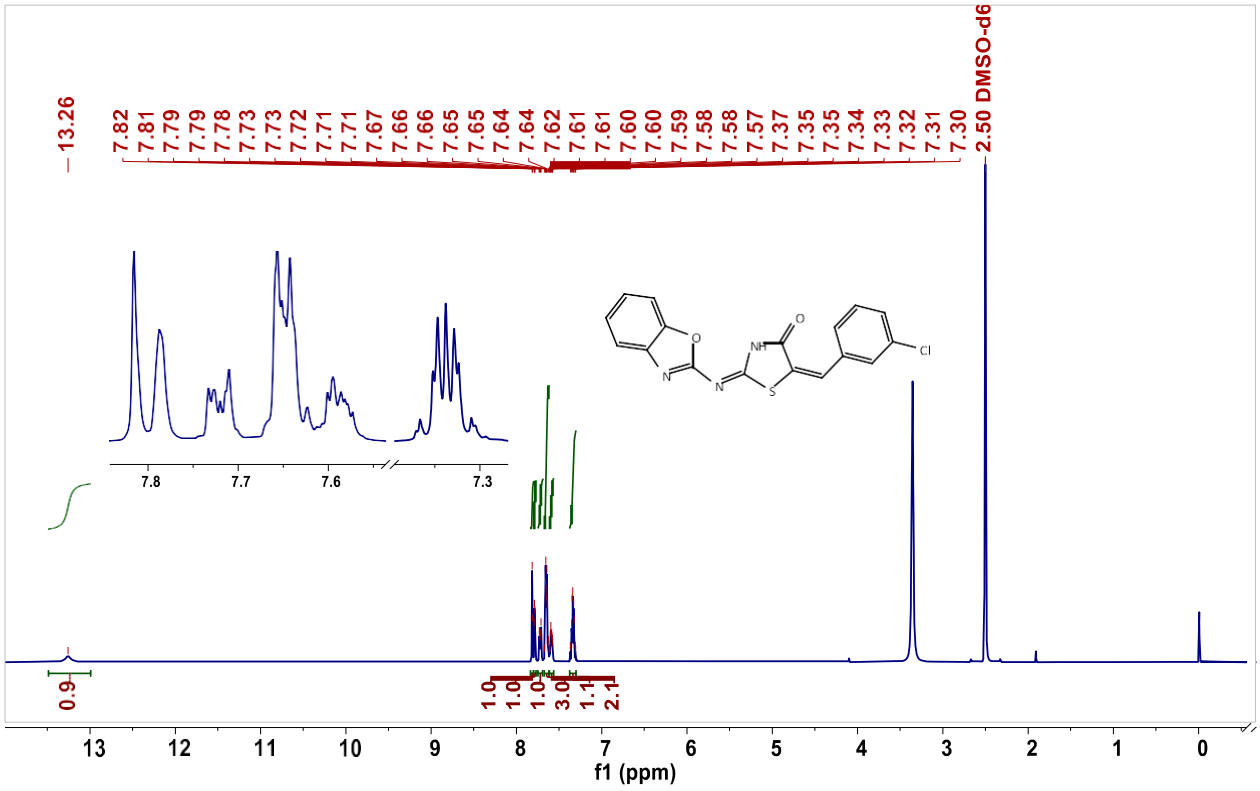

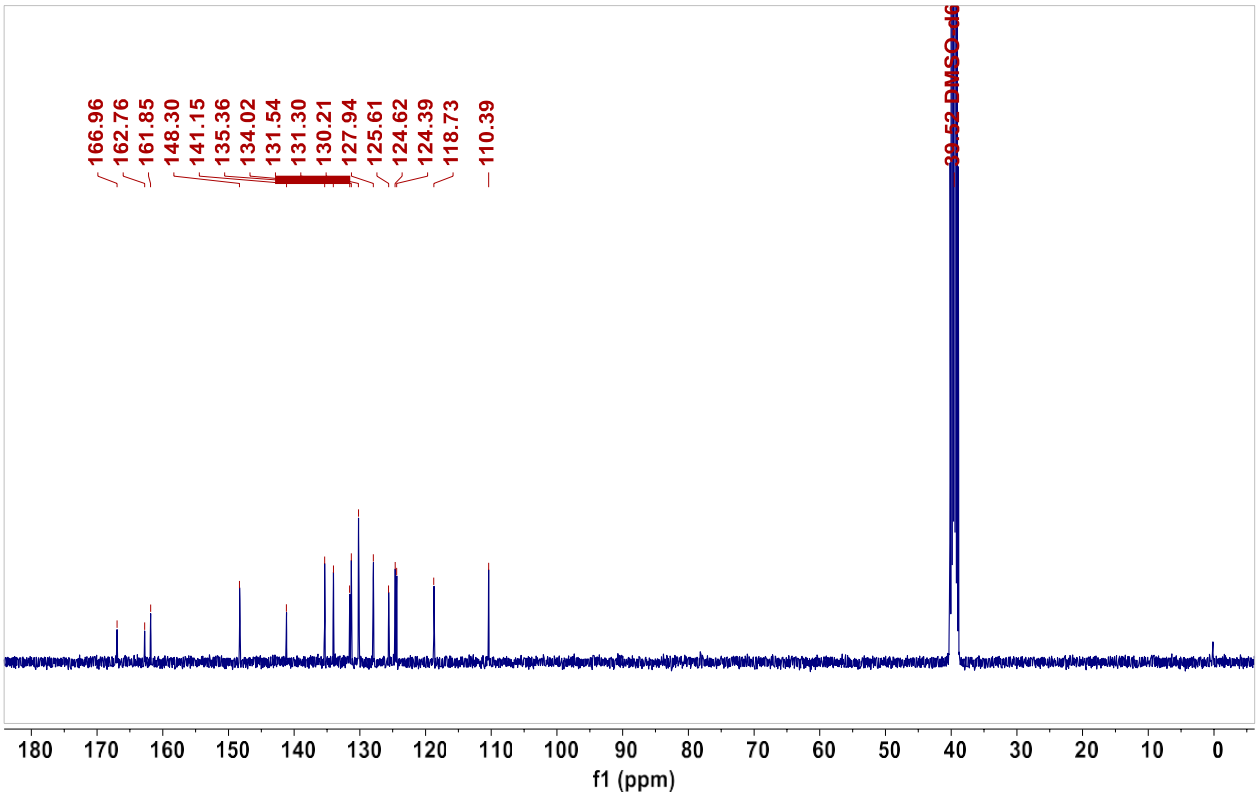

$^{1}H/^{13}C$-NMR spectra of BT

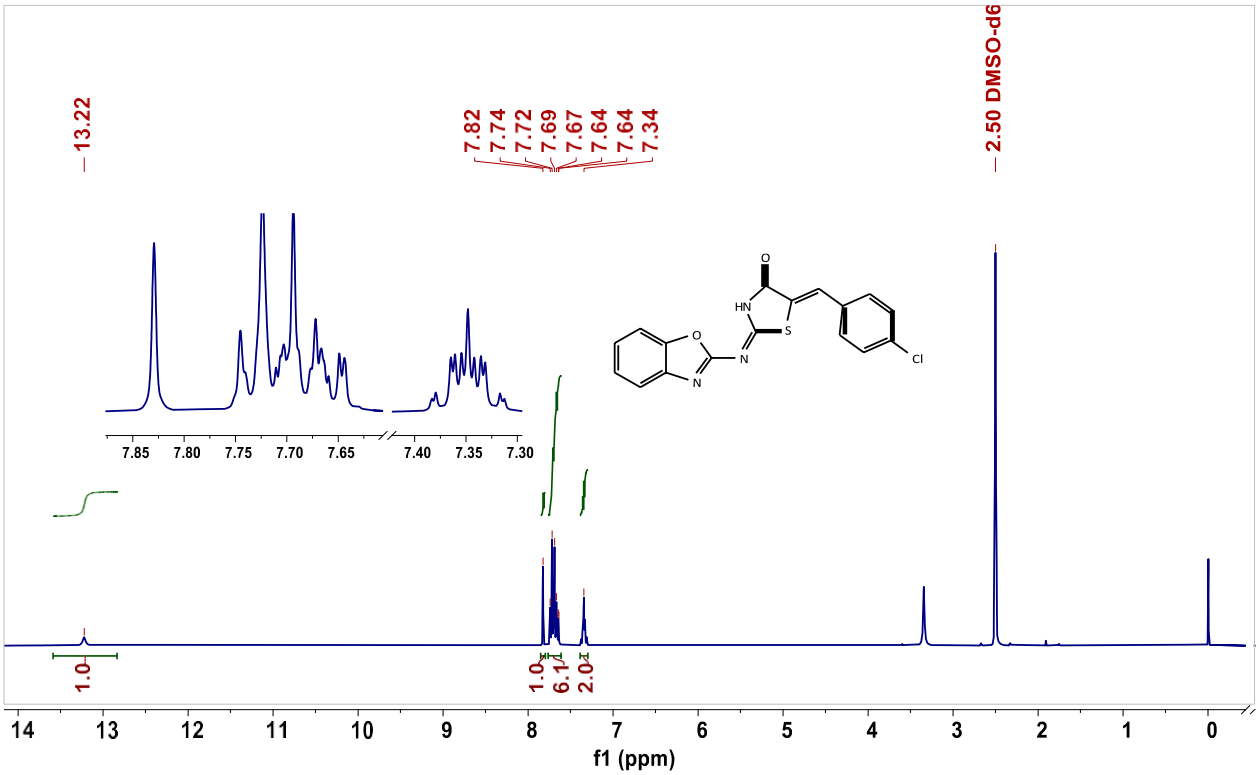

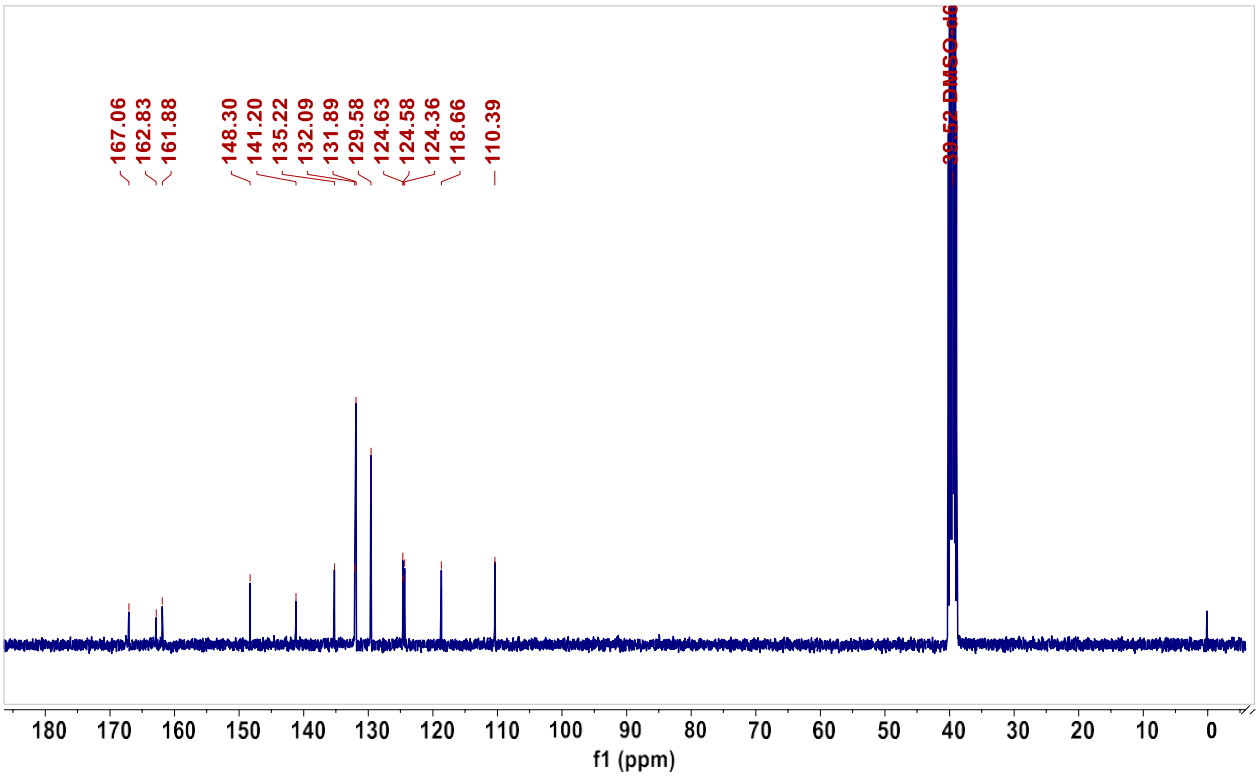

[1]H-NMR spectra of BT6

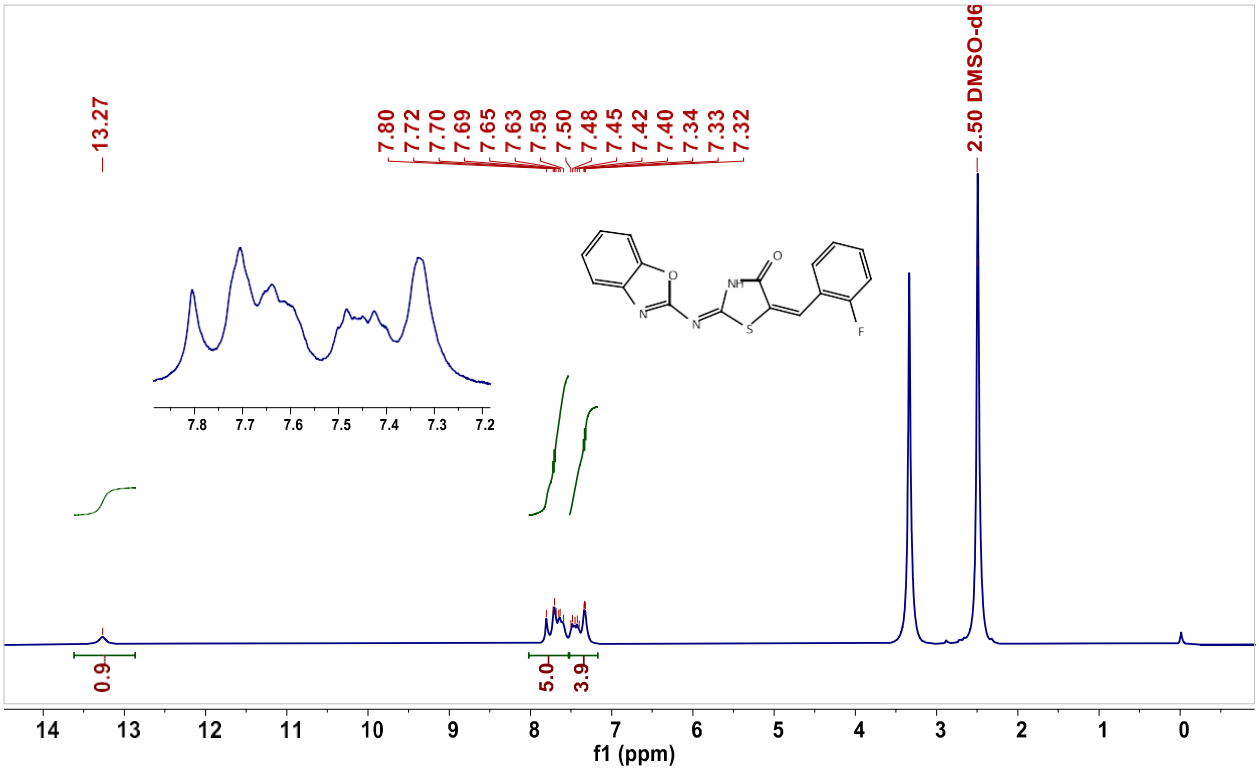

$^{1}H/^{13}C$-NMR spectra of BT

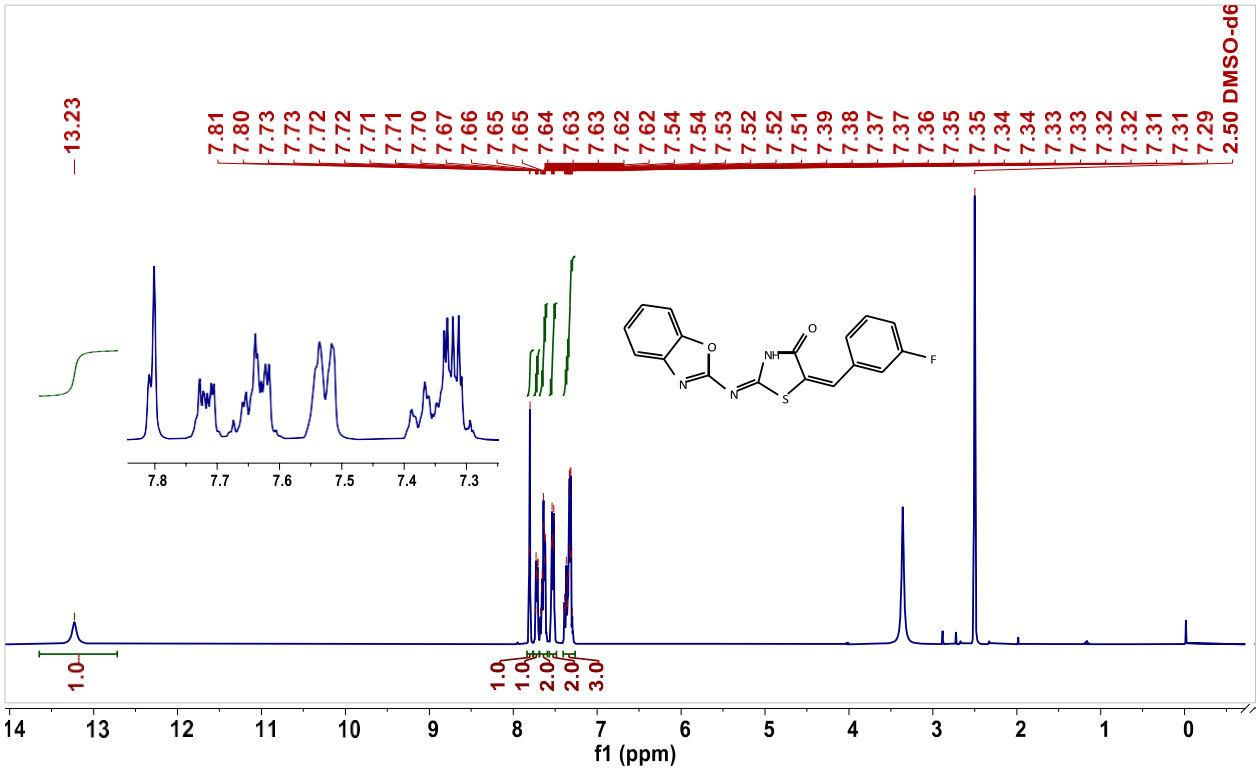

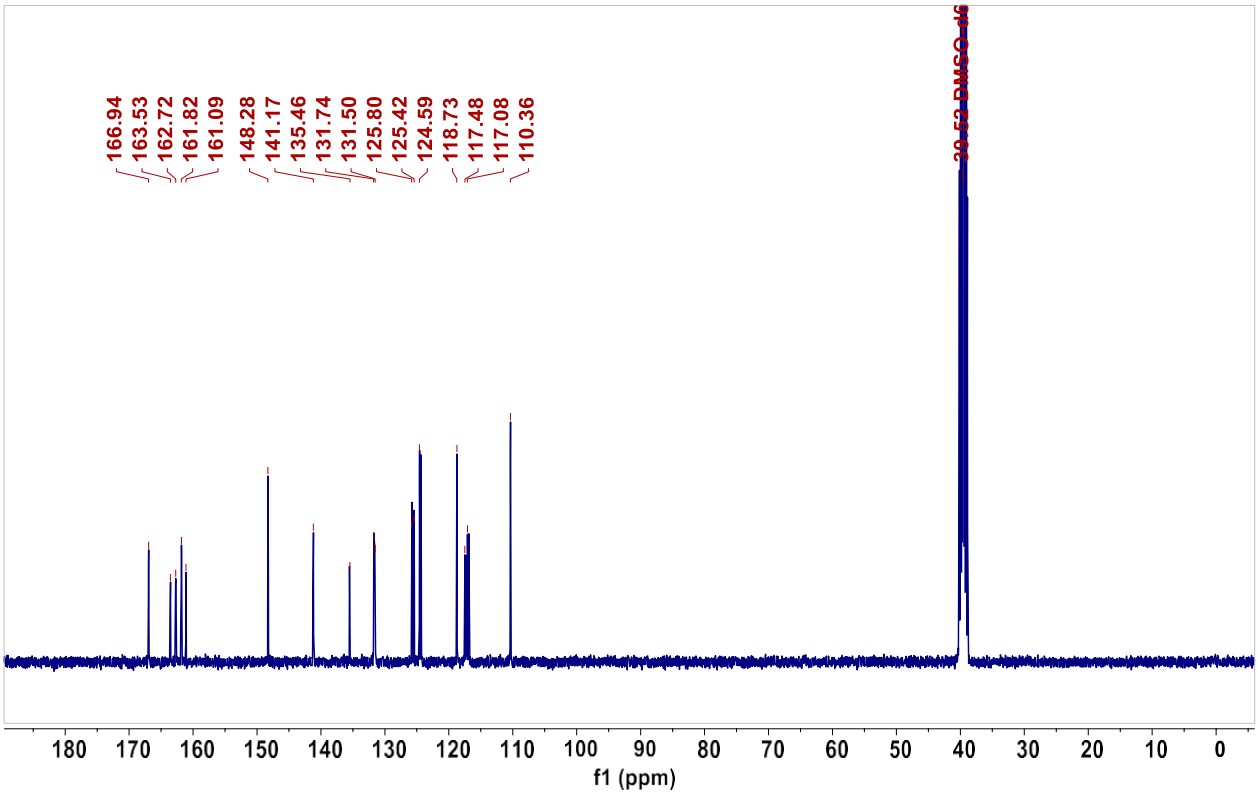

$^{1}H/^{13}C$-NMR spectra of BT

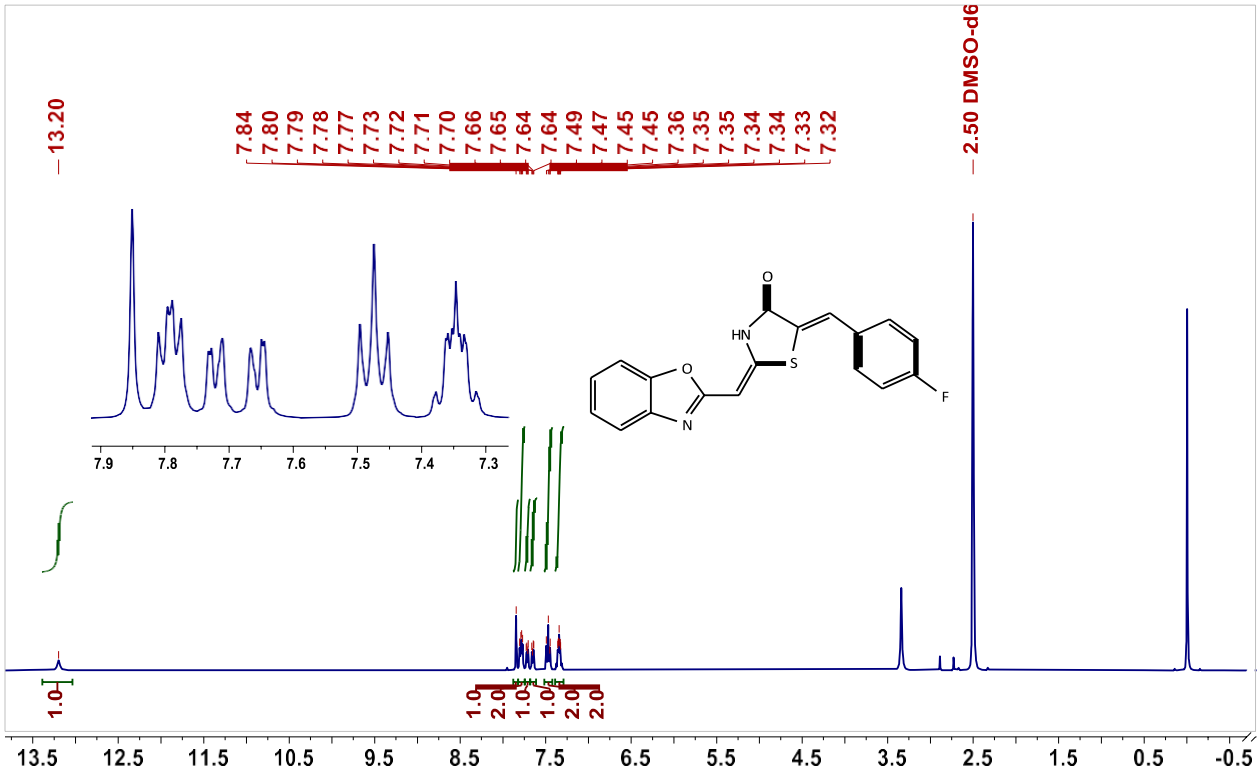

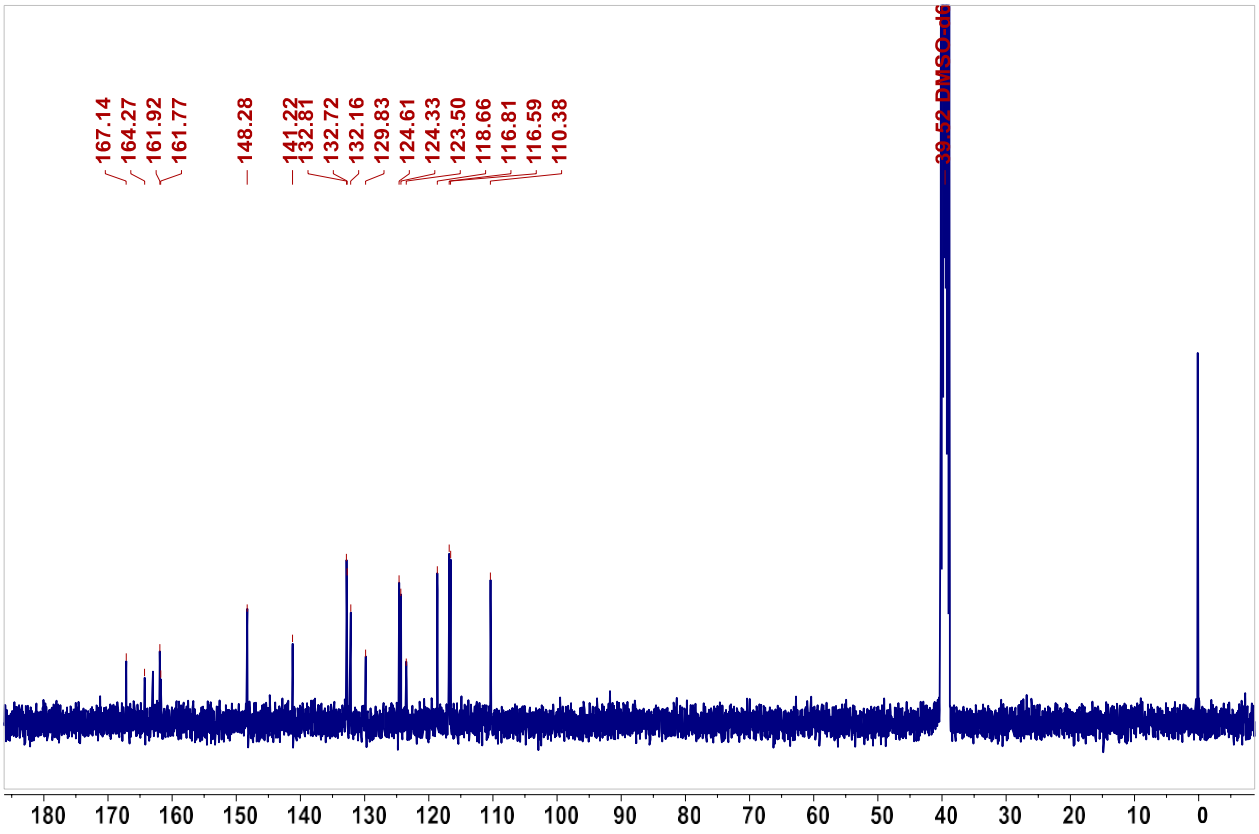

$^{1}H/^{13}C$-NMR spectra of BT

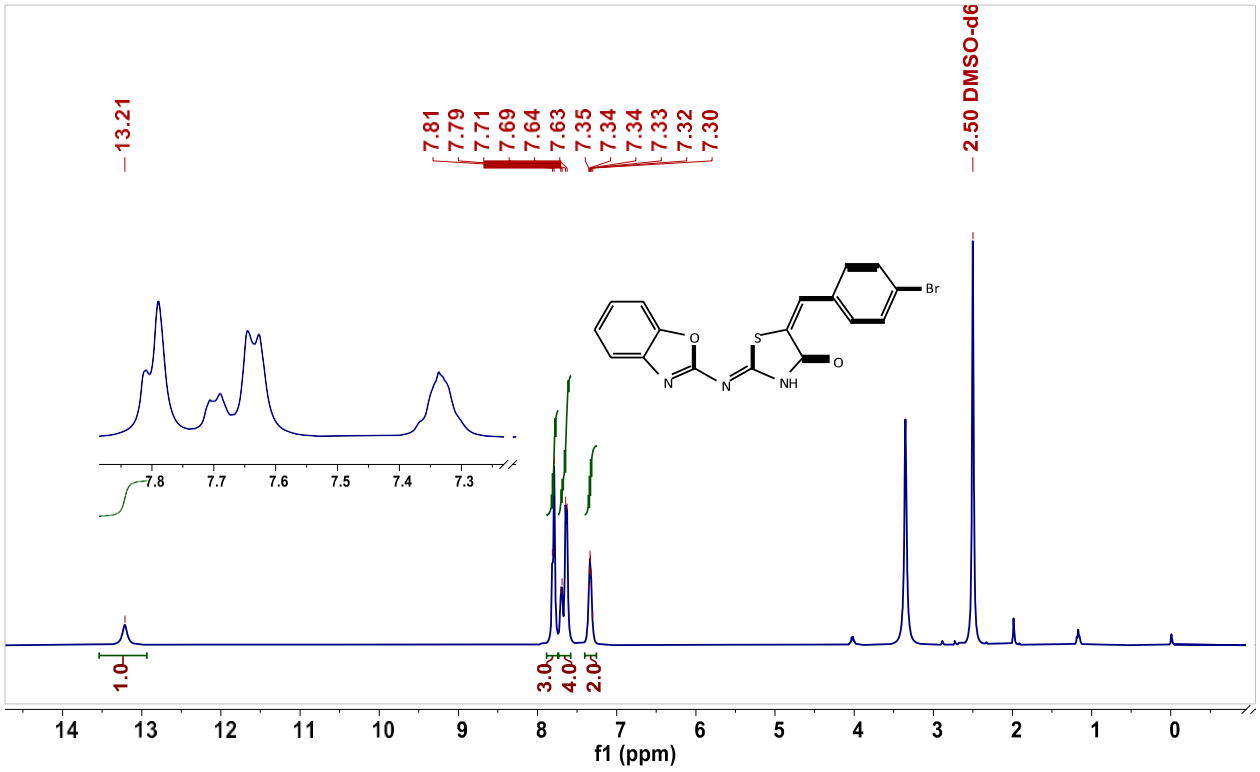

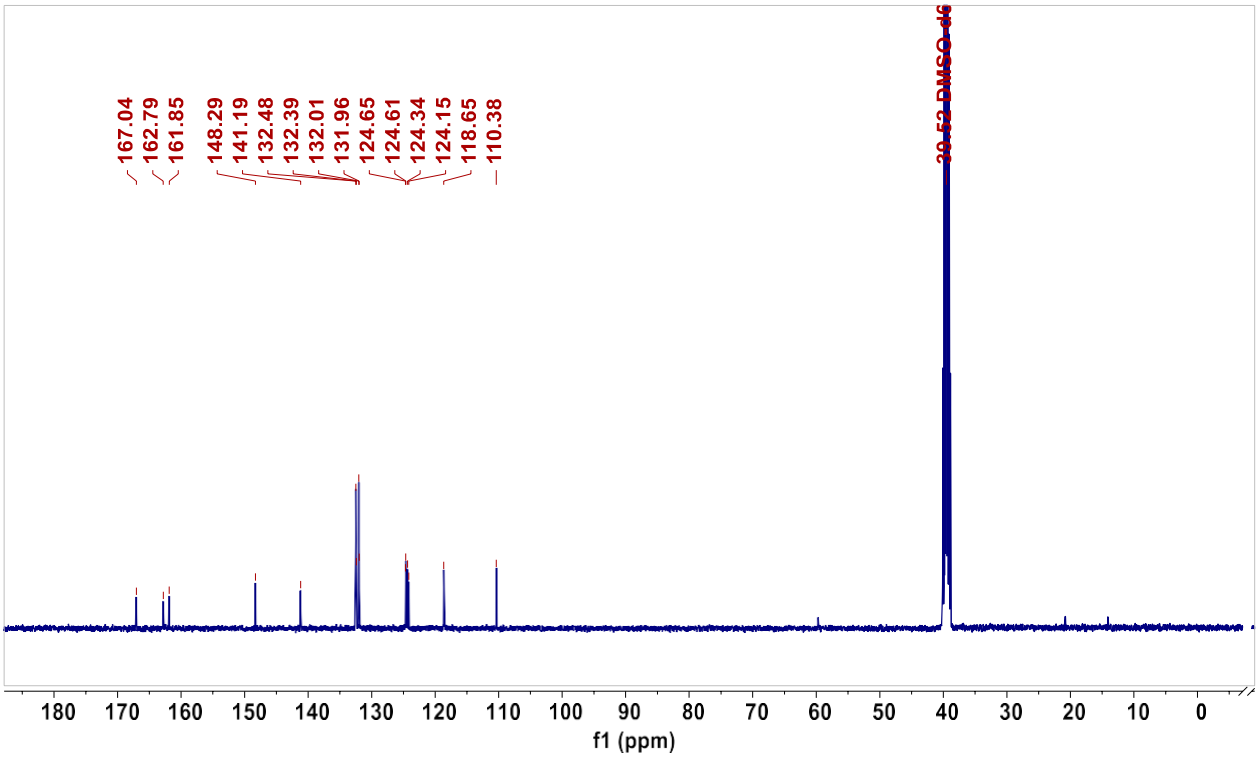

$^{1}H/^{13}C$-NMR spectra of BT16

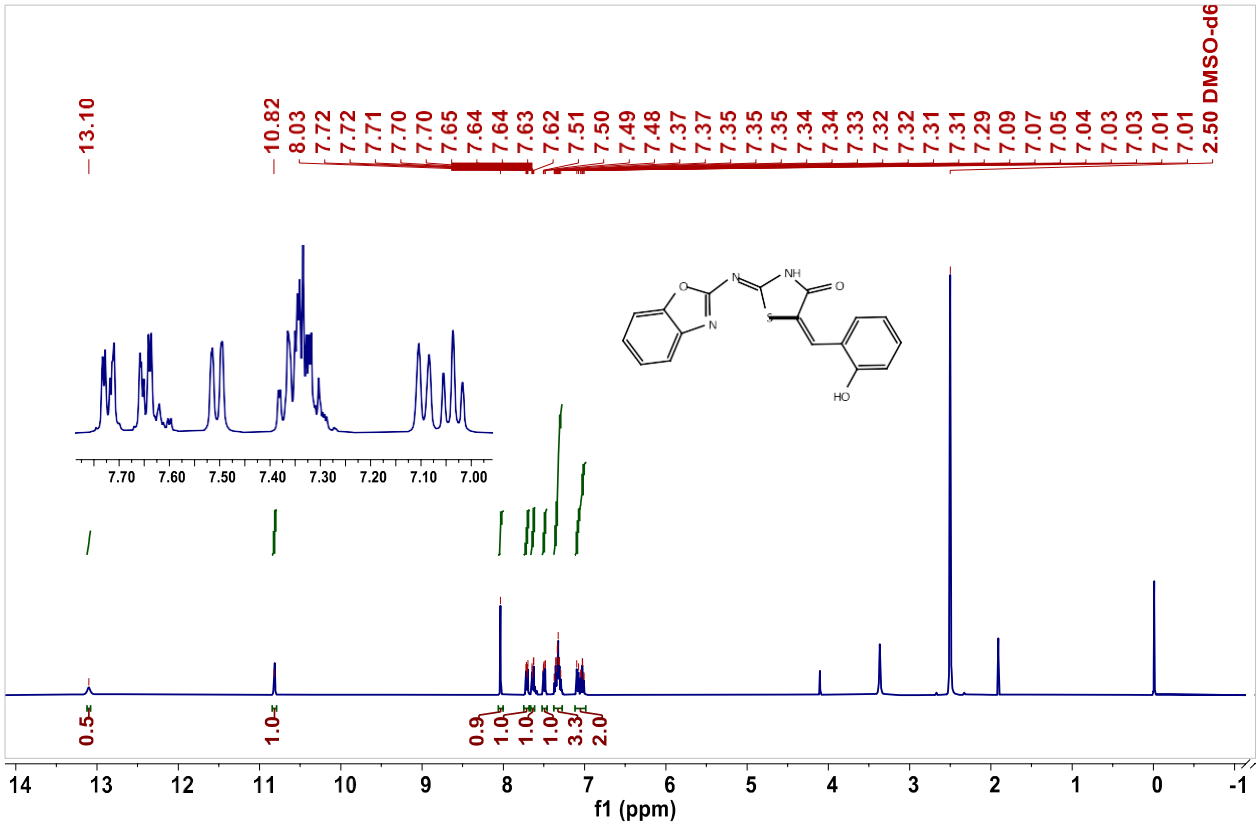

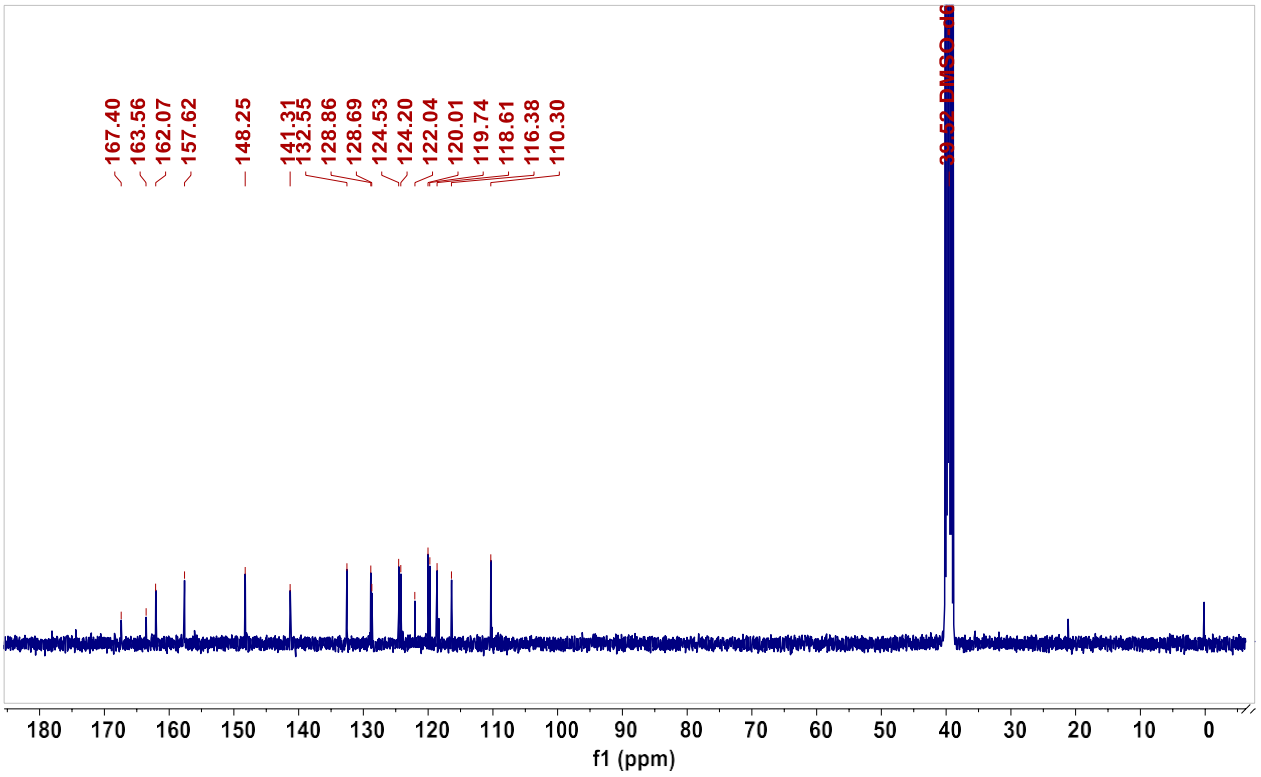

$^{1}H/^{13}C$-NMR spectra of BT17

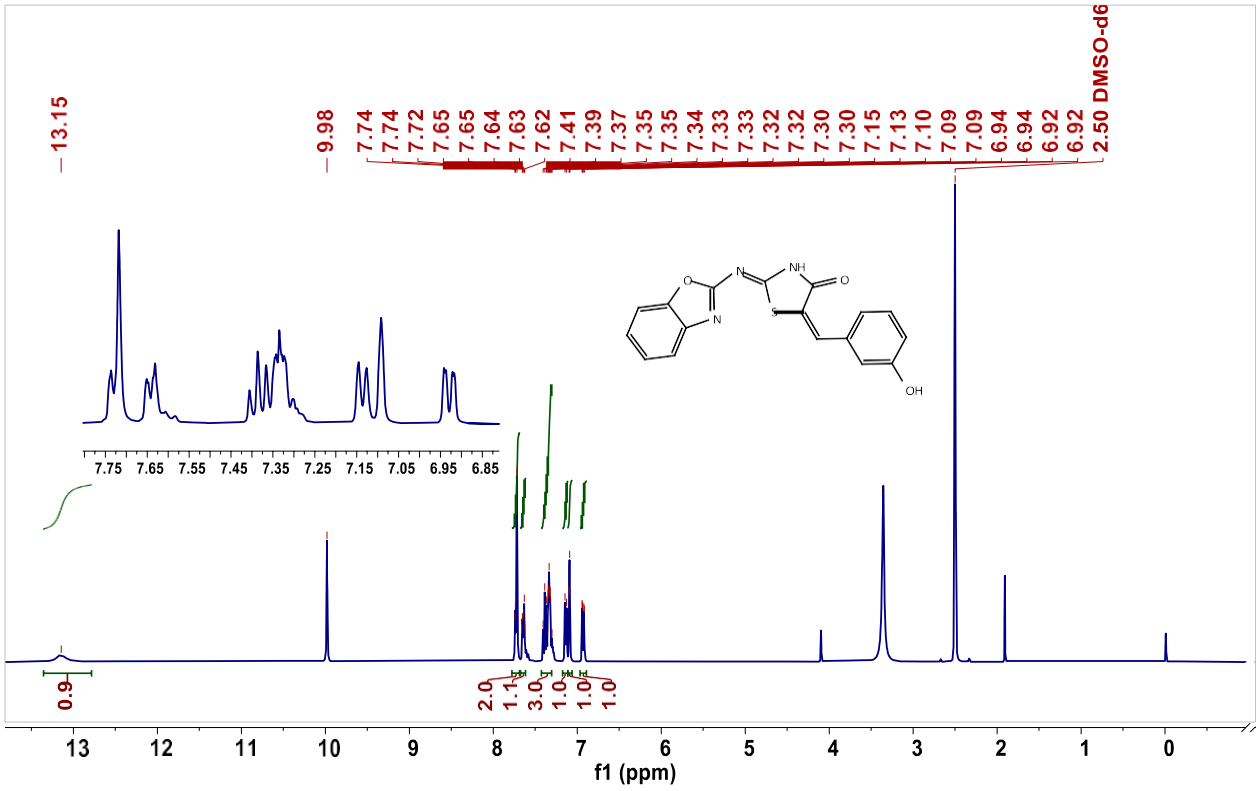

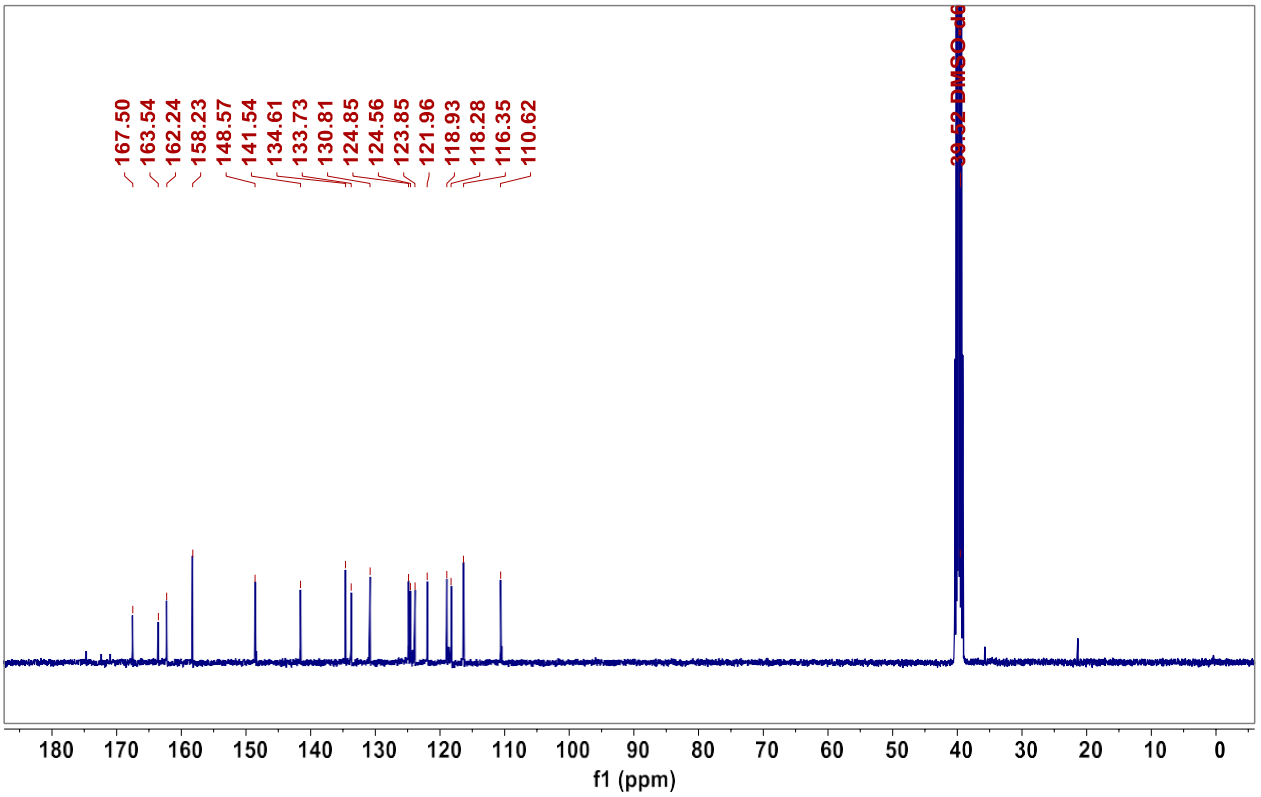

$^{1}H/^{13}C$-NMR spectra of BT18

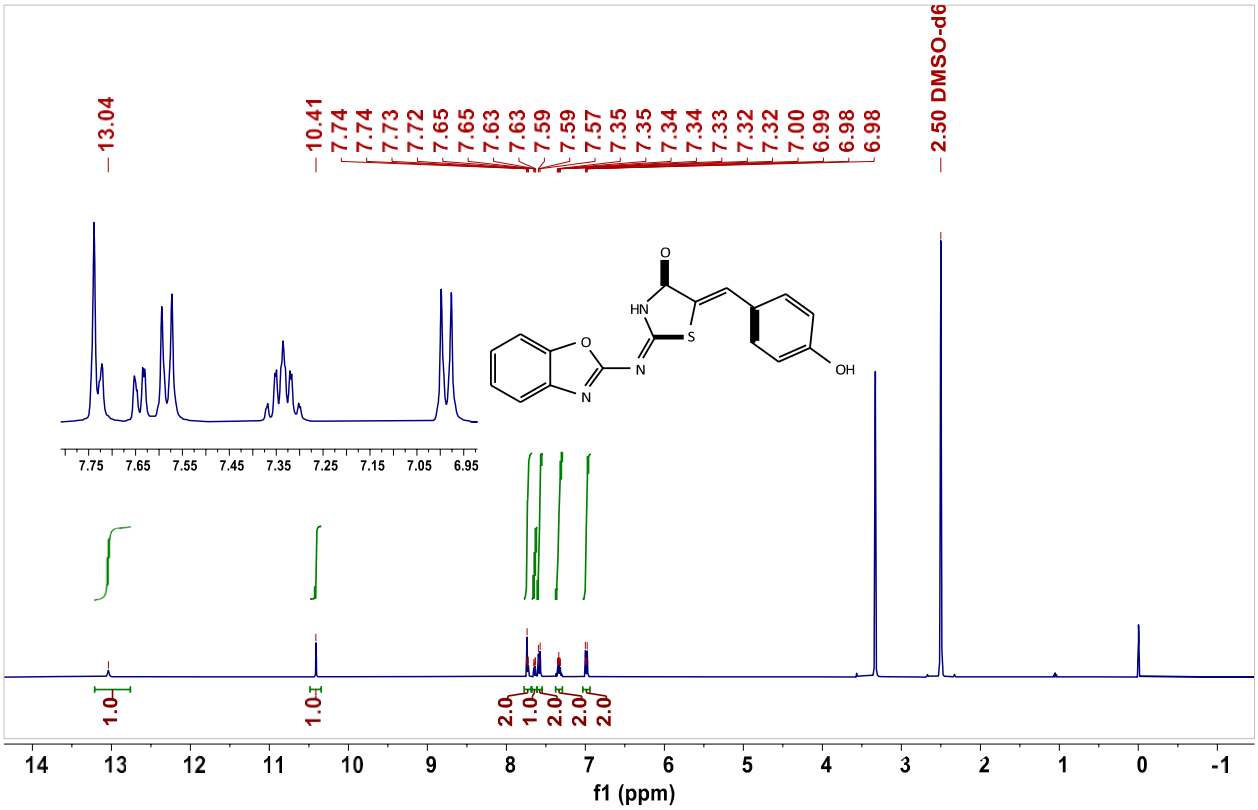

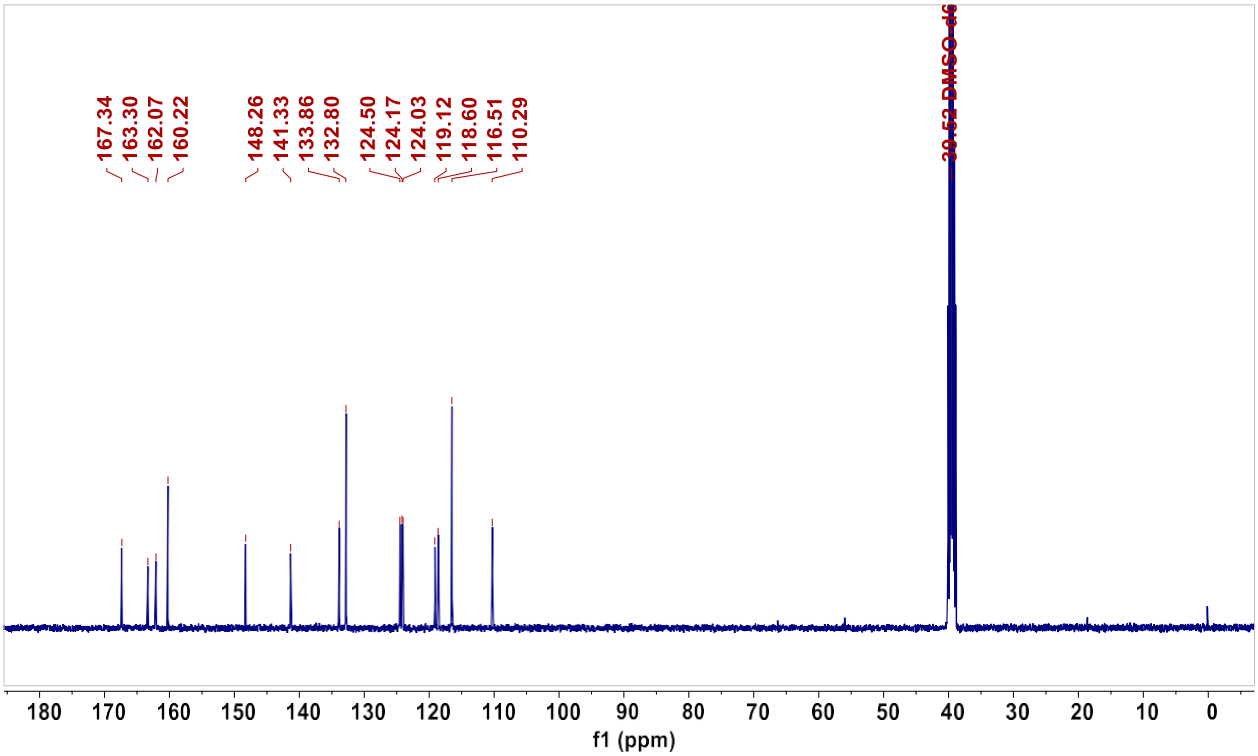

$^{1}H/^{13}C$-NMR spectra of BT19

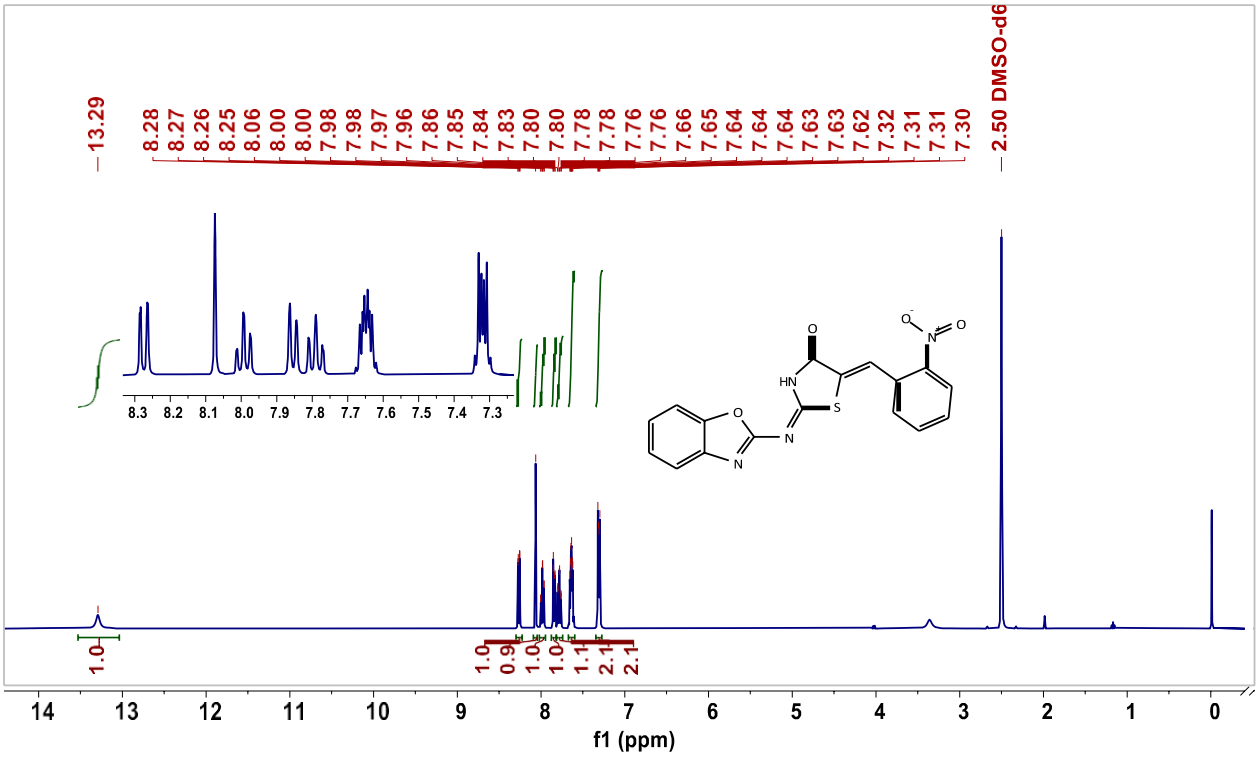

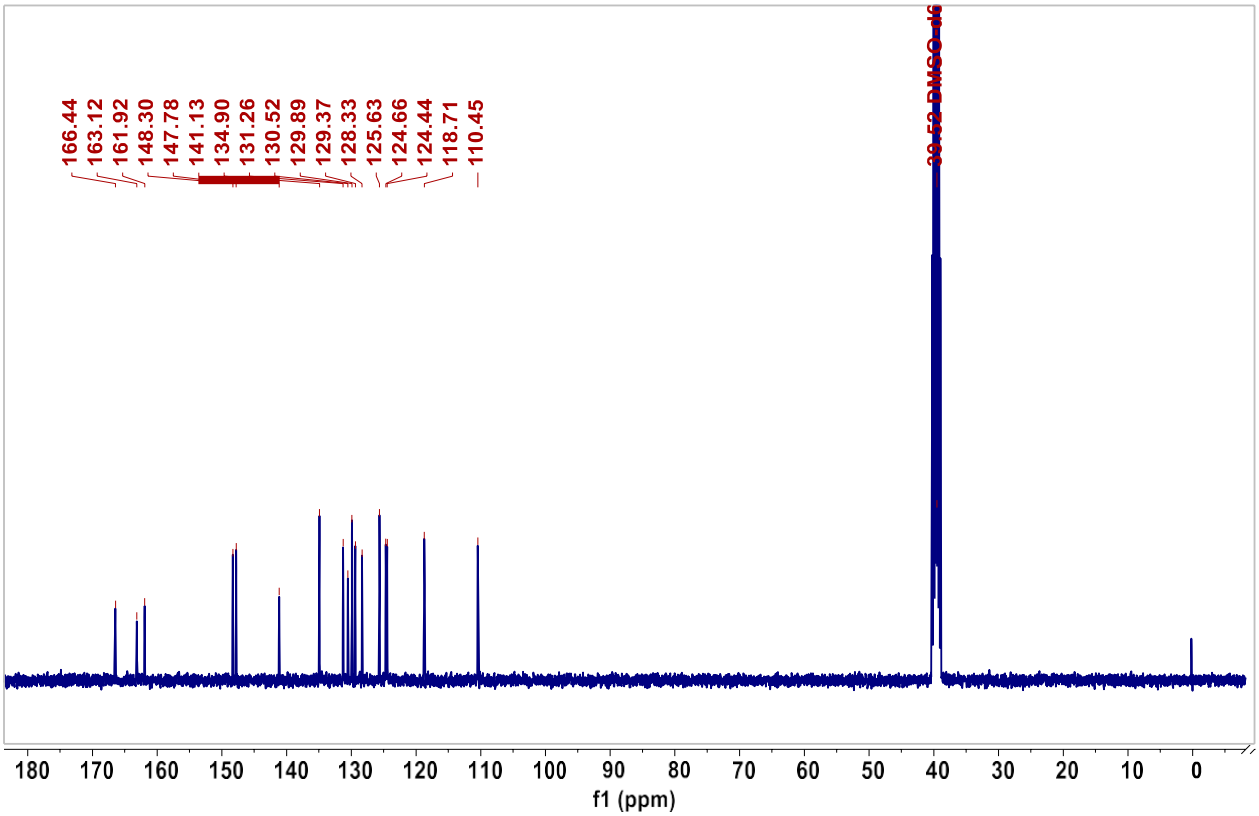

$^{1}H/^{13}C$-NMR spectra of BT20

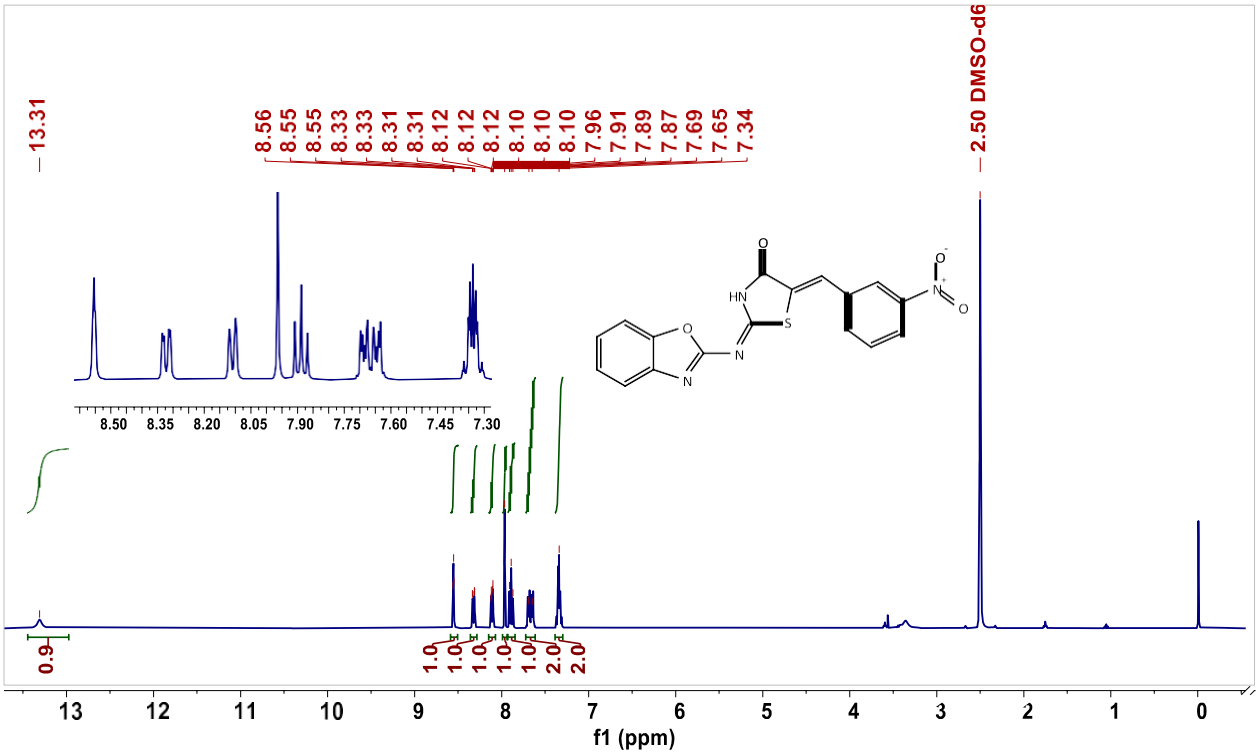

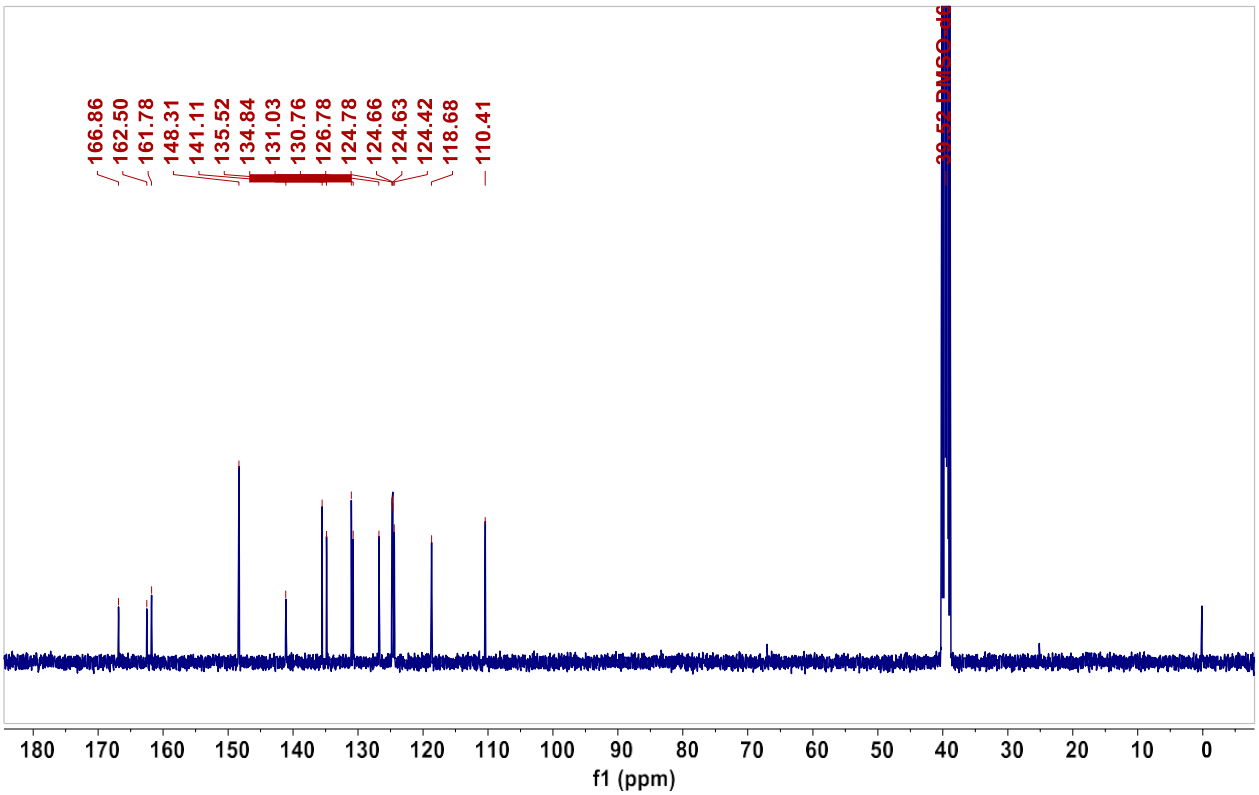

[1]H-NMR spectra of BT15

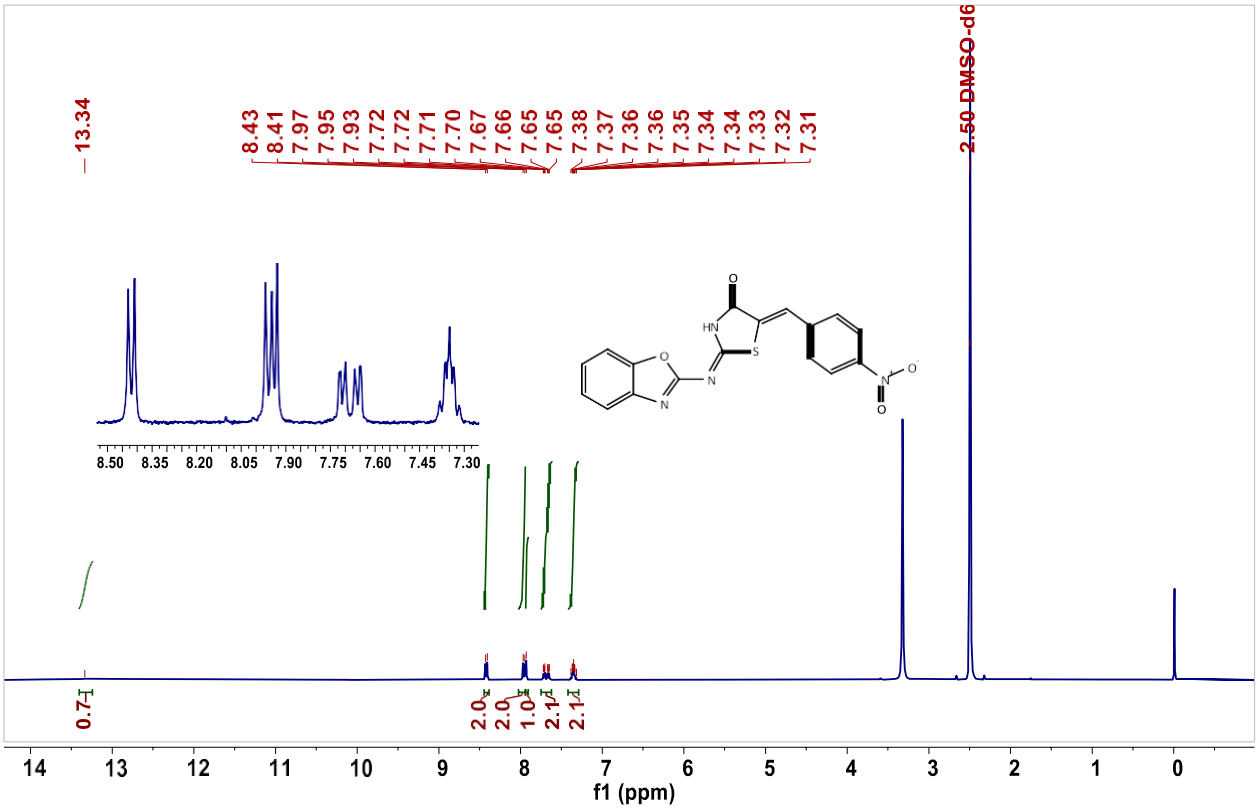

$^{1}H/^{13}C$-NMR spectra of BT2

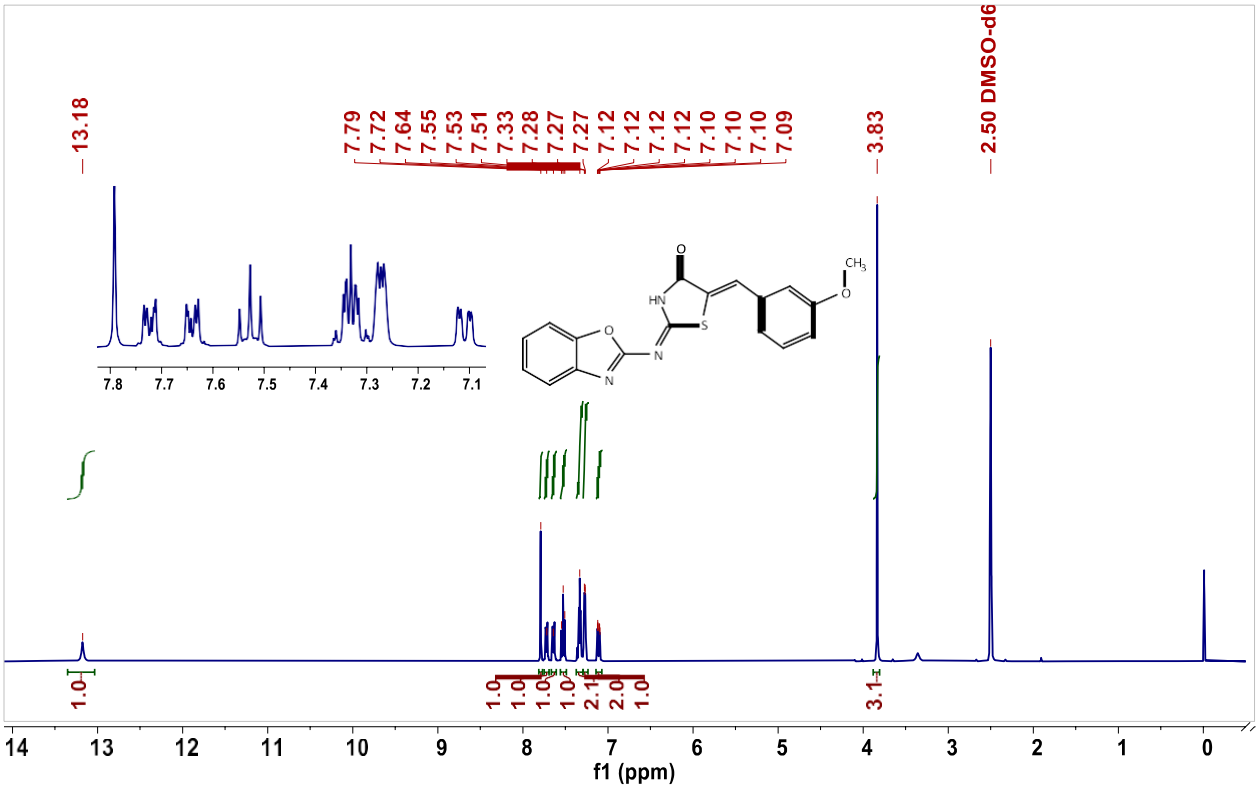

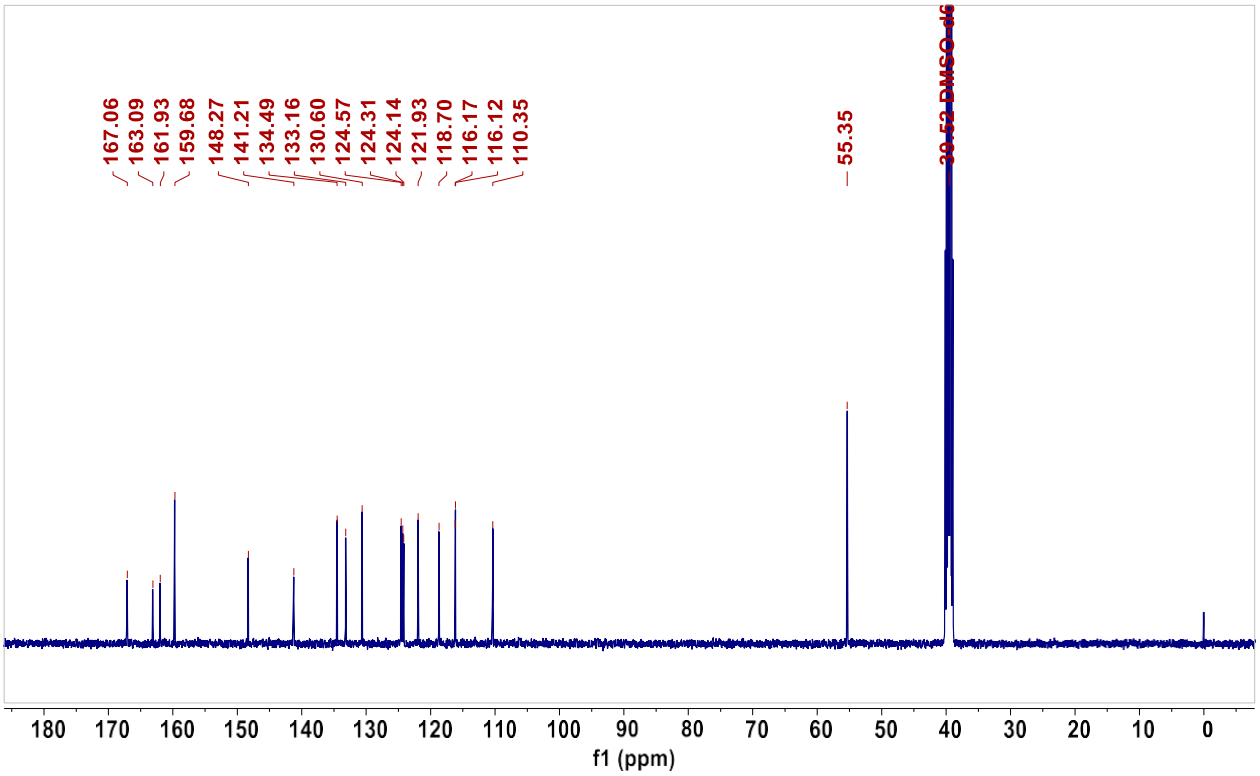

$^{1}H/^{13}C$-NMR spectra of BT3

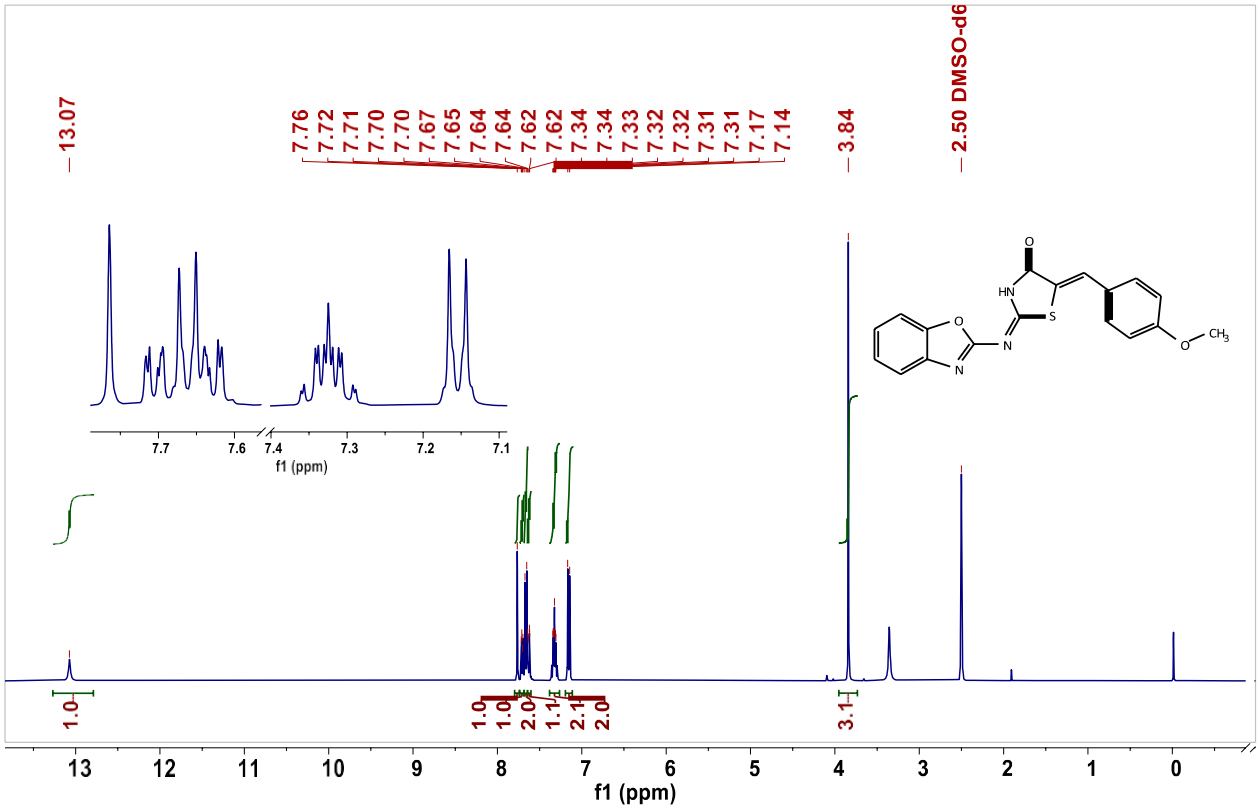

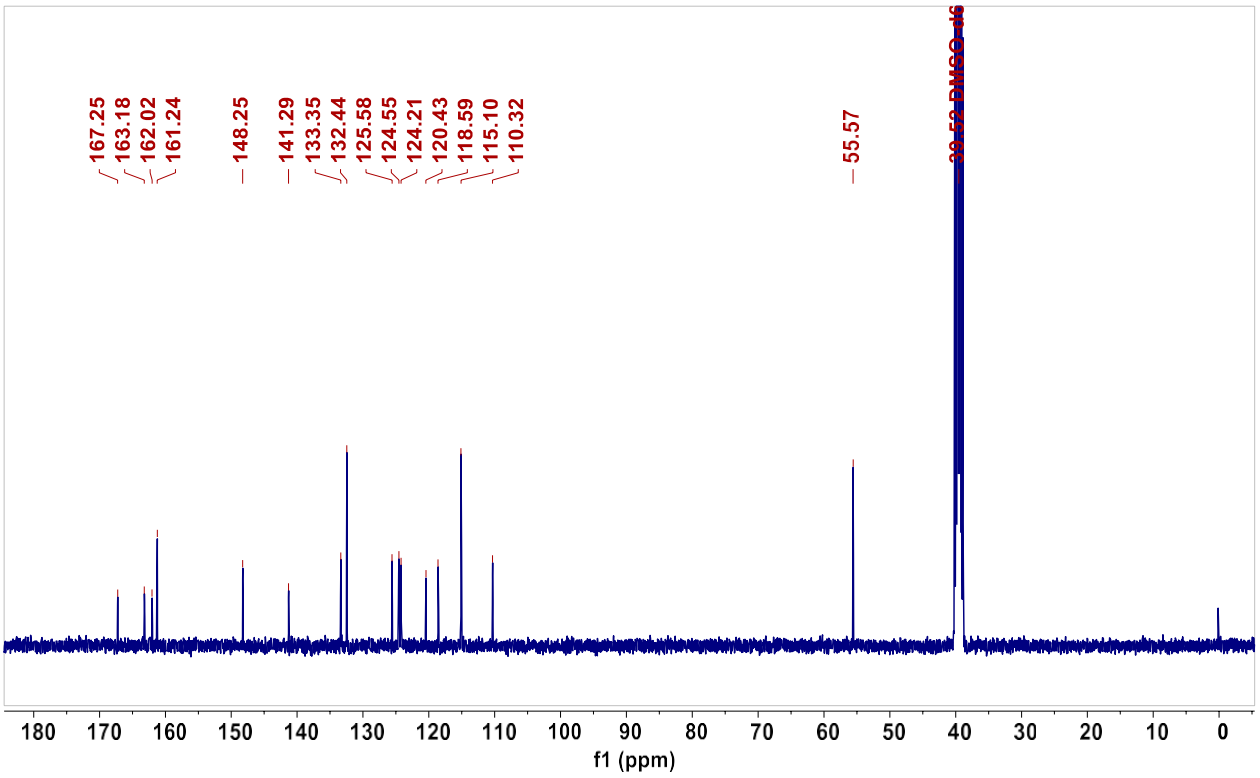

$^{1}H/^{13}C$-NMR spectra of BT4

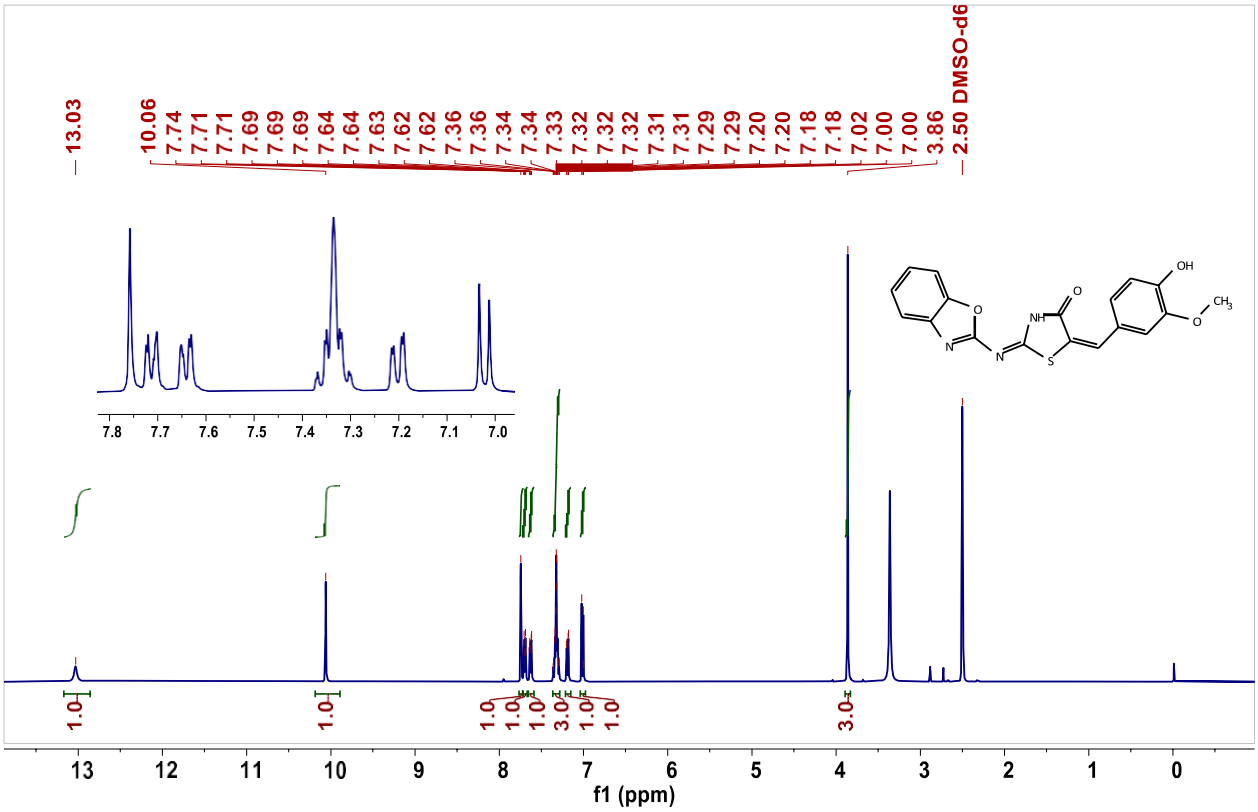

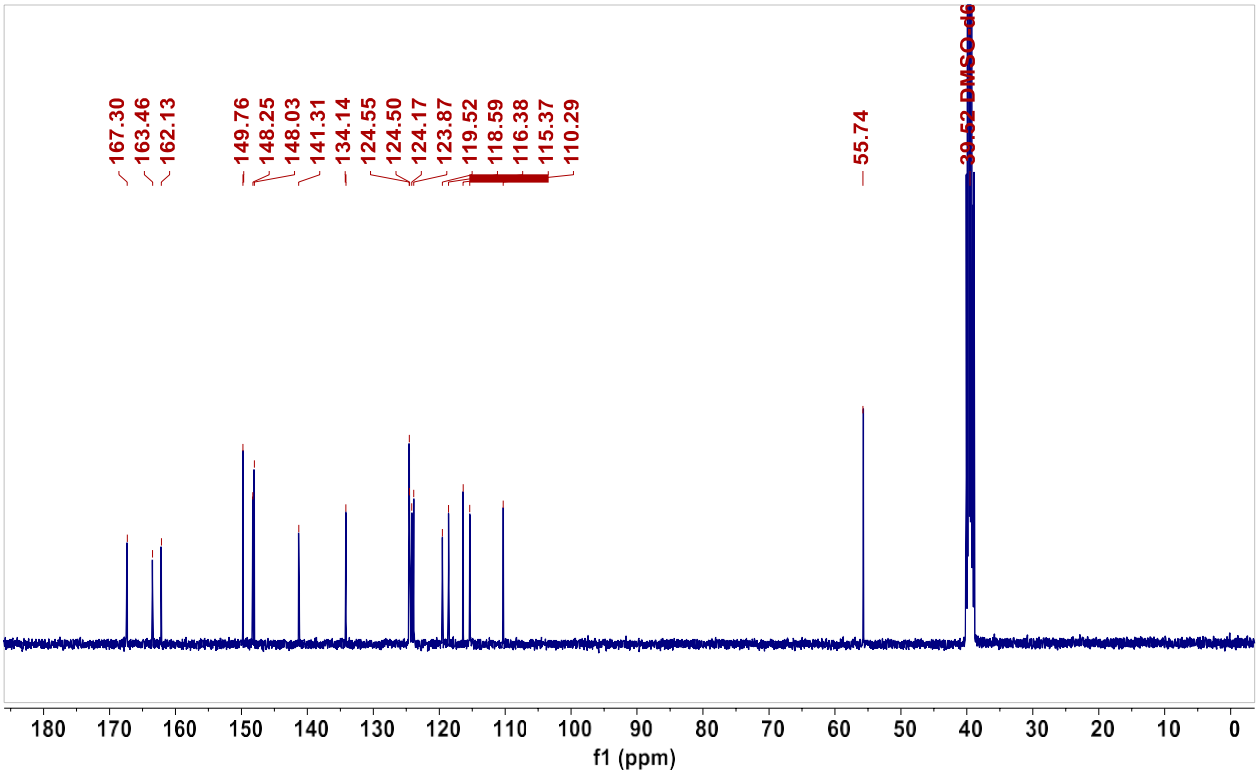

$^{1}H/^{13}C$-NMR spectra of BT5

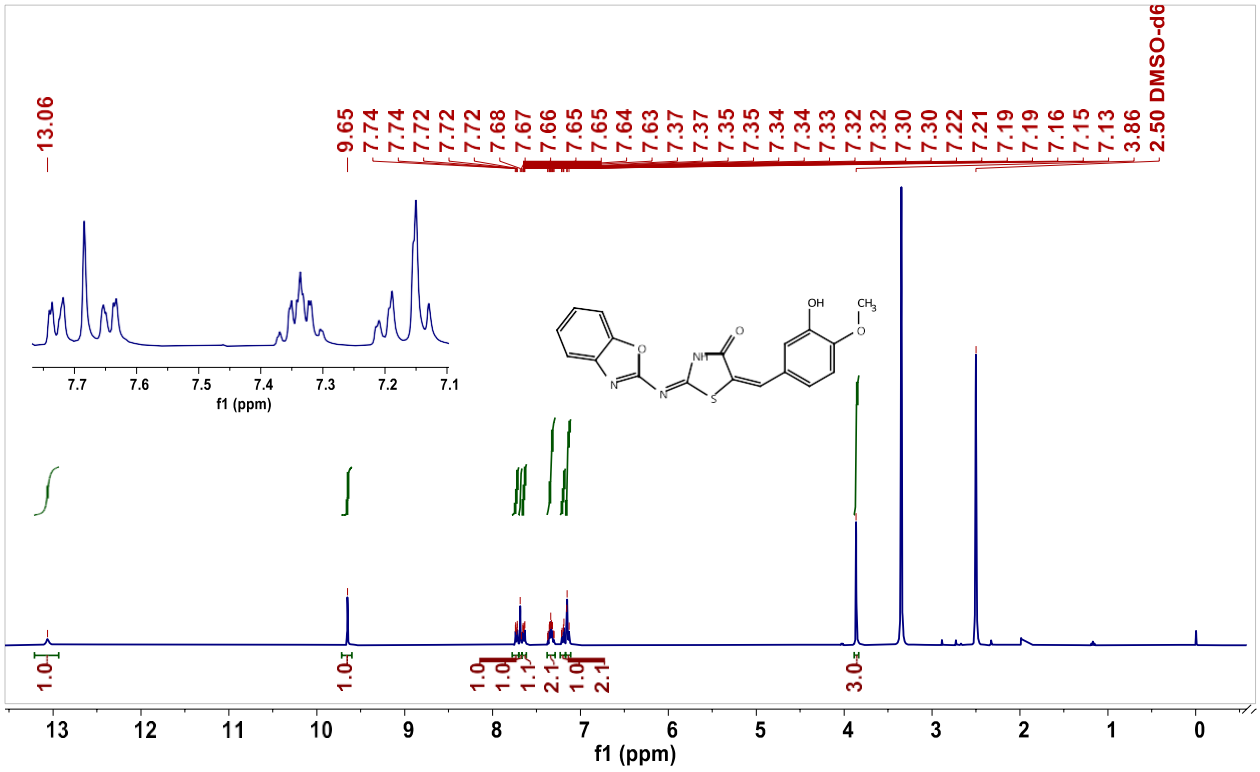

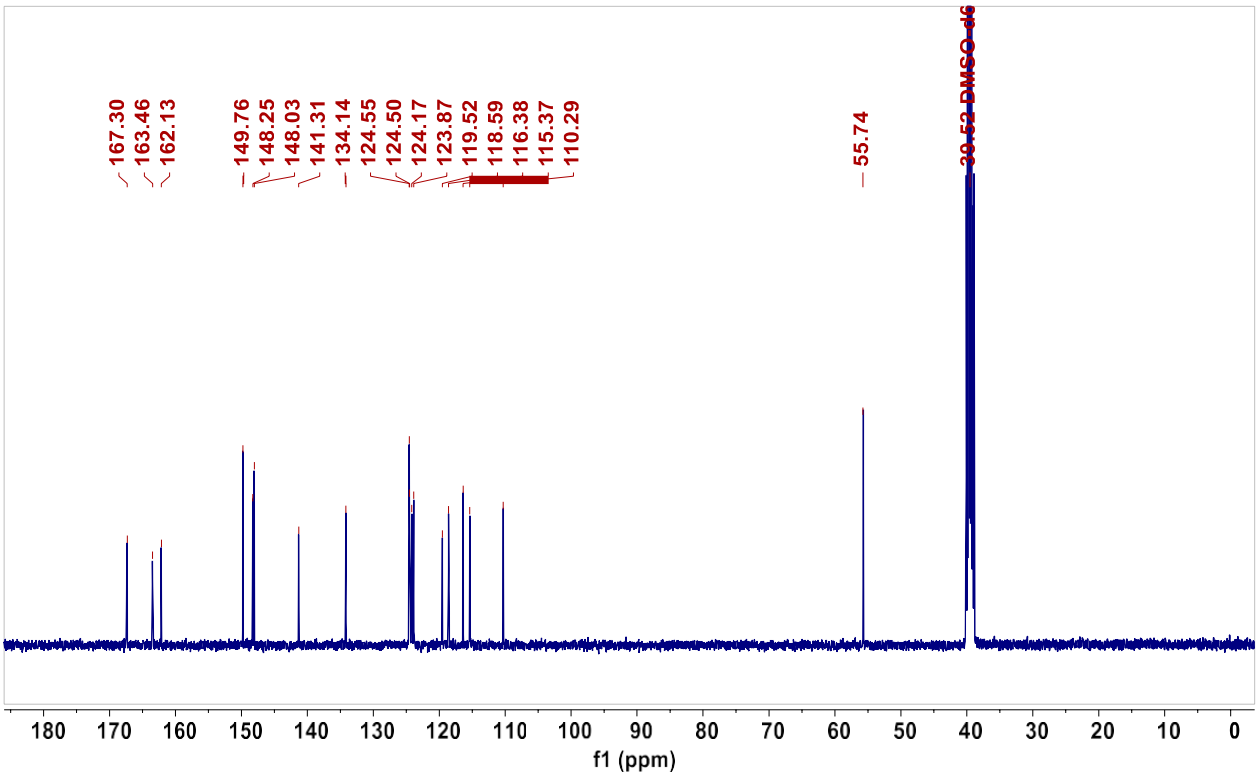

^{13}C-NMR spectra of BT20

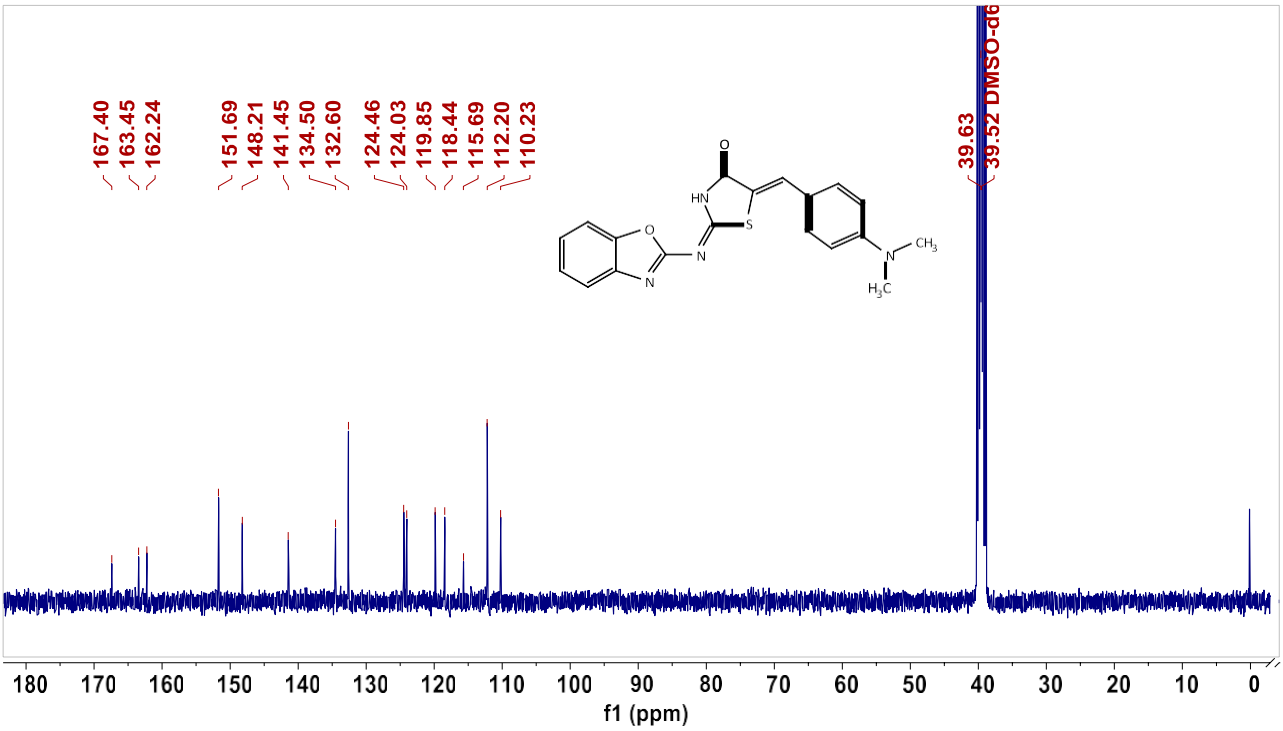

$^{1}H/^{13}C$-NMR spectra of BT7

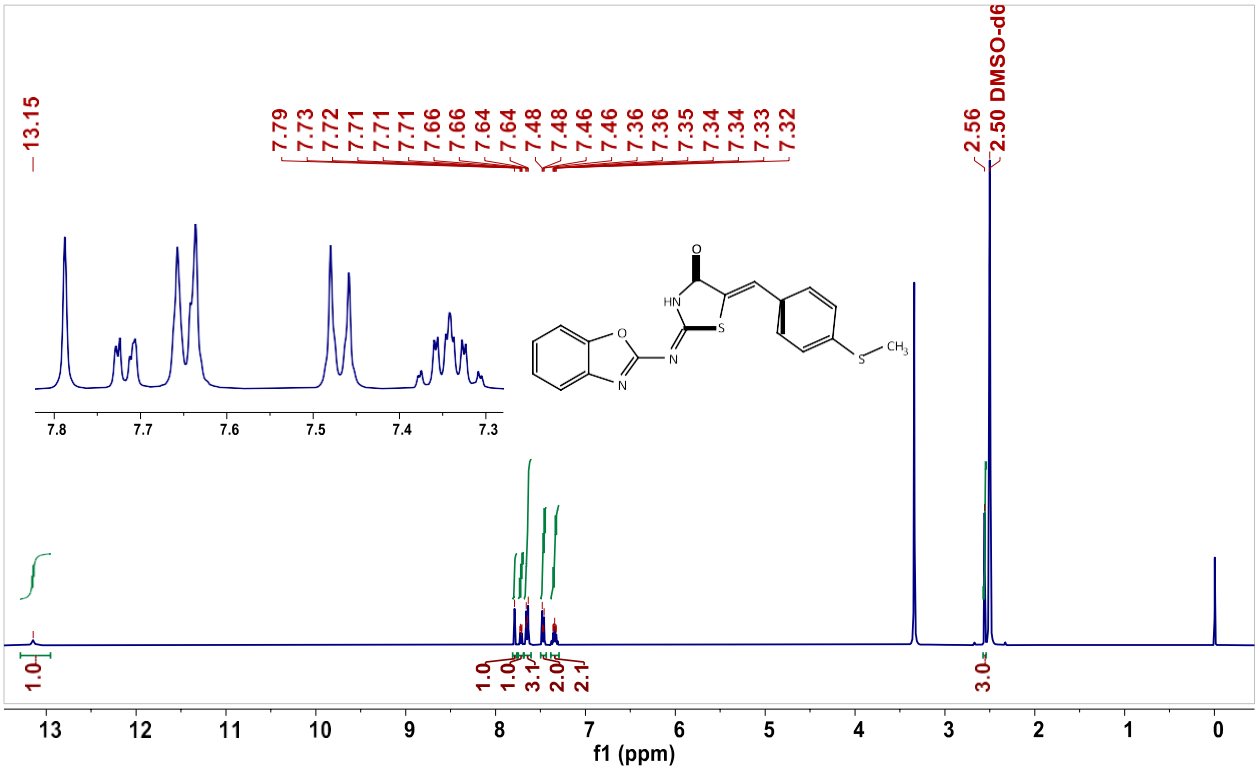

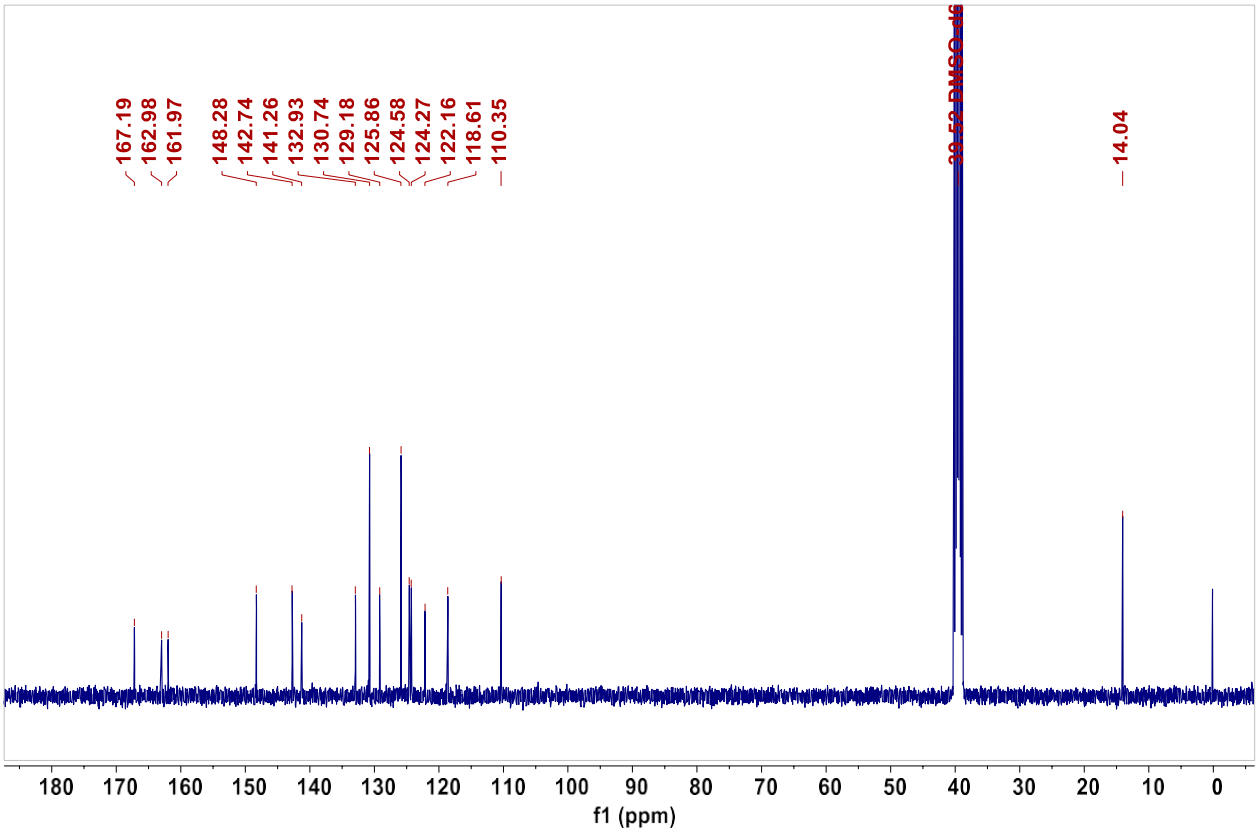

$^{1}H/^{13}C$-NMR spectra of BT8

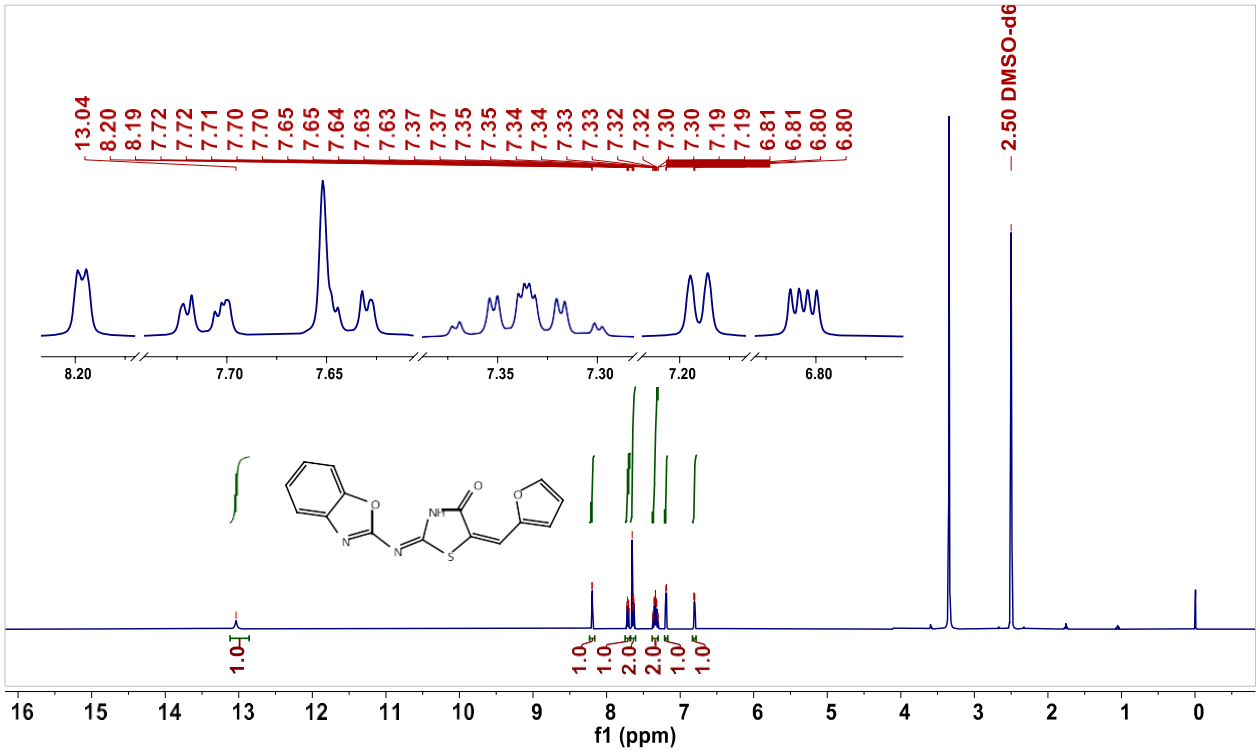

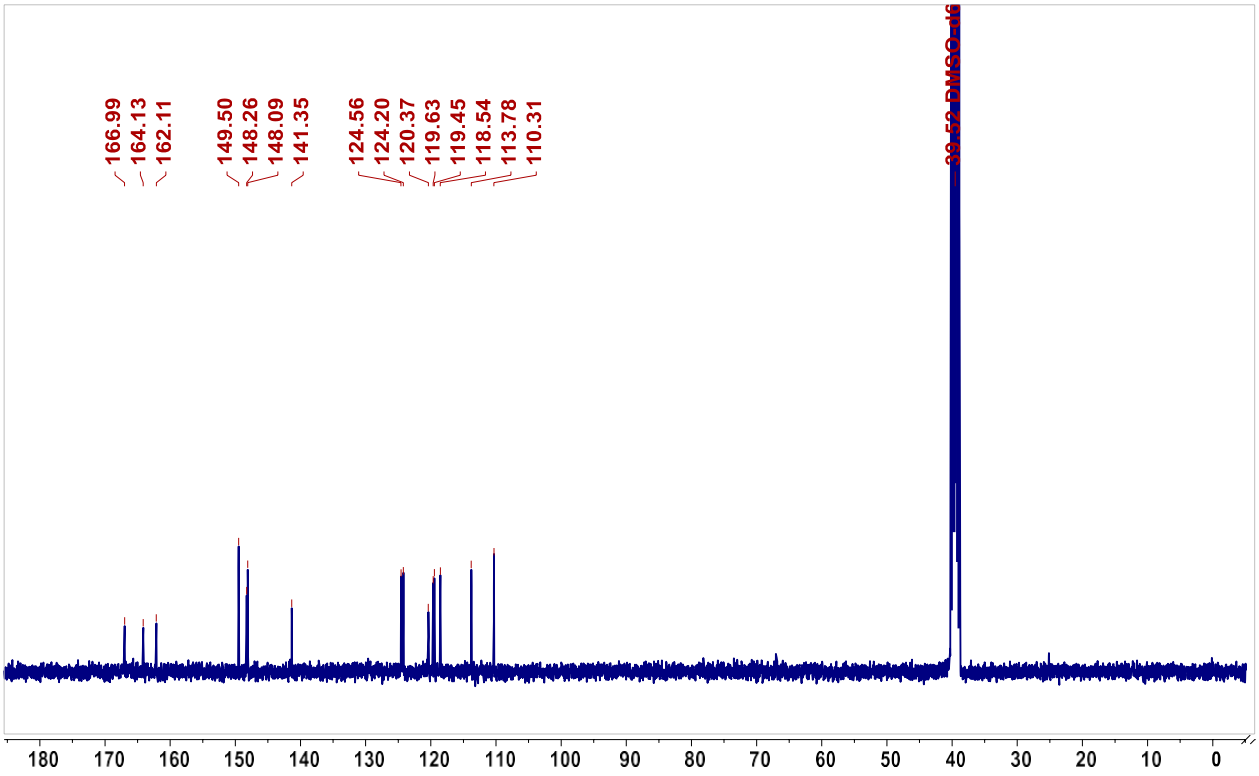

$^{1}H/^{13}C$-NMR spectra of BT9

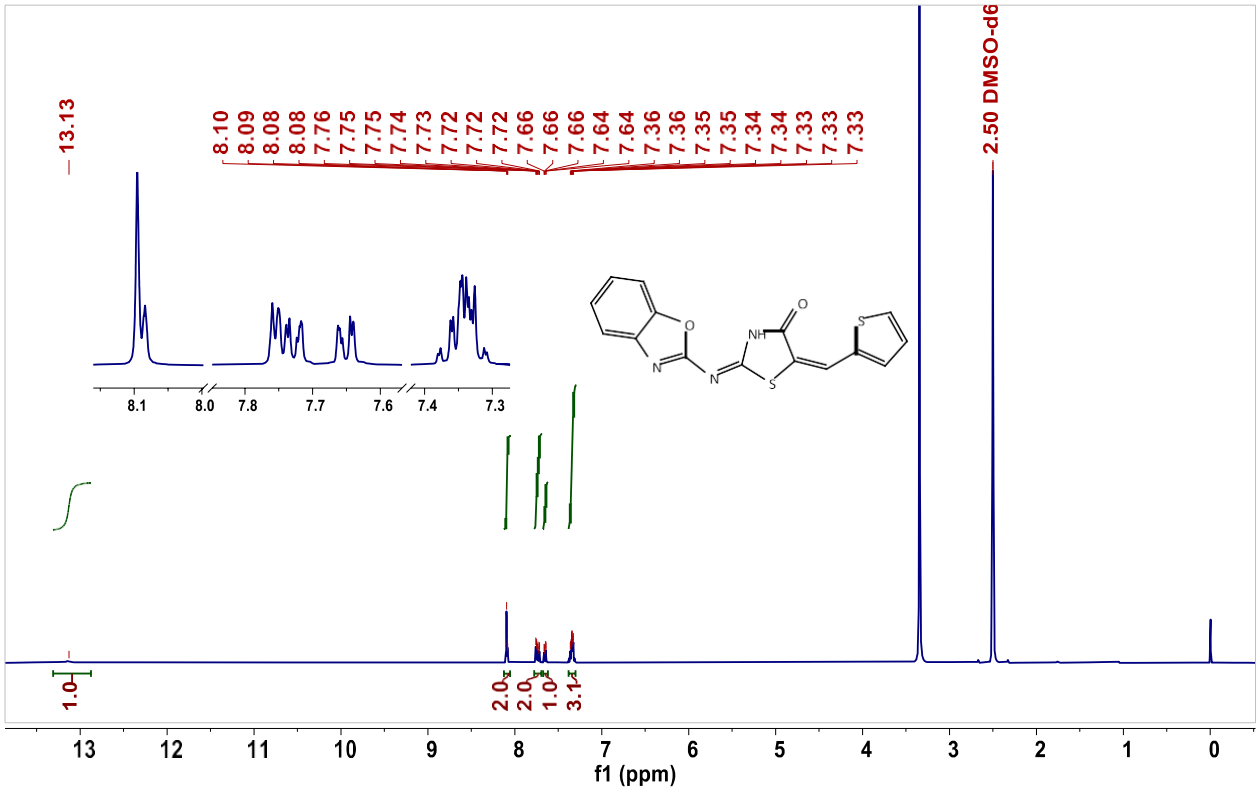

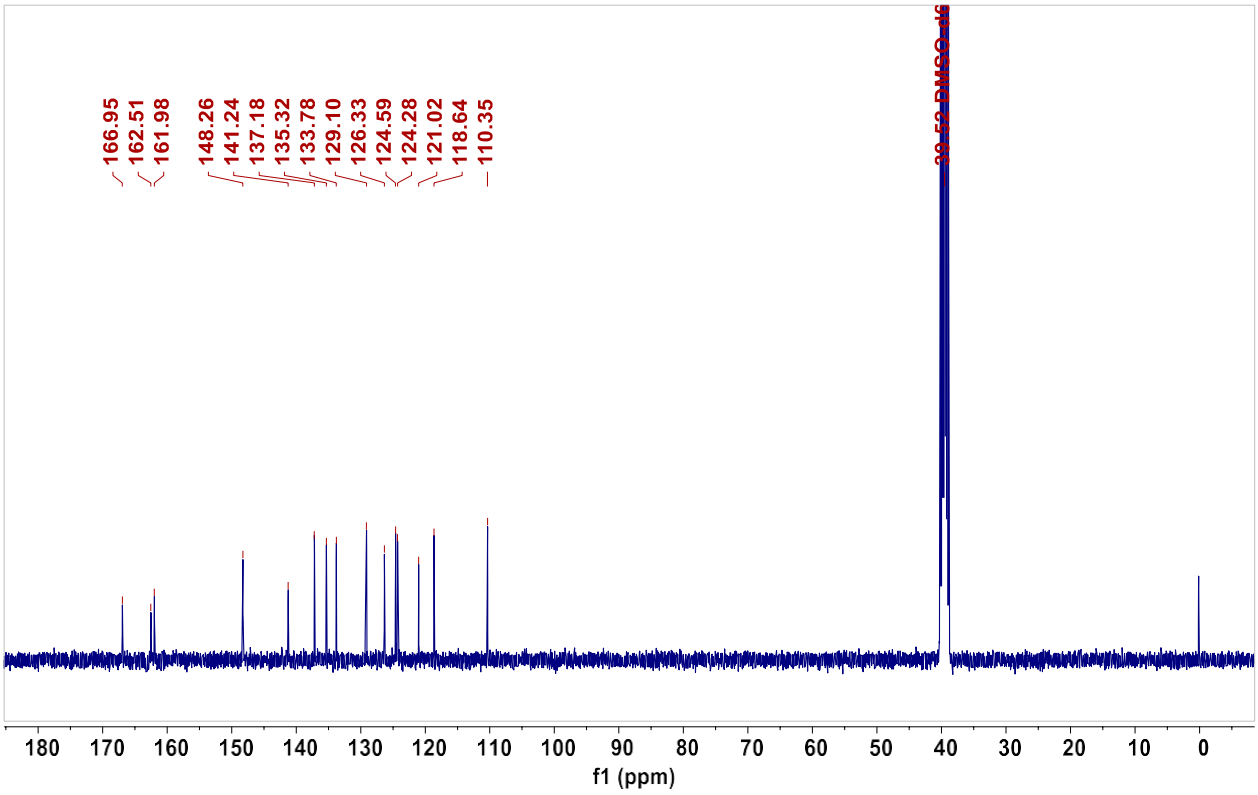

$^{1}H/^{13}C$-NMR spectra of BT10

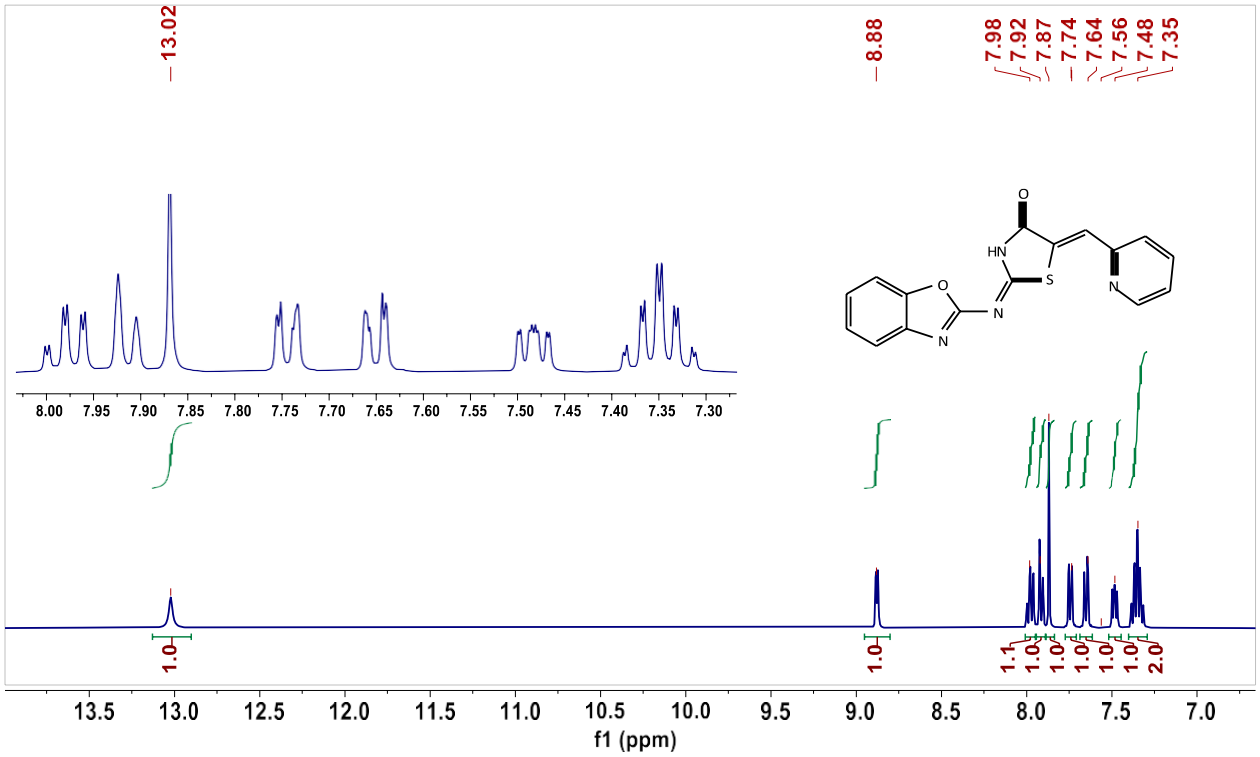

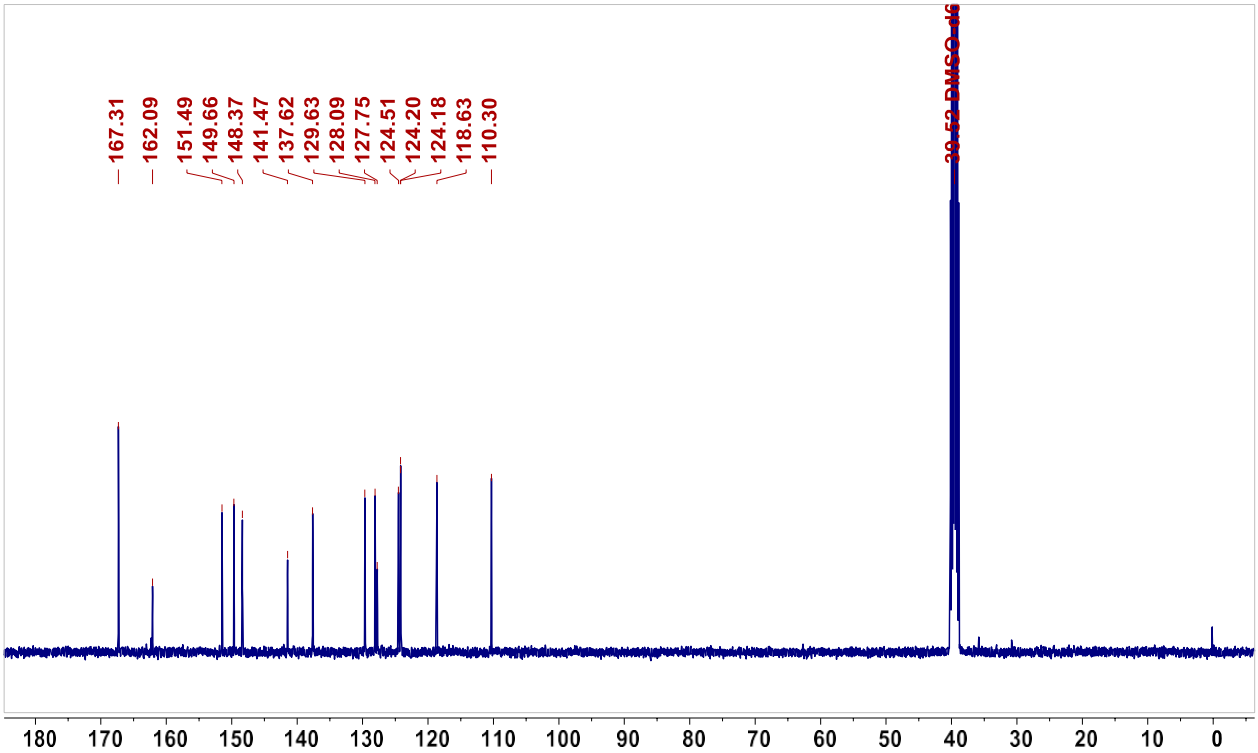

$^{1}H/^{13}C$-NMR spectra of BT11

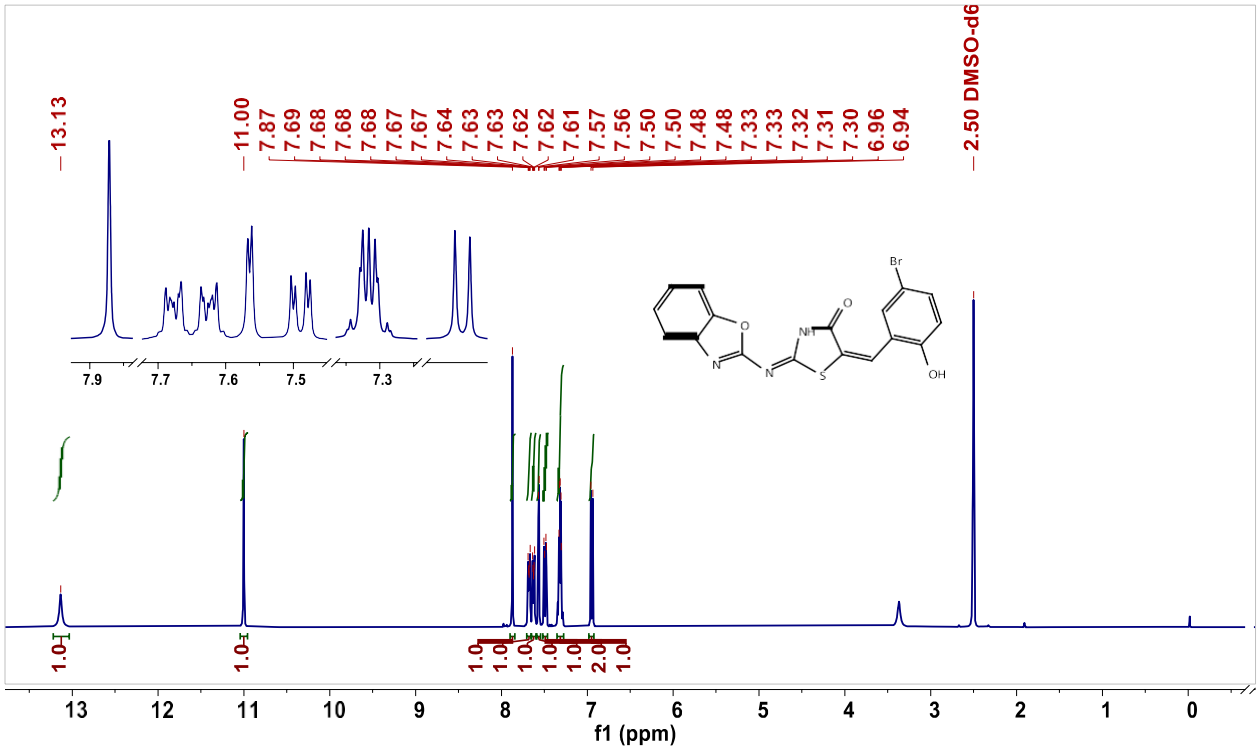

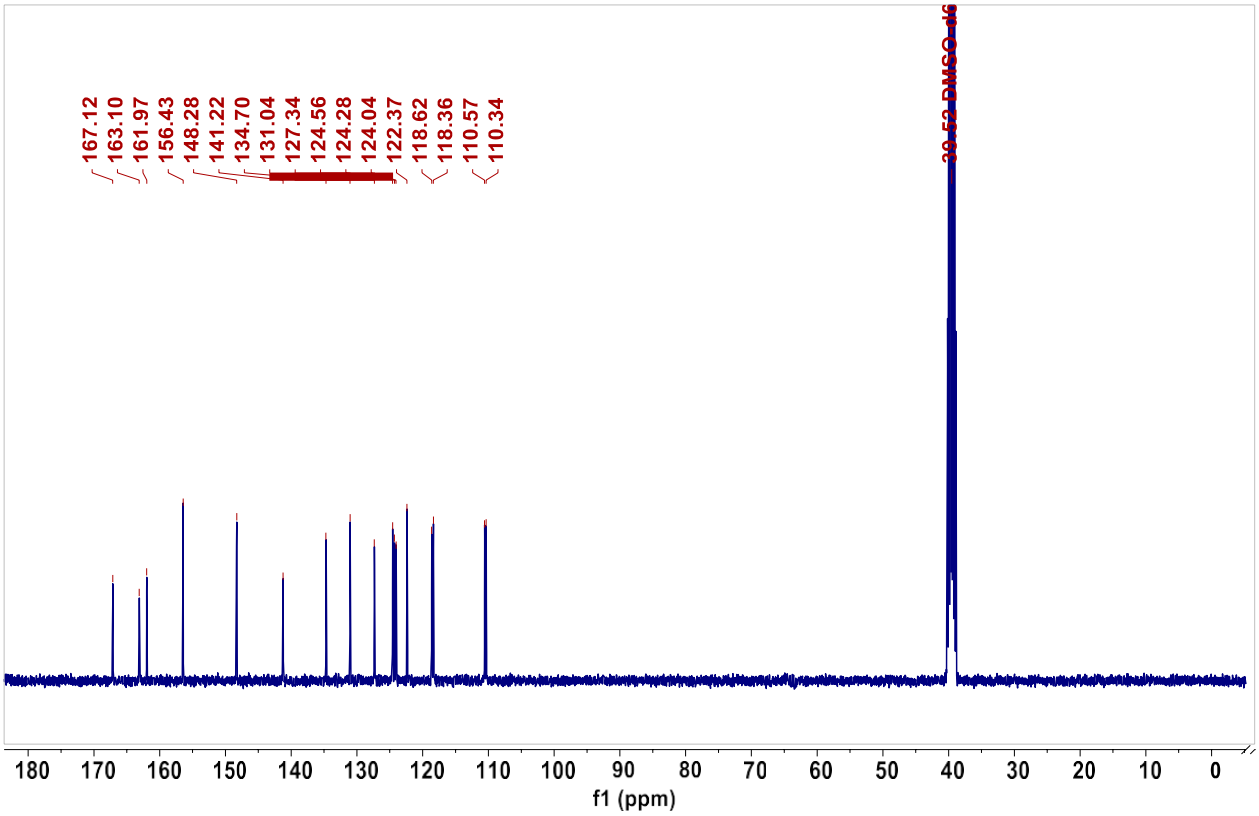

$^{1}H/^{13}C$-NMR spectra of BT12

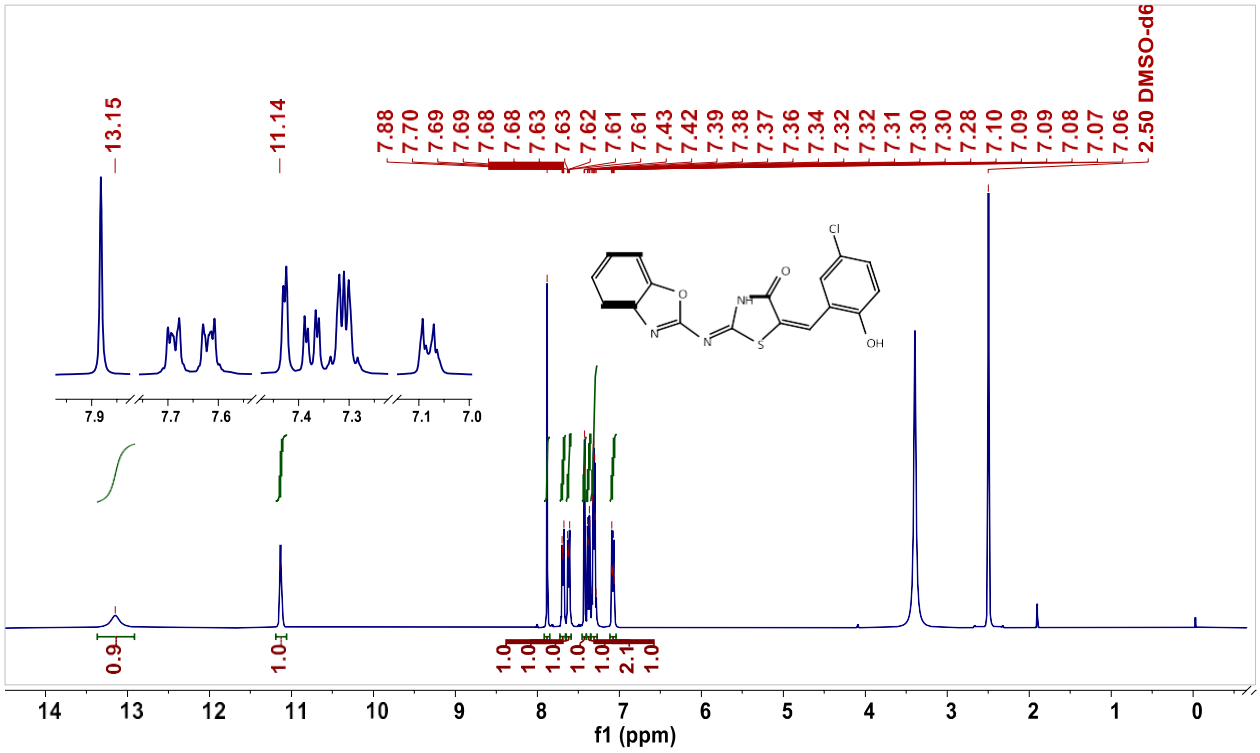

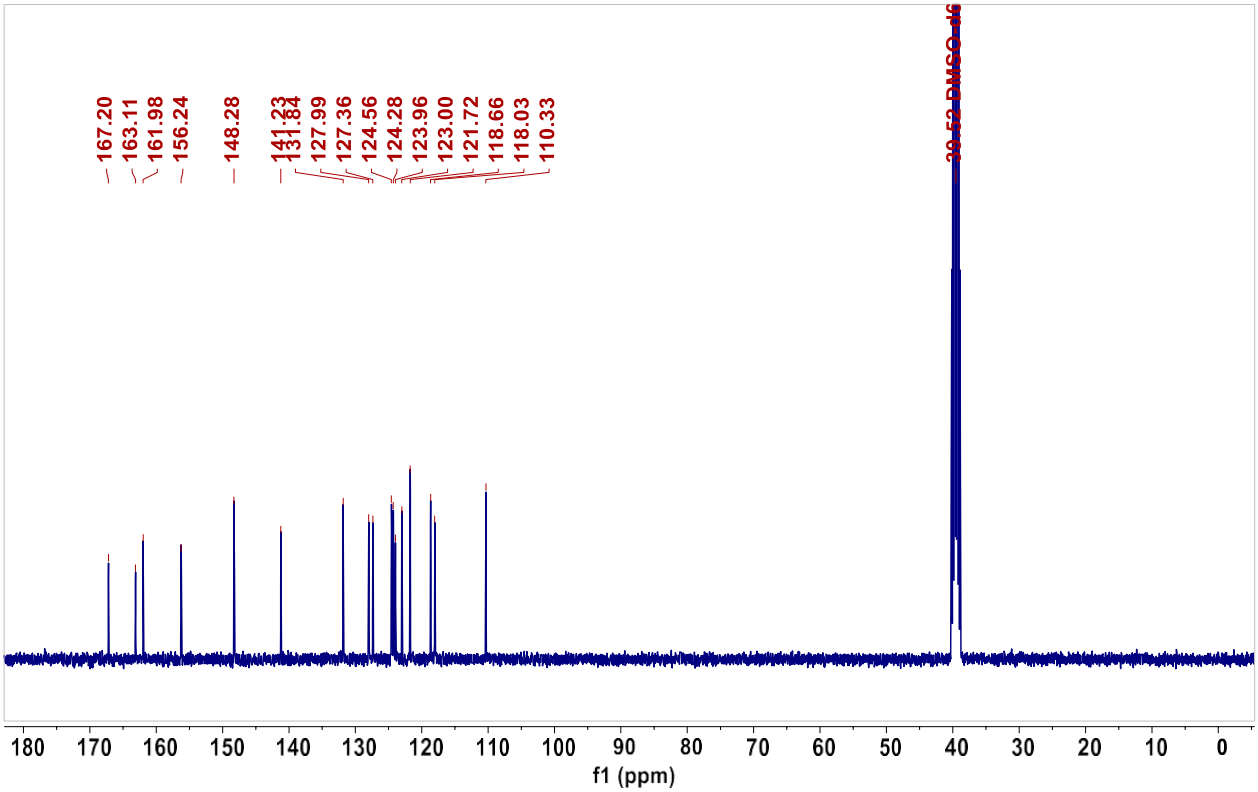

3. Mass Spectra of B-T hybrids

Mass spectrum of BT1

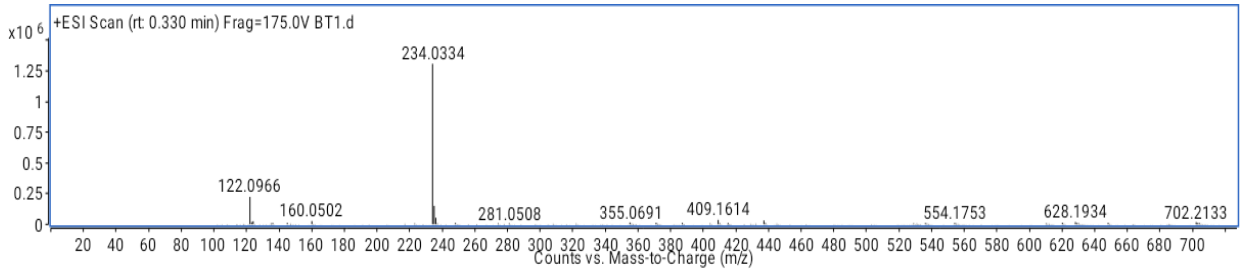

Mass spectrum of BT2

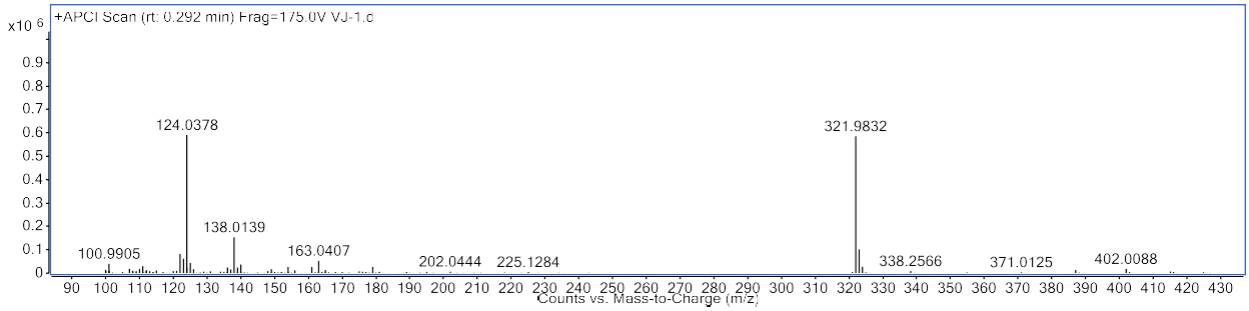

Mass spectrum of BT3

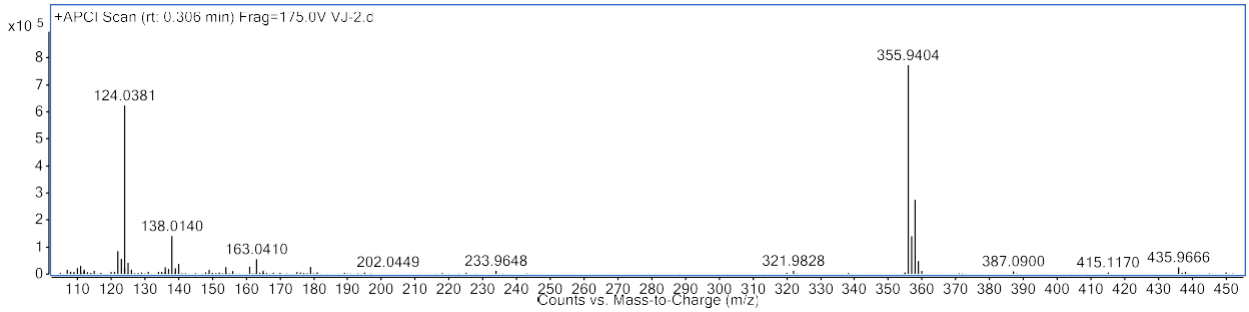

Mass spectrum of BT4

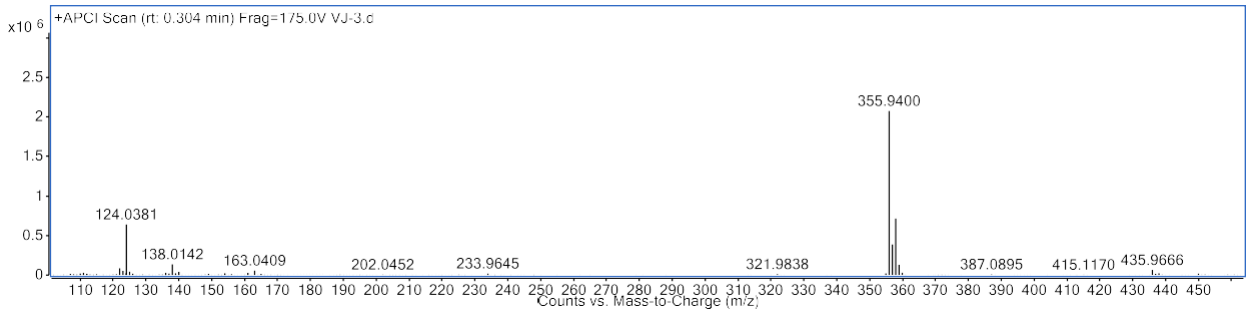

Mass spectrum of BT5

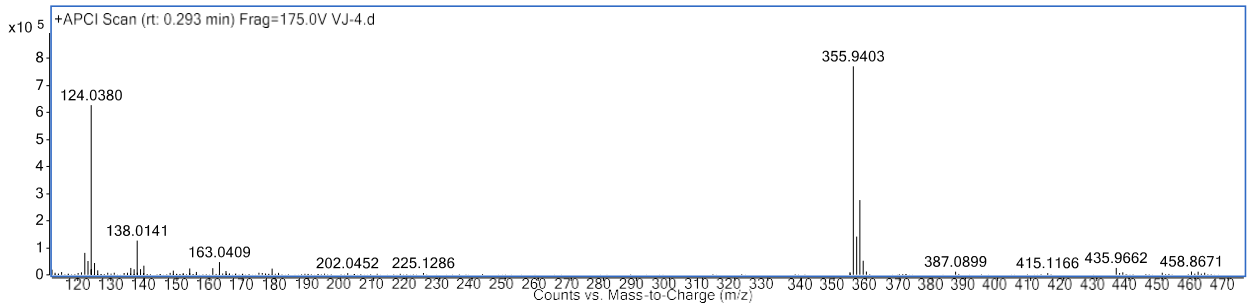

Mass spectrum of BT6

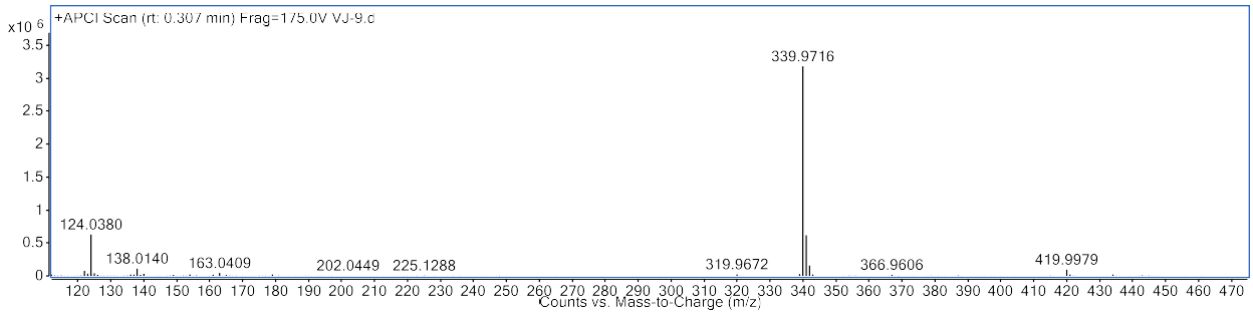

Mass spectrum of BT7

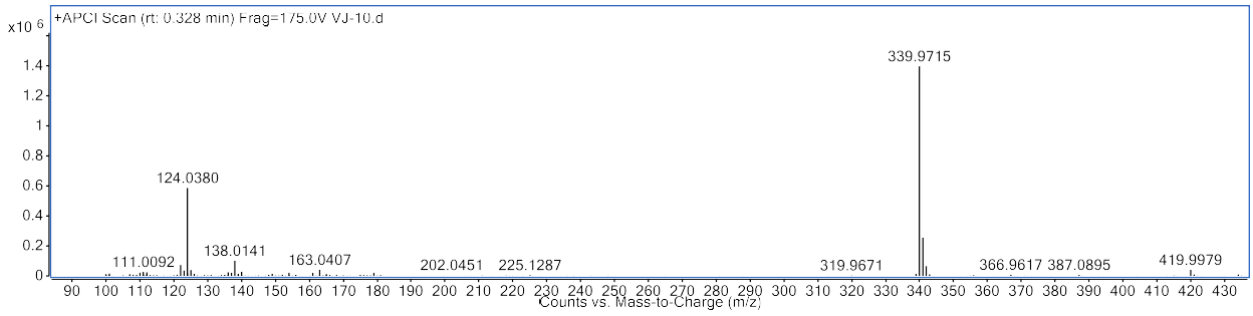

Mass spectrum of BT8

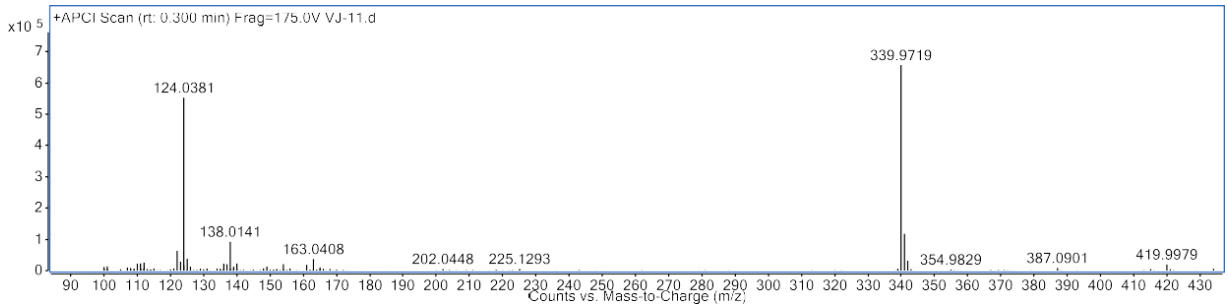

Mass spectrum of BT9

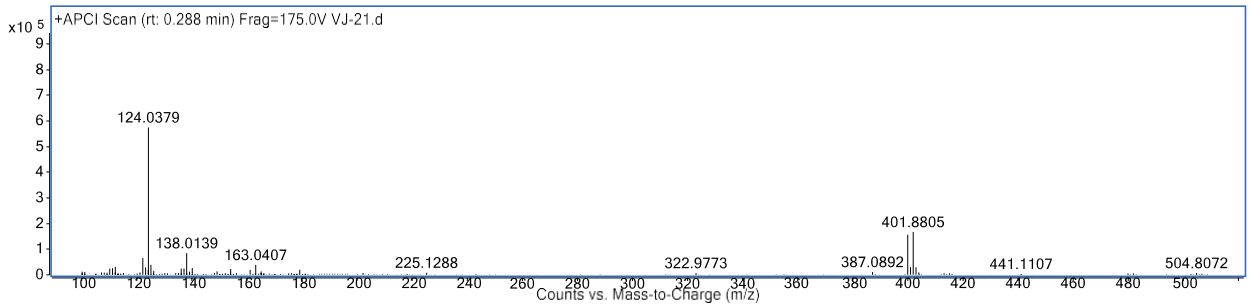

Mass spectrum of BT10

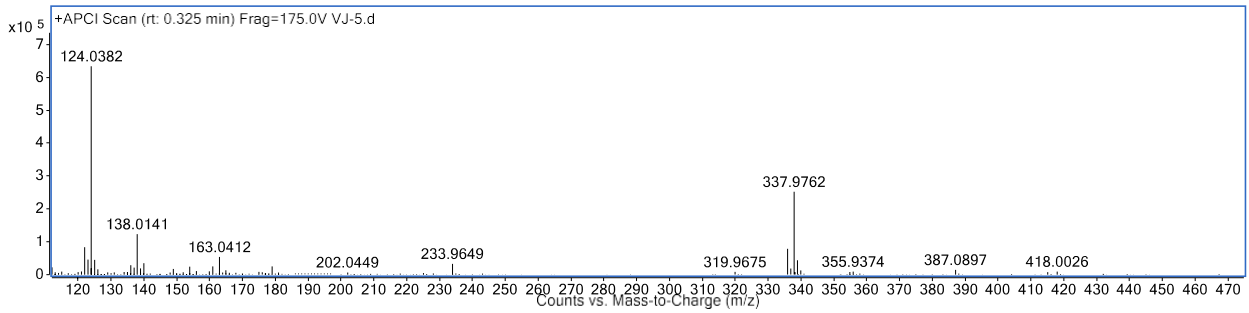

Mass spectrum of BT11

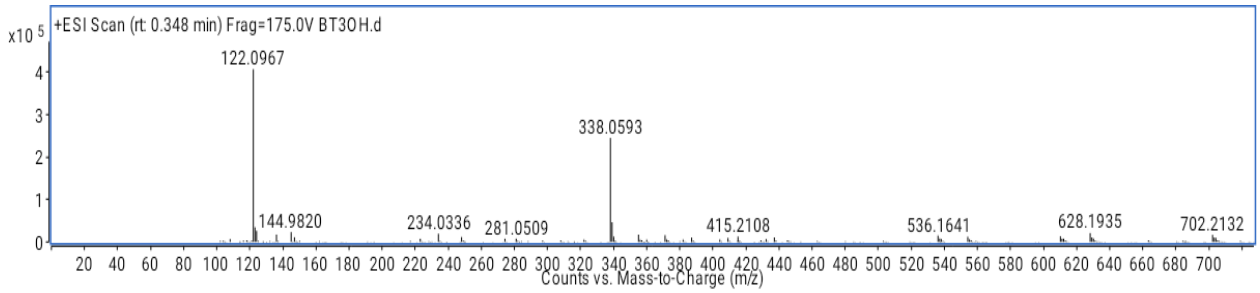

Mass spectrum of BT12

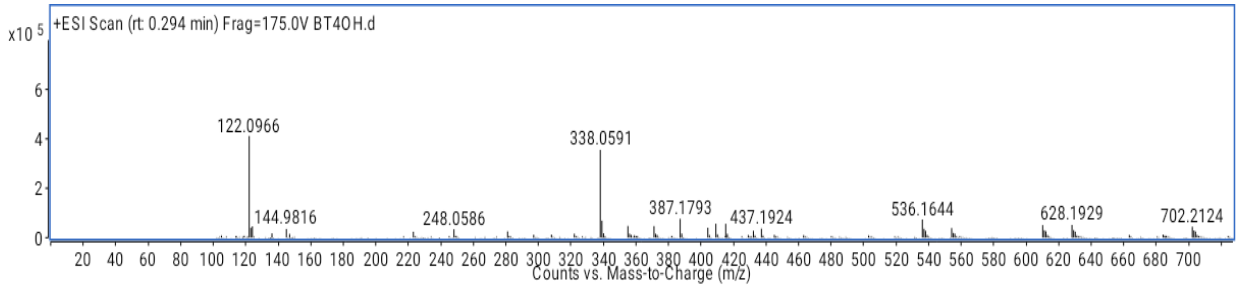

Mass spectrum of BT13

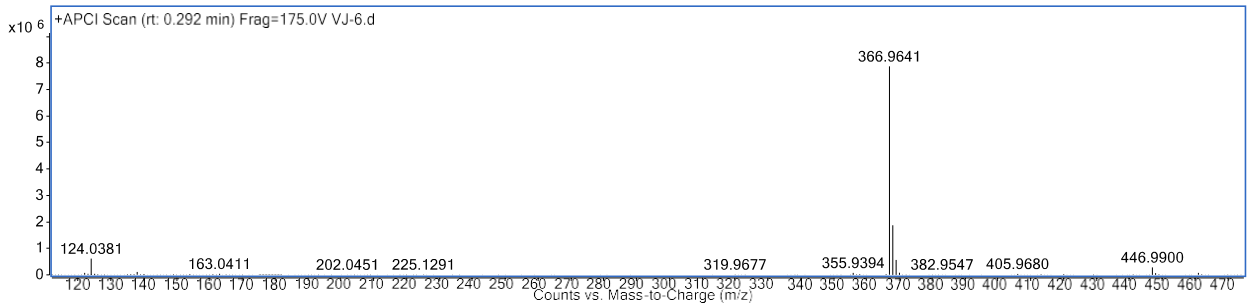

Mass spectrum of BT14

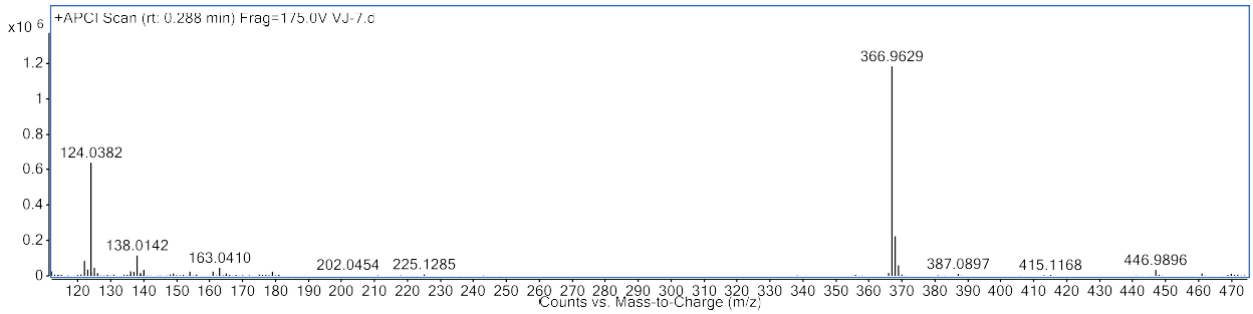

Mass spectrum of BT15

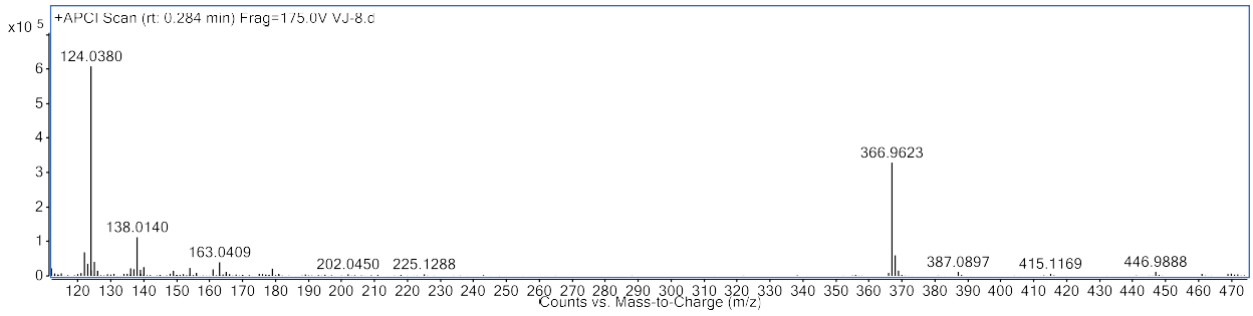

Mass spectrum of BT16

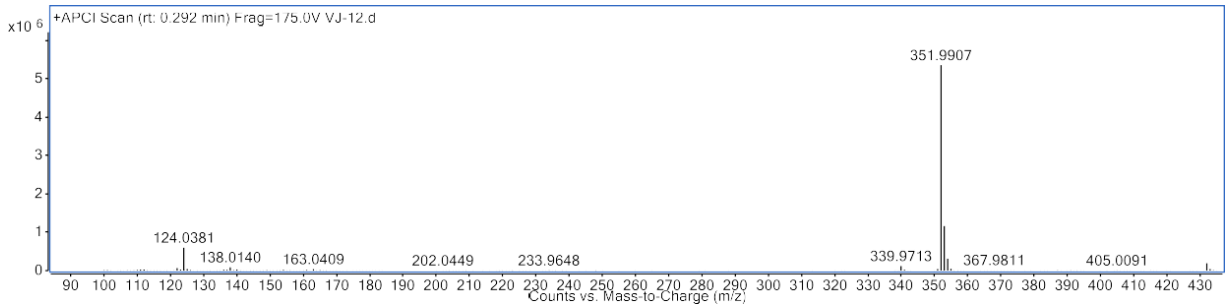

Mass spectrum of BT17

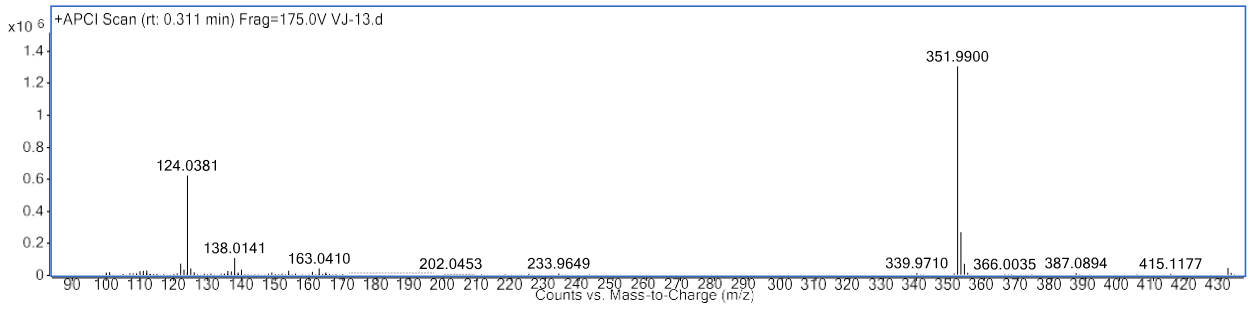

Mass spectrum of BT18

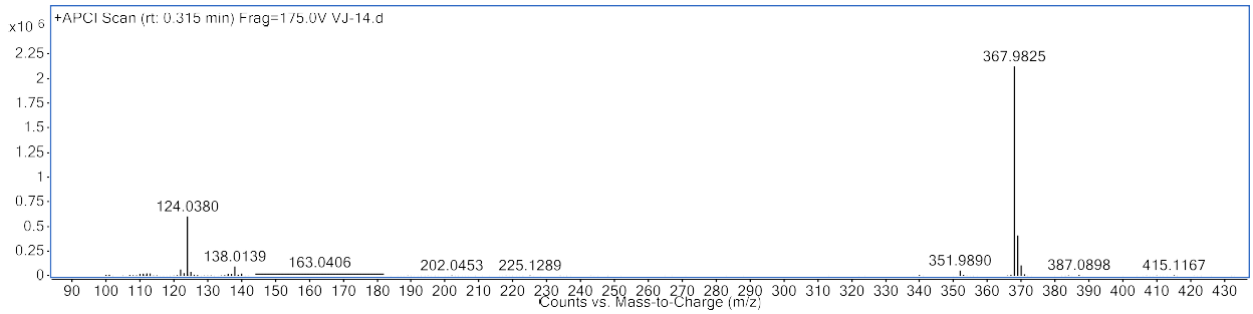

Mass spectrum of BT19

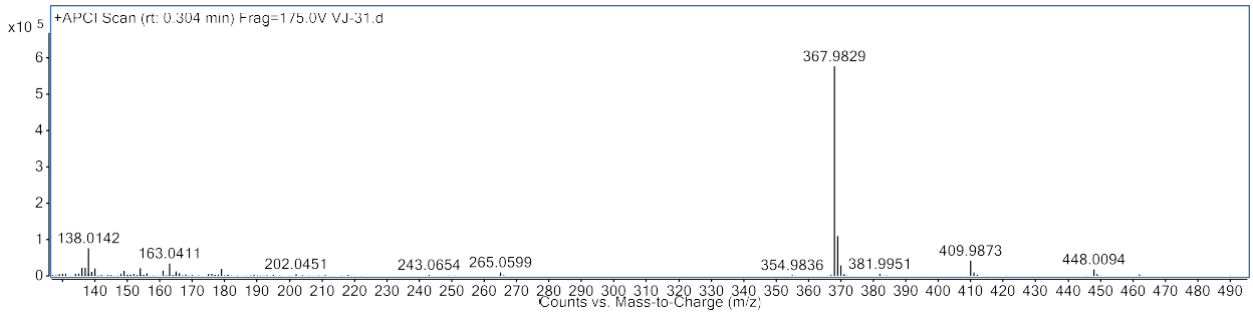

Mass spectrum of BT20

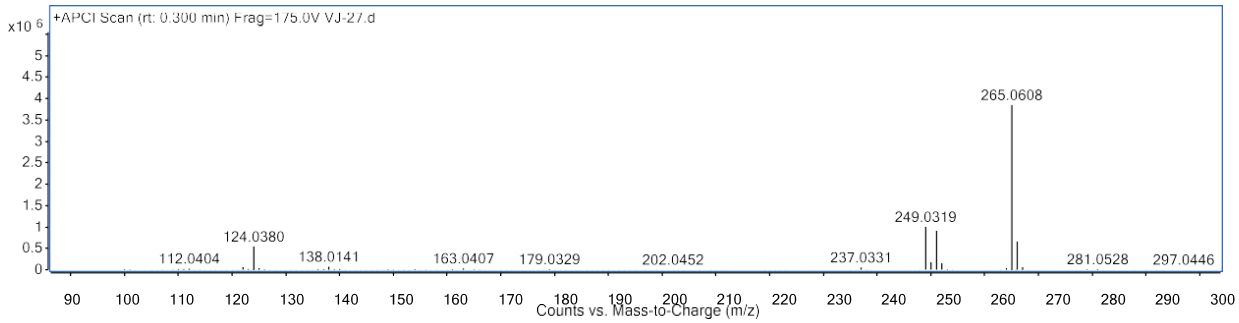

Mass spectrum of BT21

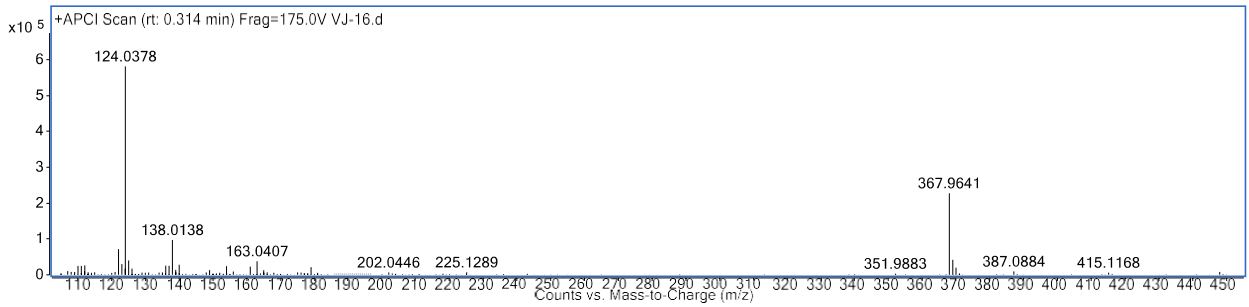

Mass spectrum of BT22

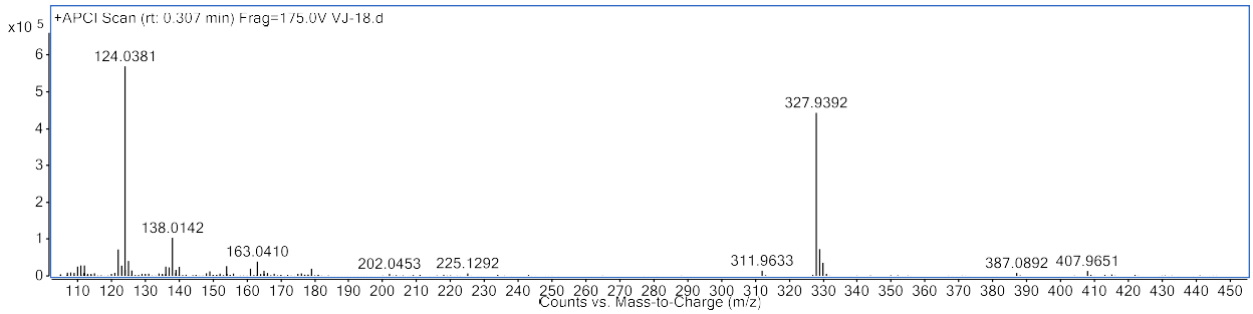

Mass spectrum of BT23

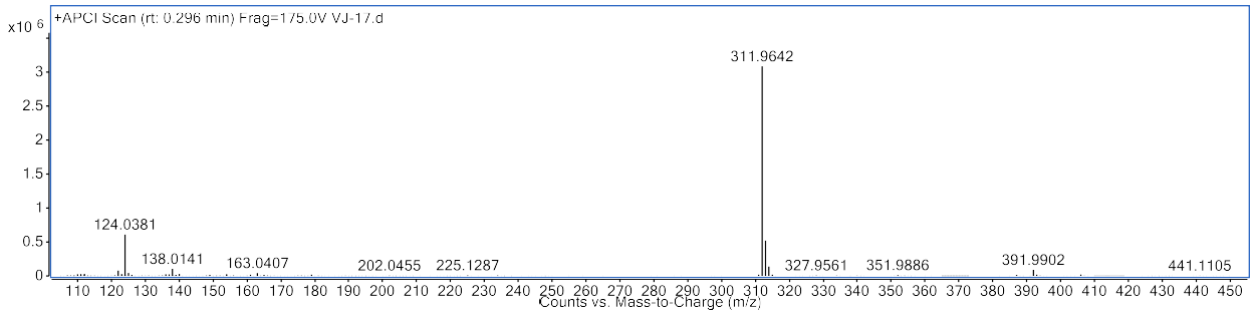

Mass spectrum of BT24

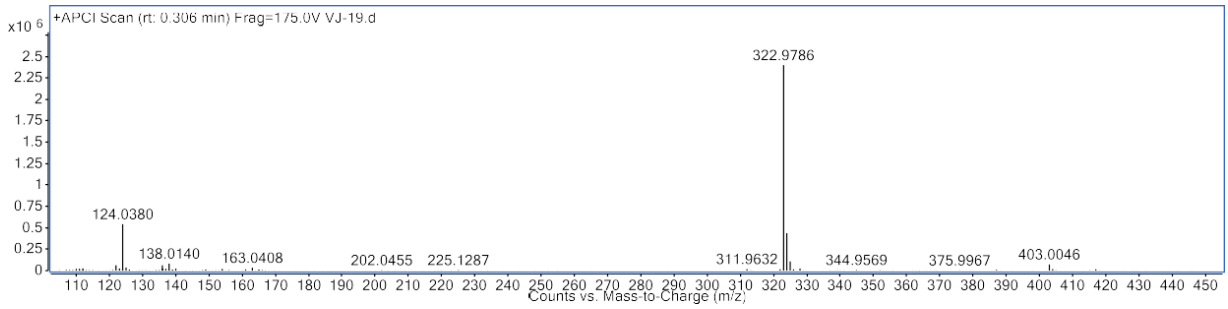

Mass spectrum of BT25

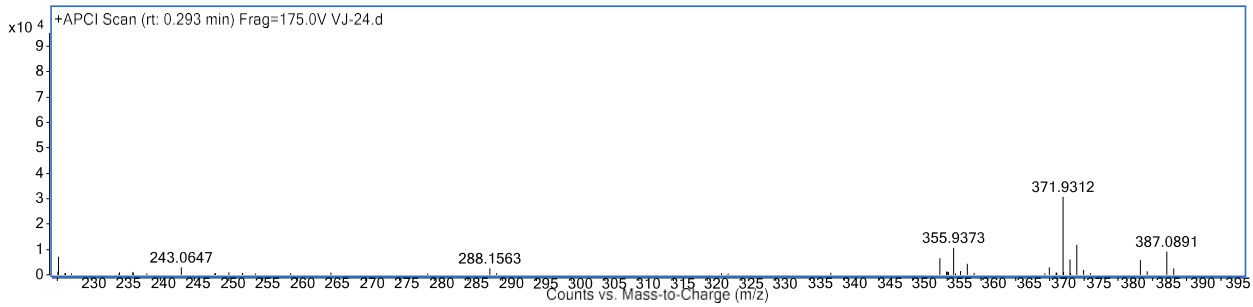

Mass spectrum of BT26

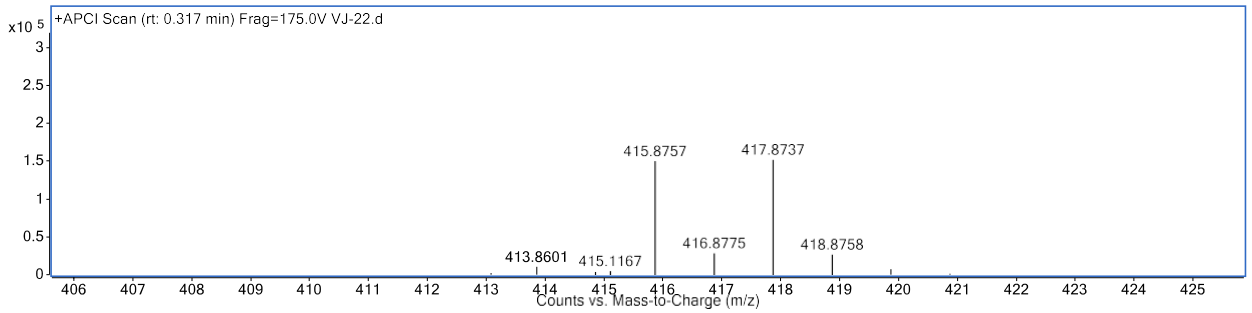

4. Computational methods

Crystal structures of target proteins DNA gyrase B (PDB ID: 4DUH), Mur B (PDB ID: 2Q85), and penicillin-binding protein 4 (PDB ID: 1TVF) were retrieved from RCSB PDB database (https://www.rcsb.org/). The missing residues in the protein structures were added using Modeller10.2 [1]. The 3D structures of B-T hybrids were generated in the Gaussian 16 programme and were optimized using the B3LYP/6-311++G(d,p) basis set.

Molecular Docking

Autodock suite was used to perform the docking studies of B-T hybrids with the three bacterial protein targets. Prior to docking, the proteins and ligands were prepared according to the standard protocol of Autodock Tools. By defining the key amino acid residues, a grid box was

created around the binding cavity (active site) of the protein molecule. The co-crystal ligand of the corresponding protein molecule was selected in order to define the active amino acid residues and predict the binding site. The docking was set up by utilizing the Lamarckian genetic algorithm (LGA), with a maximum of 2500000 energy evaluations, and 100 iterations of the genetic algorithms. The programme was run with the default values for the remaining parameters. The docking results were compared with the reference drugs novobiocin, thiazolidinone inhibitor [2], and cephalexin for DNA gyrase B, MurB, and PBP4 systems respectively. The structures of the reference drugs are displayed in the Figure S5.

Molecular Dynamics

Molecular dynamics simulations were performed on GROMACS 2020.1 [3] software package with the amberff99SB-ILDN [4] force field and TIP3P water model [5]. The proteins were extracted from the complexes and processed through PROTEINPREPARE module of the PlayMolecule website [6] assuming a suitable pH (7.5) for DNA gyrase B [7], 8.0 for MurB [8], and 7.4 for PBP4 [9]) before generating the topologies. The ligand topologies were generated using the ACPYPE server [10]. The complex topologies were constructed by combining the topologies of the ligands and the corresponding proteins. After explicit periodic boundary conditions-based solvation in a cubic box with a 7 Å distance from the boundaries, the complexes were neutralized with 0.15 M NaCl. With the parameters and conditions stated elsewhere [11,12], energy minimization, equilibration (NVT and NPT for 500 ps) and the production run (50 ns) were carried out. gmxMMPBSA v1.6.0[13] programme in conjunction with the MMPBSA.py [14] script and the AmberTools21 package was employed to compute the binding free-energy of protein-ligand complexes using Molecular Mechanics Generalized Born Surface Area (MM/GBSA).

5. *In silico* studies: Results and discussion

Binding and Interaction Analysis

The potential of B-T hybrids to interact with the key residues was indicated by their docking with bacterial enzymes DNA gyrase B, MurB and penicillin-binding protein 4 (PBP4) in their binding pockets. Apart from hydrophobic interactions, π-cation and hydrogen bonding interactions constituted the majority of principal interactions between selected proteins and hydroxy B-T hybrids. 2D interaction plots of B-T hybrids with the three enzymes are provided in supplementary material (Figures S7, S8 & S9). The benzoxazole unit and aryl group on the thiazolidinone ring are involved in π-cation interactions while the hydroxy group on the aryl ring of B-T hybrids is constantly involved in hydrogen bonding interactions with the key residues of the proteins. The active residues Tyr109, Asp73, Thr165, and Asn46 of DNA gyrase B are engaged in hydrogen bonding interactions, while Arg76 and Lys103 are engaged in π-cation interactions with hydroxy B-T hybrids. In the case of MurB enzyme, the residues Glu128, Arg159, Arg 214, Ser229, Asn233, and Gln288 are involved in hydrogen bonding, whereas Lys262 is involved in π-cation interactions.

In case of PBP4, the residues Ser75, Thr260, Ser116, Thr262, Glu297 and Arg300 participated in hydrogen bonding interactions with the hydroxy B-T hybrids. Table 5 displays the binding energies of hydroxy B-T hybrids with the selected proteins obtained from docking studies. It is interesting to note that **BT25** and **BT26** exhibited the best binding energies from docking studies that correlated with the experimental data among all the selected hydroxy B-T hybrids with the three bacterial enzymes (Table S1).

Table S1. Binding energies of BT hybrids obtained from docking studies.

Compound	Binding Energy (kcal mol^{-1})		
	DNA gyrase B	**MurB**	**PBP4**
BT1	-7.13	-6.09	6.53
BT10	-9.61	-7.61	-8.11
BT11	-9.93	-7.23	-8.38
BT12	-9.80	-7.39	-7.76
BT18	-9.35	-7.44	-7.44
BT19	-9.75	-7.32	-7.71
BT25	**-9.96**	**-7.86**	**-8.13**
BT26	**-9.93**	**-7.89**	**-8.13**
Novobiocin	-9.29	--	--
TI	--	-7.61	--
Cephalexin	--	--	-8.35

Molecular Dynamics (MD) Simulations

In order to gain dynamic insights into the structural or conformational changes of protein-ligand complexes and identify the residual interactions that stabilize the ligands at the binding site, the initial ligand geometries produced by the docking studies on the crystal structures of the selected antibacterial targets were subjected to MD simulations for 50 ns. Various parameters such as RMSD, Radius of gyration (Rg), RMSF and hydrogen bonds were analyzed to check the stability of

each system. In case of DNA Gyrase B (GyrB), it can be observed that **BT25**, **BT26** and Novobicin (Novo) complexes were equilibrated in the range of RMSD value 0.1 to 3.5 nm as shown in Figure S1(a). The fluctuation of the GyrB backbone and the protein-ligand stability can both be explained by the average RMSD value of each trajectory. The average values of RMSD of protein backbone of apo structure, **Gyr-Novo**, **GyrB-BT25** and **GyrB-BT26** complexes are 1.8±0.32 Å, 1.7±0.1 Å, 2.6±0.63 Å and 1.7±0.20 Å respectively. These results indicate that except **GyrB-BT25** complex, all the other systems exhibited relatively greater stability. Figure S2(a) illustrates the total residual fluctuations (RMSF) of the GyrB apo-structure and complexes. The solvent exposed residues in the region of 81 to 89 and 101 to 123 were found to have high fluctuations in case of all the systems. The maximum average RMSF value was observed in case of novobiocin complex and the minimum average value was observed with **BT26** complex. Figure S1(b) displays the radius of gyration plots of GyrB complexes and its apo structure. These stable Rg plots clearly indicate that all systems were rigid and compact during the course of simulation.

Results of protein backbone RMSD analysis of the MurB complexes and protein indicate that all the trajectories achieved stability within 5 ns (Figure S1(c)). The average values of RMSD of protein backbone of apo structure, **MurB-TI**, **MurB-BT25** and **MurB-BT26** complexes are 1.6±0.17 Å, 1.7±0.1 Å, 1.6±0.16 Å, and 1.6±0.19 Å respectively. Figure S2(b) depicts the overall residual fluctuations of the MurB systems. With the apo structure, all of the MurB complexes displayed a similar pattern of residual fluctuations. The solvent exposed regions from 182 to 201 and 235 to 262 exhibited high fluctuations in all the systems, indicating a higher degree of conformational flexibility. The MurB complexes and apo structure showed comparable Rg and the average Rg's

were between 20.84±0.16 Å and 20.89±0.1 Å, indicating that all systems remained rigid during the simulation (Figure S1(d)).

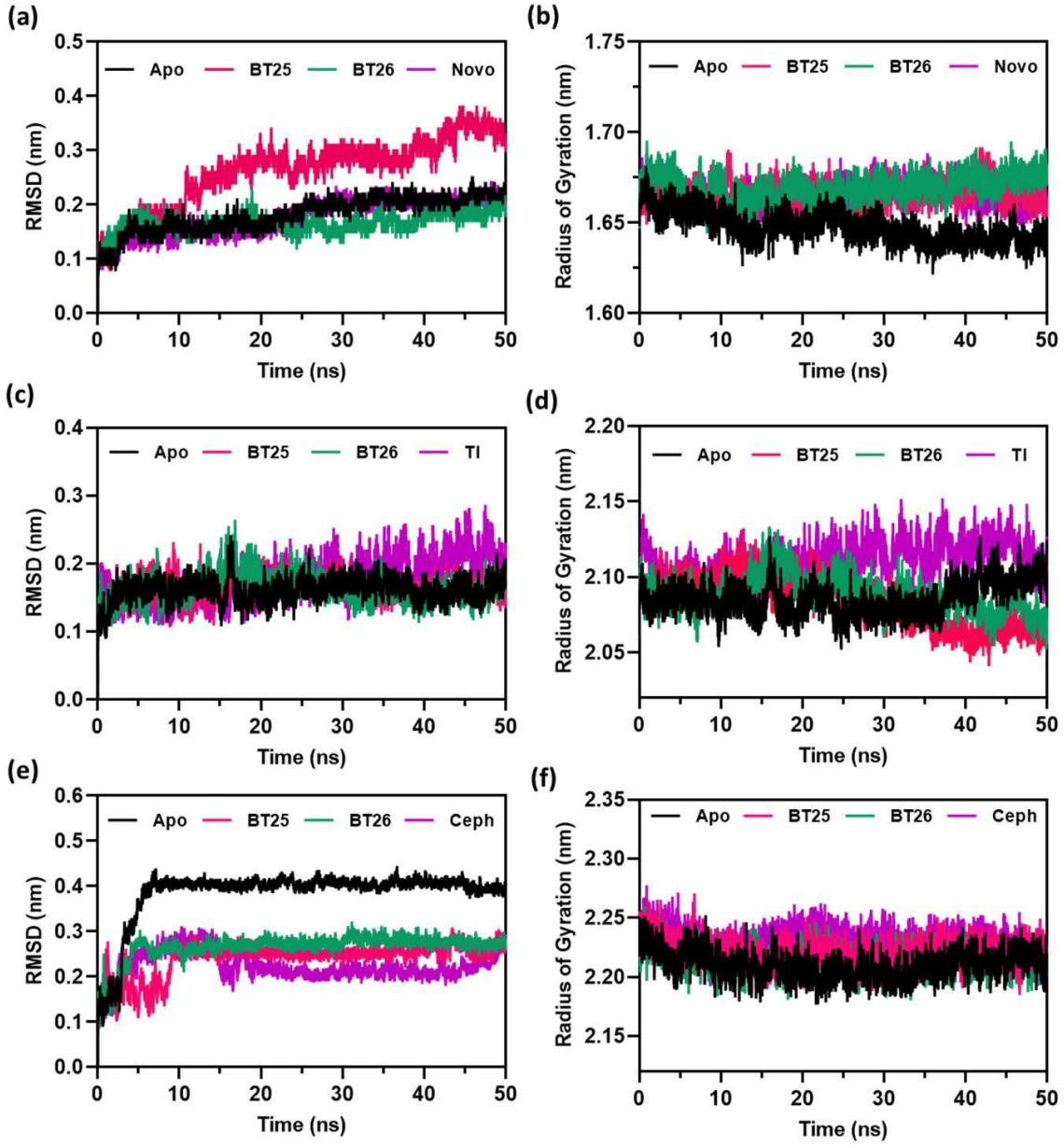

Figure S1. Results of molecular dynamic simulations of hydroxy B–T hybrids against the selected bacterial enzymes. The RMSD plots of GyrB-systems, MurB-systems and PBP4-systems are displayed in (a), (c), and (e), respectively. The radius of gyration plots of GyrB-systems, MurB-systems and PBP4-systems are displayed in (b), (d), and (f), respectively.

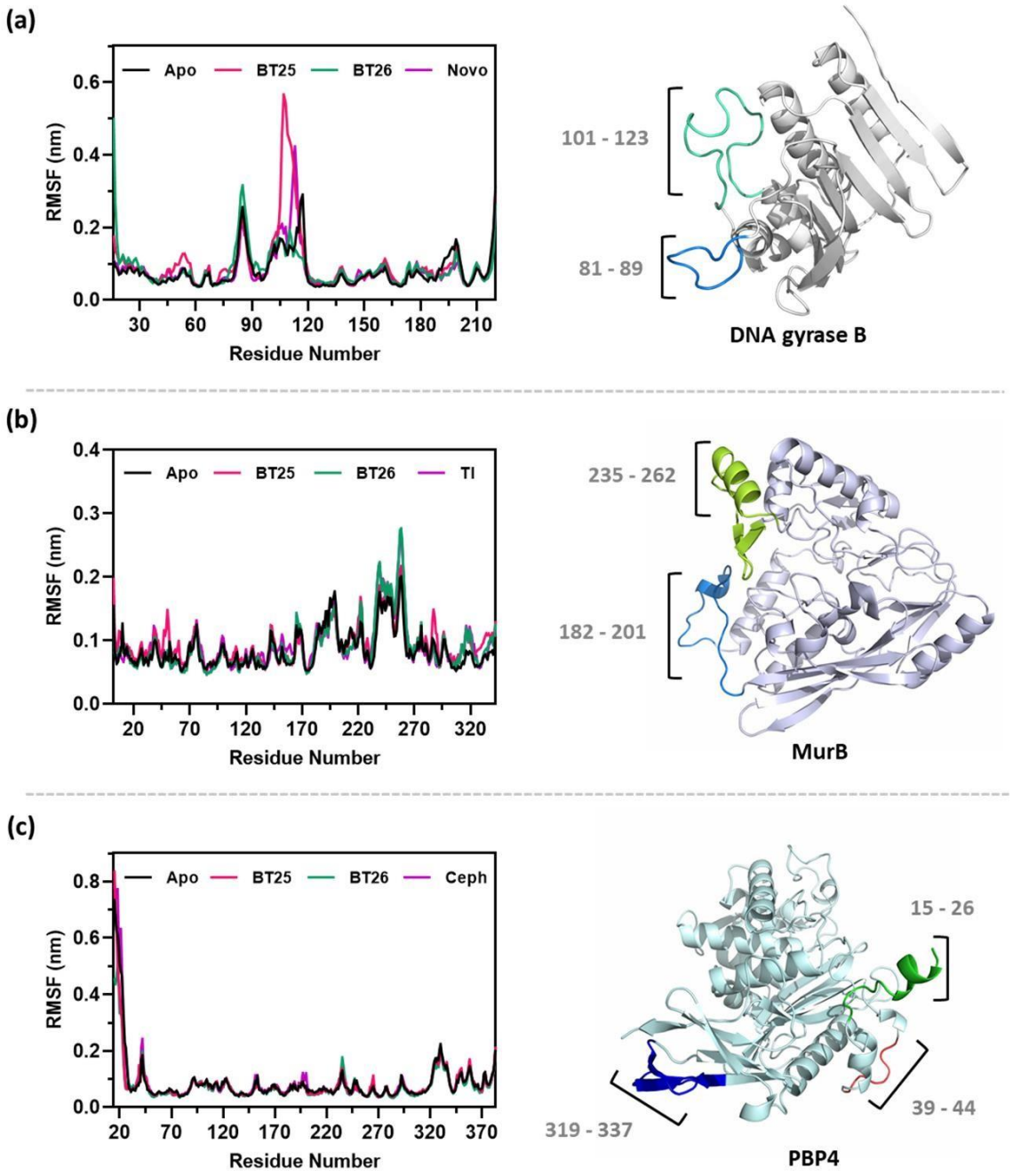

Figure S2. Results of molecular dynamic simulations of hydroxy B–T hybrids against the selected bacterial enzymes. The RMSF plots of GyrB-systems, MurB-systems and PBP4-systems are displayed in (a), (b), and (c), respectively. The residues with high fluctuations are identified and presented with different colors in the respective protein structures.

According to the protein backbone RMSD of complexes, the PBP4 trajectories achieved stability during the first 7 to 10 ns (Figure S1(e)). However, the complexes showed comparatively lower RMSD values between 2.4±0.4 Å and 2.6±0.4 Å than the average RMSD displayed by the apo structure (3.8±0.6 Å), indicating that the interactions between the ligands and the active region of PBP4 may increase the stability of the enzyme. In terms of the RMSF data from Figure S2(c), PBP4 systems had very minimal residual fluctuations when compared to other two target enzymes. From the Figure S1(f), the highly stable Rg plots indicate that all the systems are compact and very rigid. The molecular dynamics simulation results indicate that the PBP4 systems exhibit remarkable stability among the three systems studied.

Therefore, following a thorough analysis of the MD trajectories of all the systems, we may draw the conclusion that the proposed hydroxy B-T hybrids can form stable complexes with the three bacterial enzymes GyrB, MurB and PBP4.

Hydrogen bonding Interaction analysis

The stability of a protein-ligand complex is significantly influenced by hydrogen bonding interactions. Using the 'g_hbond' module of GROMACS and the 'Hydrogen Bonds' plugin of VMD, the hydrogen-bonding interactions between binding site residues of the bacterial proteins and the hydroxy B-T hybrids were investigated during the course of the simulation.

According to the H-bond plots obtained from molecular dynamics trajectories (Figure 3), when compared to novobiocin and **BT25**, **BT26** forms relatively fewer H-bonds with the DNA gyrase B (Figure S3). Average 2, 1 and 2 numbers of H-bonds were found for ligands **BT25**, **BT26** and novobiocin complexed with DNA gyrase B enzyme, respectively.

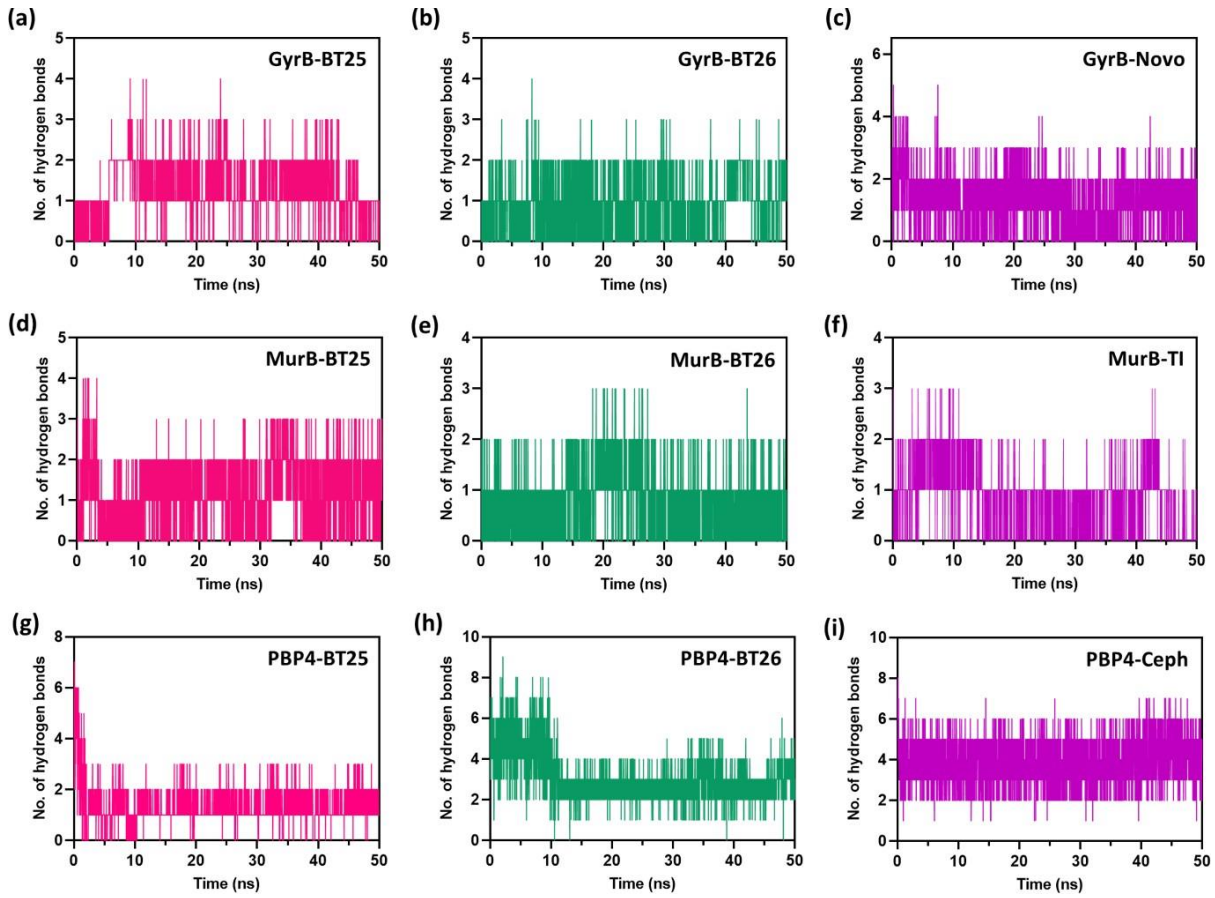

Figure S3. The first set of plots (a, b, c) represents the number of hydrogen bonds exhibited by the **BT25** (a), **BT26** (b) and Novobiocin (c) with DNA gyrase B throughout the simulation. The second set of plots (d, e, f) represents the number of hydrogen bonds exhibited by the **BT25** (d), **BT26** (e) and Thiazolidinone inhibitor (f) with MurB enzyme throughout the simulation. The third set of plots (g, h, i) represents the number of hydrogen bonds exhibited by the **BT25** (d), **BT26** (e) and cephalexin (f) with PBP4 throughout the simulation.

Novobiocin and ligand **BT25** formed hydrogen bonds with 14 and 25 different residues in the binding pocket during the course of the simulation, with Asn46 and Asp73 having the highest occupancy at 15% and 78%, respectively. Whereas, **BT26** interacted with 23 residues, with Gly101 having the maximum occupancy at 11%. In case of MurB systems, on an average, only one hydrogen bond could be observed for each of the three ligands at any given time during the simulation. Thiazolidinone inhibitor (**TI**), **BT25**, and **BT26** established hydrogen bonds with 29, 29,

and 33 distinct amino acids, with Tyr125, Gly126, and Gly126 having the highest occupancy at 30%, 40% and 40%, respectively. On the contrary, in the case of PBP4 complexes, an average of 3 to 4 hydrogen bonds was observed between the ligands and the active site amino acid residues. It is noteworthy to note that cephalexin, **BT25**, and **BT26**, all exhibit a maximum of 7, 9 and 7 hydrogen bonds during the simulation, respectively. Cephalexin, **BT25**, and **BT26** formed hydrogen bonds with 21, 30 and 28 different amino acids, respectively, with Ser75, Glu297 and Arg300 having the maximum occupancy at 64%, 50% and 67%. PBP4 complexes displayed the maximum number of hydrogen bonds and the highest degree of stability out of the three systems that were examined. Therefore, it is demonstrated by hydrogen bonding analysis and other analyses (RSMD, RMSF and Rg) that hydrogen bonding interactions are vital for preserving the stability of the protein-ligand complexes.

Binding free energy and per-residue analysis

The binding free energy of the complexes and the per-residue contributions towards it were calculated in order to understand the contribution of the energy components and assess the strength of the interactions between the pocket residues and the ligands. The last 100 snapshots from molecular dynamics simulations of protein-ligand systems were used to assess the binding free energy using molecular mechanics generalized born surface area (MM/GBSA). Using the interaction entropy approximation (IE) in gmxMMPBSA tool, the entropy contribution to the binding free energy was estimated. Figure S4 demonstrates the total binding free energy and individual energy contributions in case of the GyrB, MurB and PBP4 systems, respectively. The total binding free energy for all the three systems was favorably impacted by the Van der Waals (VDWAALS), electrostatic (EEL), and non-polar component of solvation (ESURF) energy terms.

However, the polar component of solvation energy (EGB) suggested an unfavorable contribution to the calculations of the thermodynamic free energy of the complexes.

MMGBSA results in the case of GyrB systems indicated that novobiocin exhibited the maximum relative binding free energy (-30.16 kcal mol^{-1}) followed by **BT25** (-22.08 kcal mol^{-1}) and **BT26** (-14.83 kcal mol^{-1}). Further, the binding free energies of all the systems were decomposed into residual contributions in order to identify the hot spot residues responsible for the binding. The residues that exhibited $\Delta G_{bind} \geq$ -1.5 kcal mol^{-1} were discussed. The major contributors to the binding free energy of **GyrB-BT25** complex were Glu50 (-3.44 kcal mol^{-1}), Ile78 (-2.78 kcal mol^{-1}), and Thr165 (-1.95 kcal mol^{-1}). The primary contributions for the free energy of **GyrB-BT26** complex originated from Ile78 (-2.14 kcal mol^{-1}), Ile94 (-2.16 kcal mol^{-1}), and Phe104 (-3.93 kcal mol^{-1}). On the other hand, Ile78 (-2.53 kcal mol^{-1}), Asn46 (-2.20 kcal mol^{-1}), and Ile94 (-1.71 kcal mol^{-1}) made the significant contributions to the binding free energy of **GyrB-Novo** complex. Overall, according to per-residue decomposition, the hot spot residues interacted with the inhibitors in case of DNA gyrase B include Asn46, Ala47, Glu50, Val71, Asp73, Arg76, Ile78, Pro79, Ile94, Lys103, Thr165, and Val167. Among the three MurB systems, the **MurB-TI** complex displayed the highest binding free energy (-31.99 kcal mol^{-1}) followed by **MurB-BT25** (-23.8 kcal mol^{-1}) and **MurB-BT26** (-21.21 kcal mol^{-1}). Decomposition analysis showed that Tyr125 (-1.97 kcal mol^{-1}), Tyr190 (-1.96 kcal mol^{-1}), Leu218 (-1.87 kcal mol^{-1}) and Gly228 (-1.71 kcal mol^{-1}) were the main residues that bind MurB and the thiazolidinone inhibitor. The residues Tyr190 (-2.03 kcal mol^{-1}), Ala124 (-1.71 kcal mol^{-1}), Gly126 (-1.5 kcal mol^{-1}), and Tyr125 (-1.48 kcal mol^{-1}) were the key contributors towards the binding free energy of the MurB-BT25 complex, whereas Tyr190 (-3.45 kcal mol^{-1}) and Ala124 (-1.68 kcal mol^{-1}) significantly contributed to the binding free energy

of **MurB-BT26** complex. The hot spot residues in case of **BT25** and **BT26** from MurB enzyme were identified as Gly123, Ala124, Tyr125, Tyr190, Leu218, Gly288, Pro252, Tyr254, Ala264, Gly266, Trp267, and Leu290.

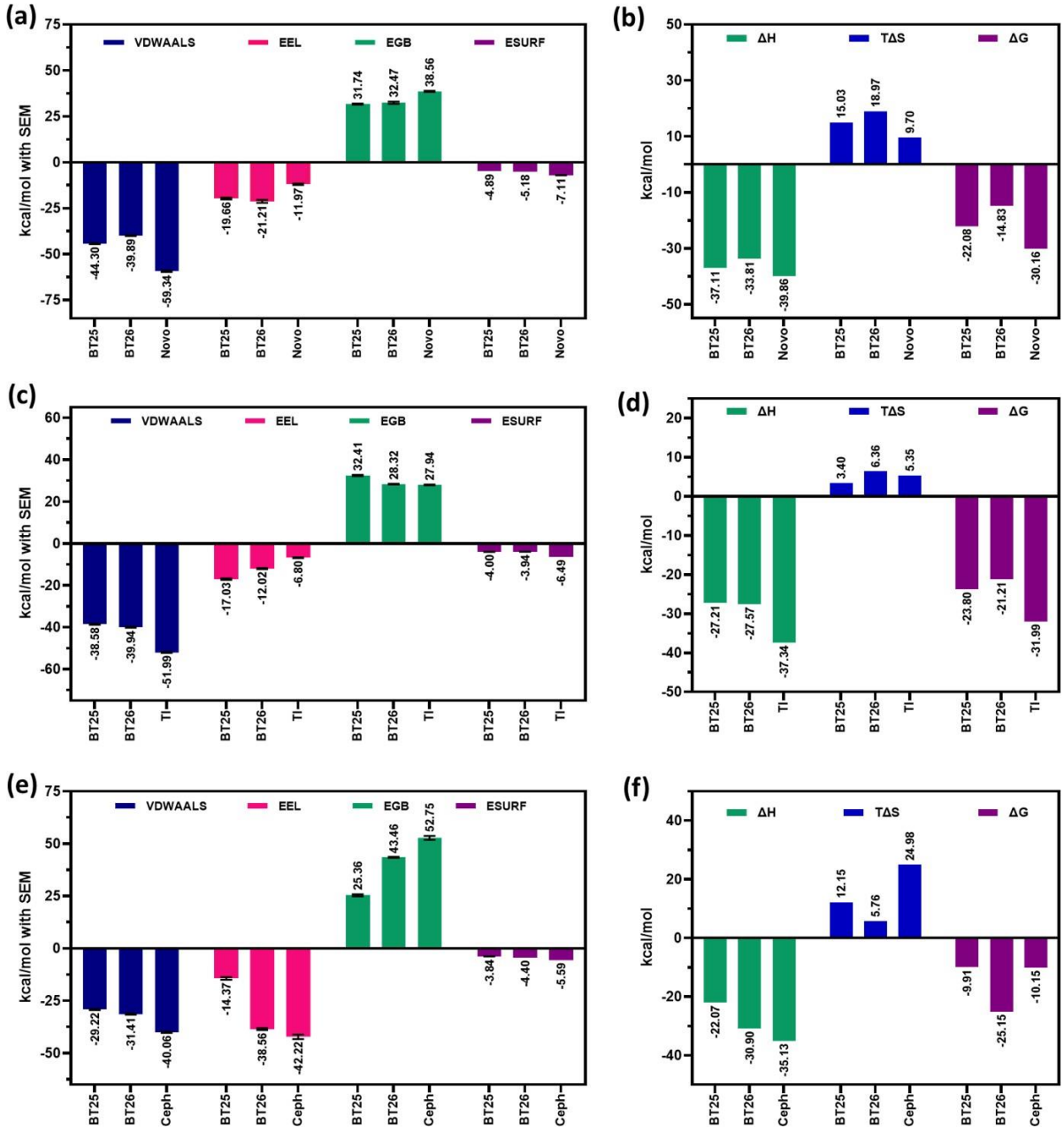

Figure S4. Contribution of individual energy terms towards the binding free energy in case of DNA gyrase B (a), MurB (c), and PBP4 (e) systems. The relative binding free energies along with the enthalpy and entropy contributions are presented for DNA gyrase B (b), MurB (d), and PBP4 (f) systems.

The resultant ΔG of **PBP4-BT25**, **PBP4-BT26**, and **PBP4-Ceph** complexes was found to be -9.91 kcal mol^{-1}, -25.15 kcal mol^{-1} and -10.15 kcal mol^{-1}, respectively. In this case, **BT26** displayed highest ΔG with significant contributions from Phe241 (-3.15 kcal mol^{-1}), Arg300 (-2.64 kcal mol^{-1}) and Phe243 (-1.21 kcal mol^{-1}). On the other hand, as a result of reduced electrostatic and higher entropy contributions, the **PBP4-BT25** complex had higher value of ΔG. The main contributors for the free energy of **PBP4-BT25** complex were Phe243 (-3.08 kcal mol^{-1}), Phe241 (-2.5 kcal mol^{-1}) and Lys249 (-1.58 kcal mol^{-1}). The **PBP4-Ceph** complex suffered from high contribution from entropy component. The residues–Ser262, Phe241 and Ser75 made significant contributions to the binding free energy of the **PBP4-Ceph** complex with each contributing -4.44 kcal mol^{-1}, -3.65 kcal mol^{-1} and -2.83 kcal mol^{-1}, respectively. The hot spot residues in case of PBP4 were Ser75, Leu115, Ser116, Phe241, Phe243, Lys249, Ser262, Glu297 and Arg300.

6. Reference drugs for *in-silico* studies

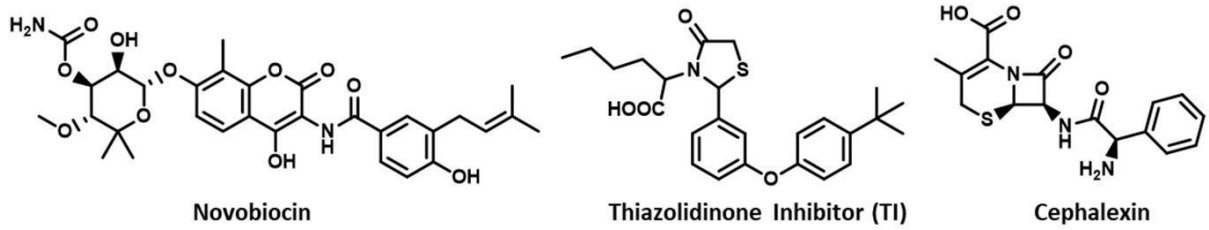

Figure S5. Reference drugs for the *in-silico* studies

7. 2D interaction plots of hydroxy B-T hybrids

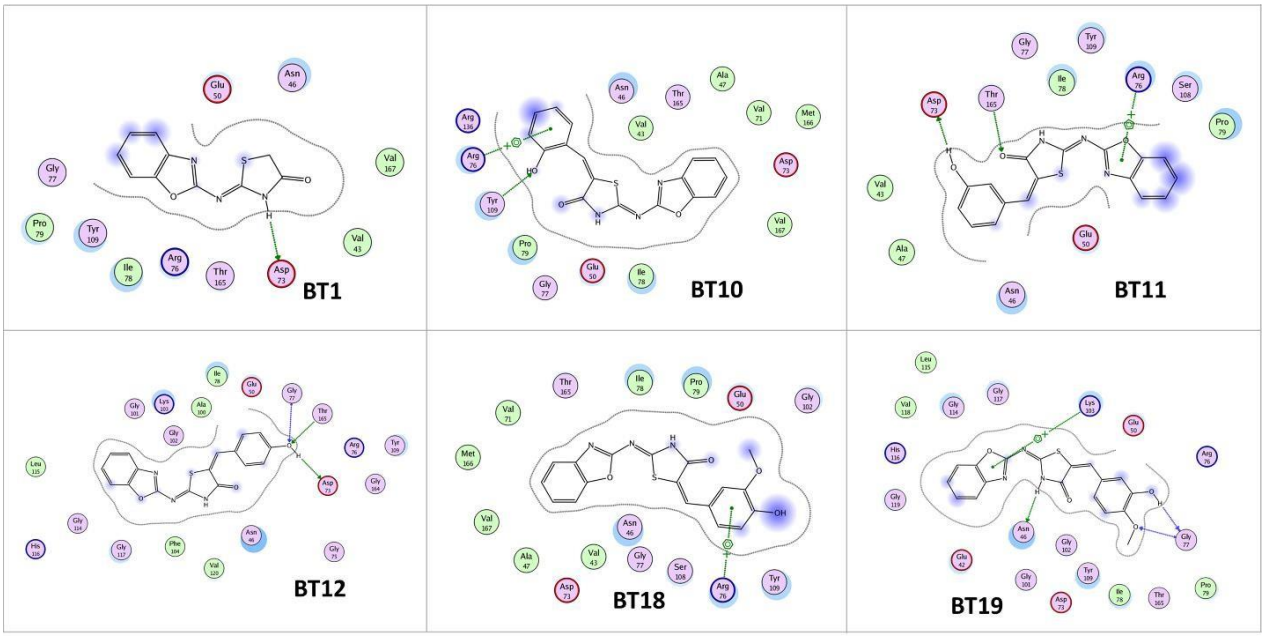

Figure S6. Interactions of selected B-T hybrids with DNA gyrase B

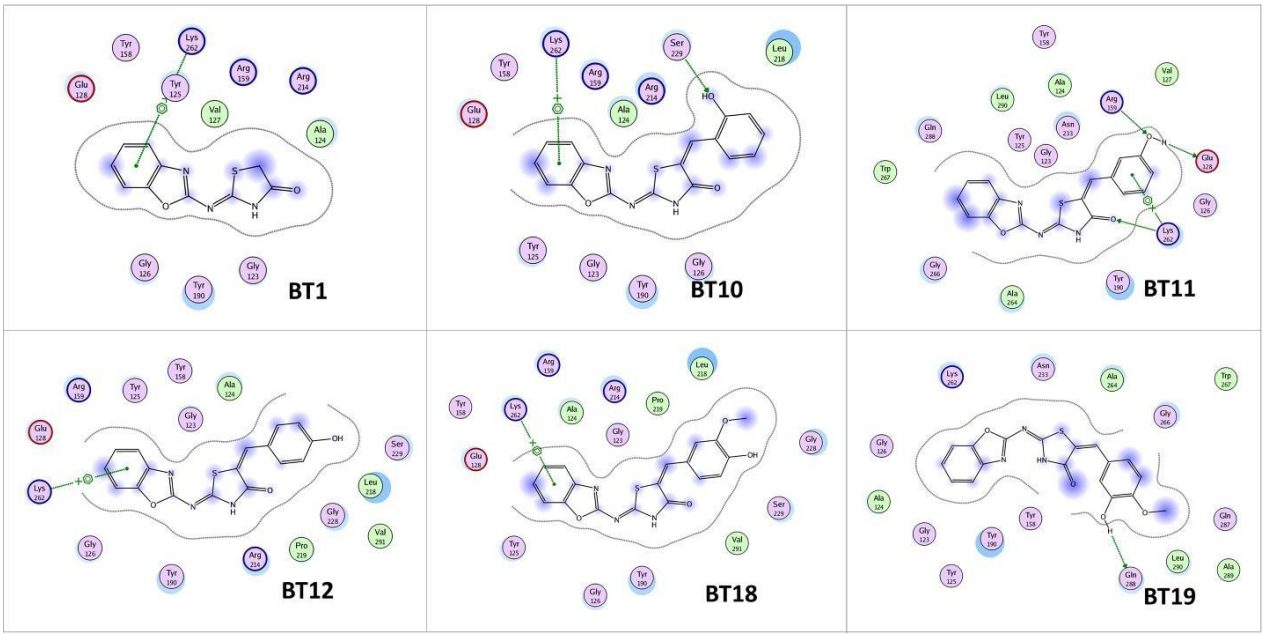

Figure S7. Interactions of selected B-T hybrids with MurB enzyme

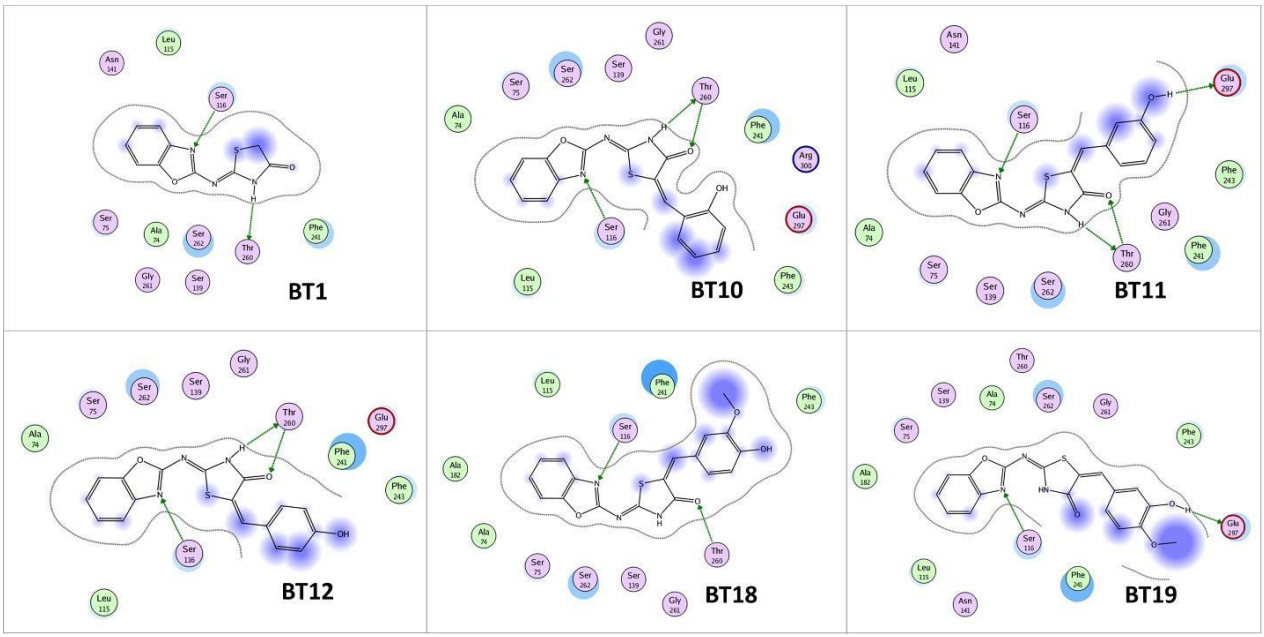

Figure S8. Interactions of selected B-T hybrids with PBP4 enzyme

8. Molecular details of the bacterial strains

Table 2 Molecular details of the bacterial strains used in the current study

Strains		Antibiotic resistant towards	Molecular details of strains
MSSA	S. aureus ATCC 29213	None	Type strain
MRSA	NRS 100	Methicillin, Tetracycline	Contains subtype I mec cassette & large variety of virulence factors
	NR 119	Methicillin, Gentamicin, Linezolid, Trimethoprim / sulfamethoxazole	Contains subtype IV mec cassette & G2576T mutation in domain V in one or more 23S rRNA genes
	NRS 129	Chloramphenicol	mecA negative
	NRS 186	Methicillin, Levofloxacin, Meropenem	USA 300 type CA-MRSA, PVL virulence factor positive & contains mec type IV cassette
	NRS 191	Methicillin, Levofloxacin, Meropenem	USA 600 type CA-MRSA, PVL virulence factor negative & contains mec type II cassette
	NRS 192	Methicillin, Levofloxacin, Meropenem, Erythromycin	CA-MRSA, PVL virulence factor negative & contains mec type II cassette
	NRS 193	Methicillin, Levofloxacin, Meropenem	CA-MRSA, PVL factor negative & contains mec type II cassette
	NRS 194	Methicillin, Meropenem	CA-MRSA, PVL virulence factor positive & contains mec type V cassette
	NRS 198	Methicillin, Levofloxacin, Meropenem	USA 100 type CA-MRSA, PVL virulence factor negative & contains mec type II cassette
VRSA	VRS 1	Methicillin, Levofloxacin, Meropenem, Vancomycin, Gentamicin, Teicoplanin & Spectinomycin	USA 100, contains mec subtype II cassette & vanA, negative for vanB, vanC1, vanC2, vanD, vanE, PVL & ACME
	VRS 4	Methicillin, Levofloxacin, Meropenem, Vancomycin, Gentamicin, Teicoplanin & Spectinomycin	USA 100, contains mec subtype II cassette & vanA, negative for vanB, vanC1, vanC2, vanD, vanE, PVL & ACME
	VRS 12	Methicillin, Levofloxacin, Meropenem, Vancomycin, Gentamicin, Teicoplanin & Spectinomycin	Data not available
Enterococcus	NR 31884	Methicillin, Gentamicin	Hemolytic, cytolytic isolate
	NR 31885	Methicillin, Gentamicin	Cytolytic isolate
	NR 31903	Vancomycin, Levofloxacin & Ceftazidime	Isolated from stool of patient before bacteraemia
	NR 31912	Gentamicin, Levofloxacin, Ceftazidime	Isolated from the stool of a human patient having dominance of vancomycin-resistant Enterococcus in stool but no bacteraemia.
Gram-negative bacteria	*E. coli* ATCC 25922	None	Type strain
	K. pneumoniae BAA 1705	mipenem, Ertapenem	Type strain
	A. baumannii BAA 1605	Ceftazidime, Gentamicin, Ticarcillin, Piperacillin, Aztreonam, Cefepime, Ciprofloxacin, Imipenem & Meropenem	Type strain
	P. aeruginosa ATCC 27853	None	Type strain

9. References

[1] A. Šali, T.L. Blundell, Comparative protein modelling by satisfaction of spatial restraints, J. Mol. Biol. 234 (1993) 779–815. https://doi.org/10.1006/jmbi.1993.1626.

[2] C.J. Andres, J.J. Bronson, S. V. D'Andrea, M.S. Deshpande, P.J. Falk, K.A. Grant-Young, W.E. Harte, H.T. Ho, P.F. Misco, J.G. Robertson, D. Stock, Y. Sun, A.W. Walsh, 4-Thiazolidinones: Novel inhibitors of the bacterial enzyme MurB, Bioorganic Med. Chem. Lett. 10 (2000) 715–717. https://doi.org/10.1016/S0960-894X(00)00073-1.

[3] M.J. Abraham, T. Murtola, R. Schulz, S. Páll, J.C. Smith, B. Hess, E. Lindah, Gromacs: High performance molecular simulations through multi-level parallelism from laptops to supercomputers, SoftwareX. 1–2 (2015) 19–25. https://doi.org/10.1016/j.softx.2015.06.001.

[4] K. Lindorff-Larsen, S. Piana, K. Palmo, P. Maragakis, J.L. Klepeis, R.O. Dror, D.E. Shaw, Improved side-chain torsion potentials for the Amber ff99SB protein force field, Proteins Struct. Funct. Bioinforma. 78 (2010) 1950–1958. https://doi.org/10.1002/prot.22711.

[5] W.L. Jorgensen, J. Chandrasekhar, J.D. Madura, R.W. Impey, M.L. Klein, Comparison of simple potential functions for simulating liquid water, J. Chem. Phys. 79 (1983) 926–935. https://doi.org/10.1063/1.445869.

[6] G. Martínez-Rosell, T. Giorgino, G. De Fabritiis, PlayMolecule ProteinPrepare: A Web Application for Protein Preparation for Molecular Dynamics Simulations, J. Chem. Inf. Model. 57 (2017) 1511–1516. https://doi.org/10.1021/acs.jcim.7b00190.

[7] K. Mizuuchi, M. Mizuuchi, M.H. O'Dea, M. Gellert, Cloning and simplified purification of Escherichia coli DNA gyrase A and B proteins, J. Biol. Chem. 259 (1984) 9199–9201. https://doi.org/10.1016/s0021-9258(17)47284-x.

[8] Y. Yang, A. Severin, R. Chopra, G. Krishnamurthy, G. Singh, W. Hu, D. Keeney, K. Svenson, P.J. Petersen, P. Labthavikul, D.M. Shlaes, B.A. Rasmussen, A.A. Failli, J.S. Shumsky, K.M.K. Kutterer, A. Gilbert, T.S. Mansour, 3,5-Dioxopyrazolidines, novel inhibitors of UDP-N-acetylenolpyruvylglucosamine reductase (MurB) with activity against gram-positive bacteria, Antimicrob. Agents Chemother. 50 (2006) 556–564. https://doi.org/10.1128/AAC.50.2.556-564.2006.

[9] M. Young, D.J. Walsh, E. Masters, V.S. Gondil, E. Laskey, M. Klaczko, H. Awad, J. McGrath, E.M. Schwarz, C. Melander, P.M. Dunman, Identification of Staphylococcus aureus Penicillin Binding Protein 4 (PBP4) Inhibitors, Antibiotics. 11 (2022) 1–17. https://doi.org/10.3390/antibiotics11101351.

[10] A.W. Sousa Da Silva, W.F. Vranken, ACPYPE - AnteChamber PYthon Parser interfacE, BMC Res. Notes. 5 (2012) 1–8. https://doi.org/10.1186/1756-0500-5-367.

[11] P. Ghanta, M. Doble, B. Ramaiah, Alkaloids of Adhatoda vasica Nees. as potential inhibitors of cyclooxygenases–an in-silico study, J. Biomol. Struct. Dyn. 0 (2021) 1–11. https://doi.org/10.1080/07391102.2021.1895887.

[12] V.S. Krishna Cheerala, P. Ghanta, S.C. Neelakantan, Design, synthesis andin silicoscreening of benzoxazole-thiazolidinone hybrids as potential inhibitors of SARS-CoV-2 proteases, RSC Adv. 11

(2021) 39328–39342. https://doi.org/10.1039/d1ra07504g.

[13] M.S. Valdés-Tresanco, M.E. Valdés-Tresanco, P.A. Valiente, E. Moreno, Gmx_MMPBSA: A New Tool to Perform End-State Free Energy Calculations with GROMACS, J. Chem. Theory Comput. 17 (2021) 6281–6291. https://doi.org/10.1021/acs.jctc.1c00645.

[14] B.R. Miller, T.D. McGee, J.M. Swails, N. Homeyer, H. Gohlke, A.E. Roitberg, MMPBSA.py: An efficient program for end-state free energy calculations, J. Chem. Theory Comput. 8 (2012) 3314–3321. https://doi.org/10.1021/ct300418h.